Nagra
Nationale
Genossenschaft
für die Lagerung
radioaktiver Abfälle

Cédra
Société coopérative
nationale
pour l'entreposage
de déchets radioactifs

Cisra
Società cooperativa
nazionale
per l'immagazzinamento
di scorie radioattive

TECHNICAL REPORT 88-31

GRIMSEL TEST SITE

RADAR CROSSHOLE TOMOGRAPHY WITH APPLICATION TO MIGRATION OF SALINE TRACER THROUGH FRACTURE ZONES

BÖRJE NIVA[1)]
OLLE OLSSON[1)]
PETER BLÜMLING[2)]

OCTOBER, 1988

[1)] SWEDISH GEOLOGICAL CO. UPPSALA, SWEDEN
[2)] NAGRA

GRIMSEL TEST SITE / SWITZERLAND
A JOINT RESEARCH PROGRAM BY

- NAGRA — National Cooperative for the Storage of Radioactive Waste, Baden, Switzerland
- BGR — Federal Institute for Geoscience and Natural Resources, Hannover, Federal Republic of Germany
- GSF — Research Centre for Environmental Sciences, Munich, Federal Republic of Germany

Parkstrasse 23 5401 Baden / Schweiz Telephon 056 / 20 55 11

Nagra
Nationale
Genossenschaft
für die Lagerung
radioaktiver Abfälle

Cédra
Société coopérative
nationale
pour l'entreposage
de déchets radioactifs

Cisra
Società cooperativa
nazionale
per l'immagazzinamento
di scorie radioattive

TECHNICAL REPORT 88-31

GRIMSEL TEST SITE

RADAR CROSSHOLE TOMOGRAPHY WITH APPLICATION TO MIGRATION OF SALINE TRACER THROUGH FRACTURE ZONES

BÖRJE NIVA[1)]
OLLE OLSSON[1)]
PETER BLÜMLING[2)]

OCTOBER, 1988

[1)] SWEDISH GEOLOGICAL CO. UPPSALA, SWEDEN
[2)] NAGRA

GRIMSEL TEST SITE / SWITZERLAND
A JOINT RESEARCH PROGRAM BY

- NAGRA — National Cooperative for the Storage of Radioactive Waste, Baden, Switzerland
- BGR — Federal Institute for Geoscience and Natural Resources, Hannover, Federal Republic of Germany
- GSF — Research Centre for Environmental Sciences, Munich, Federal Republic of Germany

Parkstrasse 23 5401 Baden / Schweiz Telephon 056 / 20 55 11

FOREWORD

Concepts which foresee the disposal of radioactive waste in geological formations lay great weight on acquiring knowledge of the proposed host rock and the surrounding rock strata. For this reason, Nagra has, since May 1984, been operating the Grimsel Test Site which is situated at a depth of 450 m in the crystalline formation of the Aar Massif. The general objectives of the research being carried out in this system of test tunnels include, in particular

- the build-up of know-how in planning, performing and interpreting underground experiments in different scientific fields and

- the aquisition of practical experience in developing, testing and applying test equipment and measuring techniques.

The Test Site (GTS) is operated by Nagra. On the basis of a German-Swiss cooperation agreement, the various experiments are carried out by Nagra, the Federal Institute for Geoscience and Natural Resources (BGR) and the Research Centre for Environmental Sciences (GSF); the latter two bodies are supported in this venture by the German Federal Ministry for Research and Technology (BMFT).

NTB 85-47 gives an overview of the GTS and a review of the status of the investigation programme as at August 1985.

VORWORT

Bei Konzepten, die die Endlagerung radioaktiver Abfälle in geologischen Formationen vorsehen, ist die Kenntnis des Wirtgesteins und der angrenzenden Gesteinsschichten von grundlegender Bedeutung. Die Nagra betreibt deshalb seit Mai 1984 das Felslabor Grimsel in 450 m Tiefe im Kristallin des Aarmassivs. Die generelle Zielsetzung für die Arbeiten in diesem System von Versuchsstollen umfasst insbesondere

- den Aufbau von Know-how in der Planung, Ausführung und Interpretation von Untergrundversuchen in verschiedenen Experimentierbereichen und

- den Erwerb praktischer Erfahrung in der Entwicklung, Erprobung und dem Einsatz von Testapparaturen und Messverfahren.

Das Felslabor (FLG) wird durch die Nagra betrieben. Die verschiedenen Untersuchungen werden aufgrund eines deutsch-schweizerischen Zusammenarbeitsvertrages durch die Nagra, die Bundesanstalt für Geowissenschaften und Rohstoffe (BGR) und die Gesellschaft für Strahlen- und Umweltforschung (GSF) durchgeführt, beide gefördert vom Deutschen Bundesministerium für Forschung und Technologie (BMFT).

Eine Uebersicht des FLG und die Zusammenfassungen der Untersuchungsprogramme sind mit Status August 1985 im NTB 85-47 enthalten.

Der vorliegende Bericht wurde im Rahmen der Zusammenarbeit zwischen den drei Partnern erstellt. Die Autoren haben ihre eigenen Ansichten und Schlussfolgerungen dargelegt. Diese müssen nicht unbedingt mit denjenigen der Nagra, BGR oder GSF übereinstimmen.

AVANT-PROPOS

La connaissance de la roche d'accueil et des couches rocheuses avoisinantes est d'importance fondamentale pour l'élaboration de concepts prévoyant le stockage de déchets radioactifs dans des formations géologiques. C'est pour cela que la Cédra exploite depuis mai 1984 le laboratoire souterrain du Grimsel à 450 m de profondeur dans le cristallin du massif de l'Aar. Les objectifs généraux des travaux menés dans ce complexe de galeries d'essais comprennent notamment:

- la constitution d'un savoir-faire dans la préparation, l'exécution et l'interprétation d'essais souterrains dans divers domaines et

- l'acquisition d'expérience pratique dans le développement, la mise à l'épreuve et l'engagement d'appareillages d'essais et de techniques de mesure.

Le laboratoire souterrain est exploité par la Cédra. Les différentes recherches sont réalisées dans le cadre d'un accord de collaboration germano-suisse par la Cédra, la "Bundesanstalt für Geowissenschaften und Rohstoffe" (BGR) et la "Gesellschaft für Strahlen- und Umweltforschung" (GSF), ces deux dernières instances étant soutenues par le Ministère allemand pour la recherche et la technologie (BMFT).

Un aperçu du laboratoire souterrain et un résumé des programmes de recherches apparaissent dans le rapport NTB 85-47 d'août 1985.

Le présent rapport a été élaboré dans le cadre de la collaboration entre les trois partenaires. Les auteurs ont présenté leurs vues et conclusions personnelles. Celles-ci ne doivent pas forcément correspondre à celles de la Cédra, de la BGR et de la GSF.

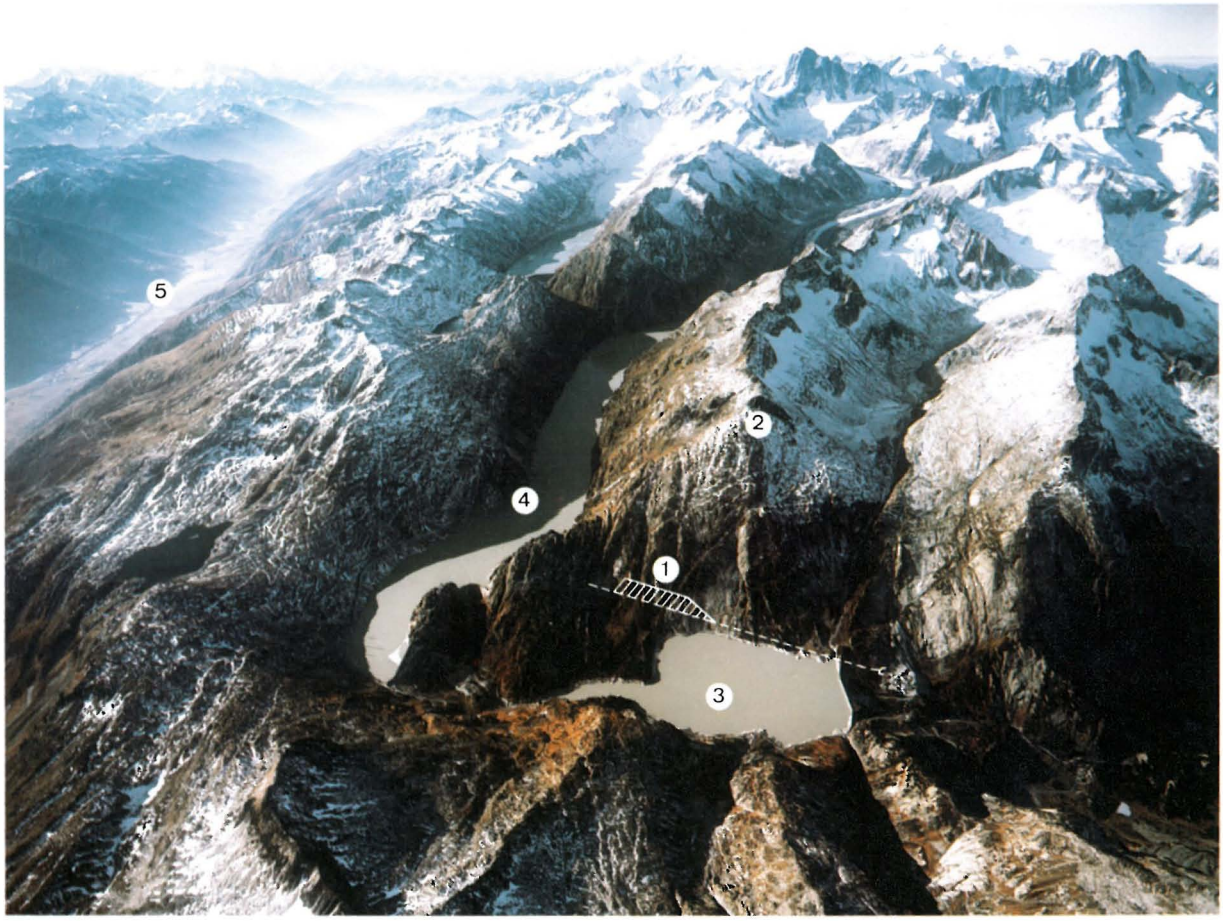

GRIMSEL-GEBIET

Blick nach Westen

1 Felslabor
2 Juchlistock
3 Räterichsbodensee
4 Grimselsee
5 Rhonetal

GRIMSEL AREA

View looking West

1 Test Site
2 Juchlistock
3 Lake Raeterichsboden
4 Lake Grimsel
5 Rhone Valley

FLG FELSLABOR GRIMSEL
GTS *GRIMSEL TEST SITE*

Situation

0 100 m

- Zugangsstollen/*Access tunnel*
- Fräsvortrieb/*by tunnel boring machine*
- Sprengvortrieb/*excavated by blasting*
- Zentraler Aaregranit ZAGR / *Central Aaregranite CAGR*
- Biotitreicher ZAGR / *CAGR with high content of biotite*
- Grimsel-Granodiorit / *Grimsel-Granodiorite*
- Scherzone/*Shear zone*
- Lamprophyr/*Lamprophyre*
- Wasserzutritt/*Water inflow*
- SB Sondierbohrung/*Exploratory borehole*
- US US Bohrung/*US borehole*

ZB	Zentraler Bereich/*Central facilities*
AU	Auflockerung/*Excavation effects*
BK	Bohrlochkranz/*Fracture system flow*
EM	El.magn. HF-Messungen/*-measurements*
FRI	Kluftzone/*Fracture zone investigation*
GS	Gebirgsspannungen/*Rock stresses*
HPA	Hydr. Parameter/*Hydr. parameters*
MI	Migration/*Migration*
MOD	Hydrodyn. Modellierung/*H. modeling*
NM	Neigungsmesser/*Tiltmeters*
UR	Untertageradar/*Underground radar*
US	Seismik/*Underground seismic testing*
VE	Ventilationstest/*Ventilation test*
WT	Wärmeversuch/*Heat test*

A — A Schnitt/*Section*

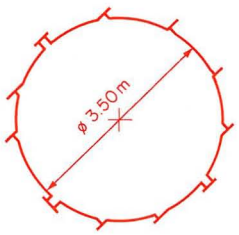

6/88

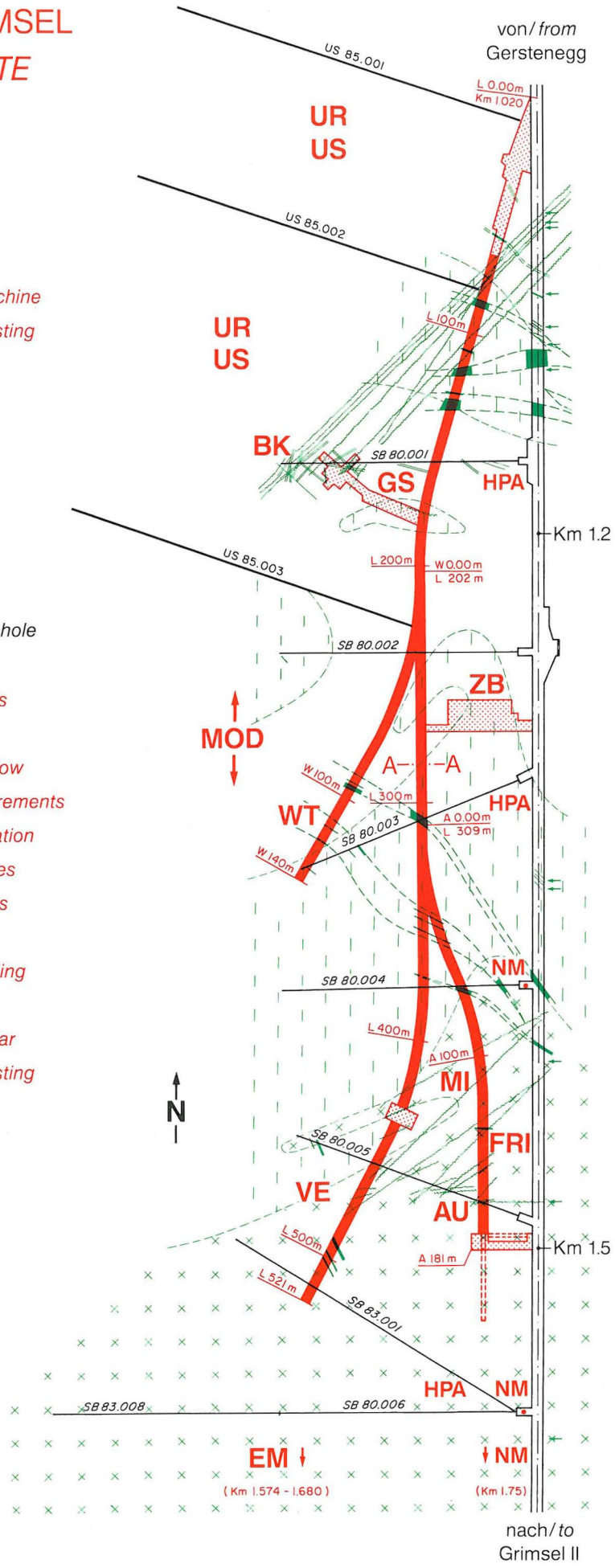

ABSTRACT

A comprehensive radar crosshole tomography survey has been carried out at the Grimsel Rock Laboratory in order to test the radar method with respect to its capability to describe geological features and to map migration of saline tracer through difference tomography. The radar survey has provided a map of the attenuation and slowness distribution of radar waves in a planar section with the dimensions 150x225 m. The program has included measurement points along parallel boreholes and a tunnel connecting these boreholes.

The slowness and attenuation tomograms give similar images of the structures at the investigated site. The largest anomalies are caused by lamprophyric dikes which are almost parallel to the boreholes while fracture zones give rise to anomalies of smaller magnitude. The attenuation tomograms have poorer resolution and contain more artifacts than the slowness tomograms. This is caused by systematic errors in the amplitude data caused by inadequate knowledge of the antenna radiation pattern for source points located in the tunnel.

The transport of saline tracer was investigated by making a tomographic inversion of the difference between data collected prior to injection of saline tracer and during injection. Two such experiments were performed with different injection points. The largest concentrations of tracer were observed close to the injection points. The tracer followed fracture zones extending from the injection points. The results clearly show the capabilities of the radar method to map tracer transport through fractured rock.

Zusammenfassung

Im Felslabor Grimsel wurde ein umfassendes Radar-Crosshole Tomographieprogramm durchgeführt. Ziel des Versuchs war es, die Methode auf ihre Eignung zur Charakterisierung von geologischen Störungen zu untersuchen und gleichzeitig mit Hilfe der Differenztomographie die Migration von Salztracer zu beobachten. Die Radarmessungen ergaben Tomogramme mit der Dämpfungs- und Slownessverteilung in einer ebenen Sektion mit einer Ausdehnung von 150 * 225 m. Grundlage für diese Ergebnisse waren Messungen in parallelen Bohrungen und dem Tunnel, von dem die Bohrungen aus gebohrt worden waren.

Die Slowness- und Dämpfungstomogramme zeigen ähnliche Abbildungen der Strukturen im Untersuchungsgebiet. Die grössten Anomalien werden durch Lamprophyre, die nahezu parallel zu den Bohrungen verlaufen, verursacht. Störungszonen werden als weniger ausgeprägte Anomalien abgebildet. Die Tomogramme der Amplitudendämpfung zeigen eine schlechtere Auflösung als die der Slowness. Die Ursache dafür liegt bei systematischen Fehlern, die durch die ungenügende Kenntnis der Abstrahlungscharakteristik der Antenne im Tunnel bedingt sind.

Der Transport des Salztracers wurde mit Hilfe einer tomographischen Inversion von Differenzdaten untersucht, die auf Messungen vor und während der Tracerinjektion basierten. Insgesamt wurden zwei Experimente mit unterschiedlichen Injektionspunkten vorgenommen. Die Resultate zeigen deutlich die einzigartige Möglichkeit der Radarmethode, den Transport des Tracers durch geklüftetes Gestein zu beobachten.

RESUME

Un vaste programme de tomographie radar entre puits a été réalisé au laboratoire souterrain du Grimsel. L'essai avait pour objet d'étudier si la méthode se prêtait é la caractérisation des perturbations géologiques tout en observant, é l'aide de la tomographie différentielle, la migration de traceurs (sel). Les mesures radar ont fourni des tomogrammes avec répartition Slowness et d'amortissement dans une section plane avec une extension de 150 x 225 m. Ces résultats se basaient sur des mesures faites dans des forages parallèles et dans le tunnel é partir duquel on avait creusé les forages.

Il ressort des tomogrammes Slowness et d'amortissement une similitude dans la représentation des structures de la région de recherches. Les anomalies majeures sont provoquées par des lamprophyres quasi parallèles aux forages. Les zones de perturbations sont représentées sous forme d'anomalies moins prononcées. Les tomogrammes de l'amortissement d'amplitudes ont une moins bonne résolution que les tomogrammes Slowness, en raison des erreurs systématiques dues é la connaissance insuffisante de la caractéristique du rayonnement de l'antenne dans le tunnel.

On a analysé le transport du traceur (sel) é l'aide d'une inversion tomographique de données différentielles se basant sur des mesures faites avant et pendant l'injection du traceur. On a procédé en tout é deux expériences avec différents points d'injection. Les résultats montrent nettement l'extraordinaire possibilité de la méthode radar d'observer le transport du traceur é travers une roche fissurée.

SUMMARY AND CONCLUSIONS

The objective of the Radar Crosshole Tomography (RCT) program carried out at the Grimsel Rock Laboratory has been to provide data on geological structures at the US-site. The results are presented as tomographic maps of radar wave attenuation and velocity of three 'fields' at the US-site. For one of the fields the tomographic measurements (phase 1) have been made three times; first a reference measurement and then two repetitions with saline water was injected at two different locations (phase 2 and 3). This was intended as a test on the capability of the radar method to map groundwater transport paths and if successful to give a map of the transport paths in the plane between the boreholes. The saline tracer increases the attenuation of the radar signal and a tomographic analysis of the difference between the second and third phases and the reference measurement will show the distribution of the tracer in the plane between the boreholes.

Tomographic surveys have been made of three areas which have been termed "fields". Fields 1 and 2 were measured with a high ray density and Field 3 which includes these two fields was measured with a lower ray density. Difference tomography to map the distribution of saline tracer was made in one of the fields (Field 2). The measurements were made with a short pulse borehole radar system (RAMAC). The total number of rays measured as a part of the RCT-programme is close to 30 000.

The RAMAC system used for the measurements has performed well during the execution of the relatively comprehensive RCT-programme. During phase 1 serious problems were caused by temperature sensitive components which caused a drift in the time base of the system. The system was modified and no problems of that type were encountered during phases 2 and 3. The comprehensive measurement programmes of each phase could be completed within the allocated time frames.

The calibration procedure applied during phases 2 and 3 provided sufficient control on any system drifts. For experiments of this type where saline tracer is injected into the rock calibration measurements have to be performed in a part of the experimental site where no saline tracer is expected to appear. Difference tomography requires a good control on

system drifts. It is essential to be able to separate effects caused by the injected salt and the measurement system itself.

The most significant errors found in the amplitude data were caused by the effect of the tunnel on the radiation pattern of the antenna. No efficient way was found to correct for this error. Therefore a significant portion of the tunnel to hole rays had to be excluded from the data set. However, the errors caused by the unknown radiation pattern cancel when the difference data is calculated with respect to the reference measurement. The effect on the difference tomograms has thus been negligeable.

The only significant errors in the travel time data occurred during phase 1 when there were relatively large drifts in the time base of the radar system. These errors could only partly be corrected for due to inadequate calibration procedures. Due to modifications of the hardware time drifts did not occur during the latter phases. The dominating errors in these data sets were quantization errors.

The main feature identified in the radar slowness and attenuation tomograms is a lamprophyre located in Field 2 which extends in a direction almost parallel to the boreholes. Two additional sets of features can also be identified which extend in almost orthogonal directions (NW and WSW). These features can be identified with good resolution in the slowness tomogram.

The slowness and attenuation tomograms show a good correlation with geological features observed in boreholes and tunnels. High resolution is obtained near the L-tunnel where the ray density is high while there is lower resolution at large distances from the L-tunnel. The distance from the tunnel where high resolution prevails is determined by the length to width ratio of the investigated field. It is therfore recommended that the length to width ratio of the investigated area is not less than 1. This will give acceptable data for at least two thirds of the area provided that measurements points are located on at least three sides of the area as has been done in this case.

The main task during the second and third phase of the RCT-programme was to investigate whether radar tomography could be used to study the spreading of a saline tracer through the rock mass and if radar tomography successfully can map the spreading of the tracer. The injection of the tracer was carried out by the Bundesanstalt für Geowissenshaften und

Rohstoffe (BGR) using the mulitpacker system that was developed for the fracture flow experiment. Saline tracer was injected from boreholes BO BK 85.009 during phase 2 and BO BK 86.003 during phase 3, both drilled from the BK-drift. The salinity of the tracer was selected to 0.9% for phase 2 and 0.8% for phase 3. This high salinity was chosen to ensure that there was a reasonable chance of measuring the increased attenuation with the radar system.

The largest concentrations of tracer were observed close to the injection points. The tracer followed fracture zones extending from the injection points. Tracer from both injection points were transported to the L-tunnel close to its intersection with the BK-drift. These transport paths did not leave a continous trace in the difference tomograms which demonstrates that the transport paths were not confined to the investigated plane. Hence, the groundwater transport at the Grimsel Rock Laboratory occurs in three dimensions. The results clearly show the unique capabilities of the radar method to map tracer transport through fractured rock.

CONTENTS

LIST OF FIGURES

Fig. 6.6 Tomographic map showing increase in radar attenuation of Field 2 from phase 1 to phase 3 obtained after removal of the rays going to the bottom of borehole BO US 85.002. Scale 1:1000. 78

LIST OF TABLES

1 INTRODUCTION

1.1 Objectives

Final disposal of spent nuclear fuel is generally based on a multi-barrier concept where one of the barriers is the host rock surrounding a repository. The safety of a future repository depends on the groundwater flow rate and transport capacity of radio-nuclides from the repository to the biosphere. In this context parameters such as groundwater gradients, hydraulic properties of the host rock, groundwater flow paths and flow velocity are essential in the description of the additional safety provided by the host rock barrier.

Groundwater flow in crystalline rock is a relatively complex process where flow essentially occurs in fractures which occupy a minor portion of the total rock volume. The development of the borehole radar technique has provided novel possibilities for investigating groundwater flow. Borehole radar is a remote sensing technique and is thus capable of giving high resolution information from observation points located far from the measuring points (boreholes or tunnels). Typical probing ranges are up to some hundreds of meters with resolution on the order of meters. For example borehole radar can be used to give a three-dimensional geometric description of fracture zones where groundwater is likely to be concentrated. It should be noted that this is a great improvement compared to "conventional" methods (e.g. core logging, geophysical logging) where information is obtained only from the immediate vicinity of the borehole (normally < 1 m) and in this case fracture zone geometry has to be inferred from boreholes separated by large distances. Remote sensing methods such as borehole radar and borehole seismics add a new degree of certainty and confidence in description of fracture zone geometry and properties (Olsson, Black, Cosma, and Pihl, 1987).

The borehole radar technique can also be used to image the actual flow paths through the rock and to provide some information about the flow velocity. The basic idea behind experiments where borehole radar is used to show groundwater flow paths is to use a difference technique. First a reference measurement is made which gives a description of the fracture system and other geological structures at the experimental site. Then saline tracer is injected

from a borehole and the measurement is repeated. Saline water increases the attenuation of radar waves and the difference between both measurements will give information on the location of the saline tracer at the time of measurement. If measurements are repeated at regular intervals it should be possible to describe the spreading of the tracer with time and hence the flow velocity.

The objective of the Radar Crosshole Tomography (RCT) program carried out at the Grimsel Rock Laboratory has been to investigate the potential of the method and to gather data on geological structures at the US-site in the form of tomographic maps of radar wave attenuation and velocity of three "fields" at the US-site. For one of the fields the tomographic measurements have been made three times; first a reference measurement and then two repetitions at which saline water was injected at two different locations. This was intended as a test on the capability of the radar method to map groundwater transport paths and if successful to give a map of the transport paths in the plane between the boreholes.

1.2 Background

A substantial development of the borehole radar technique and its application to fracture detection in crystalline rock has been made within the framework of the International Stripa Project. The work has been performed by a research group at the Swedish Geological Co. (SGAB). The development efforts have comprised the construction of a new radar system (RAMAC), a comprehensive field testing program, and interpretation of the data collected (Olsson, Falk, Forslund, Lundmark, and Sandberg, 1987). The RAMAC system can be applied both for single hole and crosshole measurements. Reflections are observed in both measurement modes and can be used to identify fracture zones or other inhomogeneities in the rock. The analysis of crosshole data has also included tomographic inversion of travel time and amplitude data. The experience gained from the Stripa Project has provided a profound insight into the processing steps required to obtain high quality tomograms from radar data.

A first test at the Grimsel Rock Laboratory with the borehole radar system developed by SGAB was performed during October 1985 (Olsson and Lundmark, 1985, Falk et. al., 1987). The testing program comprised reflection measurements in the boreholes BO US

85.001, BO US 85.002, BO US 85.003 (Fig. 1.1) and a few crosshole scans. Radar reflection ranges of up to 150 m were obtained. The strongest reflections were caused by lamprophyre dikes while fracture zones caused weaker reflexes. The crosshole measurements demonstrated the capability of the system to detect radar signals which had propagated between the holes with the largest separation (225 m) and hence that the current Radar Crosshole Tomography (RCT) program was feasible.

1.3 Scope of work

The RCT-programme has been carried out in three phases: The first phase comprised a set of reference measurements which have given a test on the capability of radar tomography to map the extent and character of geological features. In the second and third phases radar tomography measurements have been performed simultaneously with injection of a saline tracer in two different fracture zones. The saline tracer increases the attenuation of the radar signal and a tomographic analysis of the difference between the second and third phases respectively and the reference measurement will show the distribution of the tracer in the plane between the boreholes.

The measurements of the first phase of the RCT programme were carried out during a four week period in October and November 1986. The first phase comprised three sets of measurements in different areas which have been termed "fields" (Fig. 1.1). Measurements with high ray density were performed between boreholes BO US 85.001 and BO US 85.002 (Field 1) and between BO US 85.002 and BO US 85.003 (Field 2). The measurement between boreholes BO US 85.001 and BO US 85.003 (Field 3) were carried out with a reduced ray density. Each field has comprised measurement points on three sides, i.e. the bounding boreholes and the Laboratory-tunnel (L-tunnel). All investigation boreholes are parallel with a dip of approximately 15^{o}.

The measurements of the second phase were carried out during a two week period in April 1987. During this phase measurements were made of Field 2 while saline tracer was injected in a fracture zone from borehole BO BK 85.009 which extends from the BK-drift (Fig. 1.2).

The measurements of the third phase were concentrated to a one week period during December 1987. To reduce the total measurement time and hence any effects of changes in tracer distribution with time, radar

measurements were made round the clock. The saline injection was now made from a section in borehole BO BK 86.003 which extends from the BK-drift (Fig. 1.3).

The measurements of the first phase constitute a set of reference data which have been used for comparison with the results of the later phases. In the second and third phases radar measurements have been carried out simultaneously with injection of saline tracer. The saline tracer will increase the electrical conductivity of the groundwater and hence the attenuation of radar waves. The saline tracer has been expected to follow some preferred flow path through the rock and the idea is to map the path through tomographic analysis of the radar crosshole data. Radar waves are in addition to the presence of a saline tracer also attenuated by geologic features in the rock, e.g. lamprophyric dikes and fracture zones. The saline tracer is only expected to cause relatively small increases in radar attenuation compared to the variation in attenuation between for example lamprophyre dikes and relatively intact granite. Therefore the effect of saline tracer can only be expected to be revealed if the difference between two measurements is studied, one where saline tracer was absent and one where it is present. This type of difference measurement is the only one which is sensitive enough to reveal the location of tracer in the investigated area.

This report describes the results from all three phases and tries to summarize the experience and know-how gained from the project. A description is given of equipment used, experimental procedures, data processing and results from the three phases. A more detailed account of the measurement program and data processing steps for each phase has been given in three separate reports (Niva and Olsson, 1987, 1988a, 1988b).

This work has been performed under a contract between NAGRA and Swedpower. The field measurements and the analysis of the data has been performed by personnel from Swedish Geological Co. (SGAB). The radar equipment used for the measurements is the property of the Swedish Nuclear Fuel and Waste Management Co. (SKB).

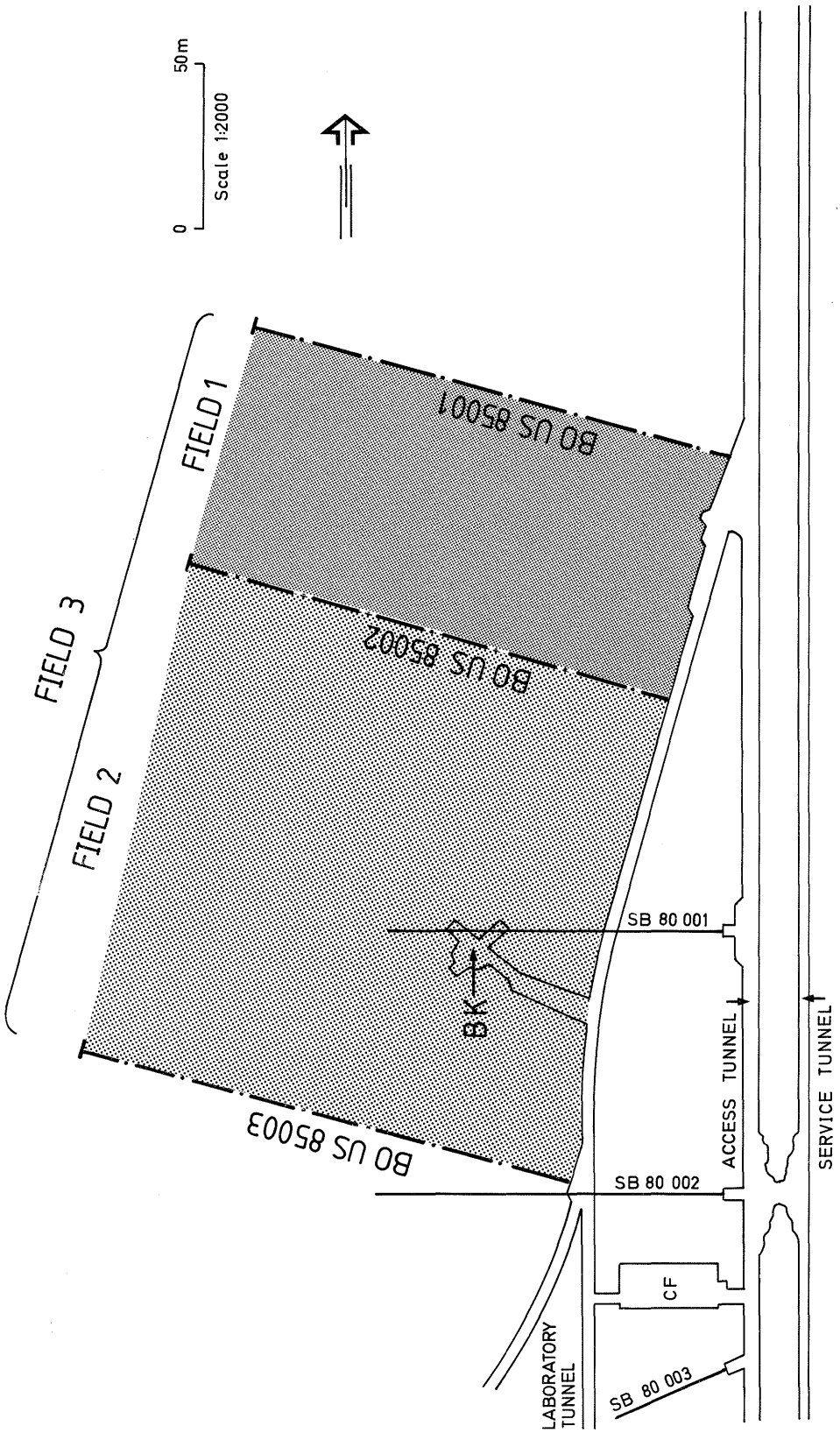

Fig. 1.1 Map of the US-site where the Radar Crosshole Tomography measurements were performed.

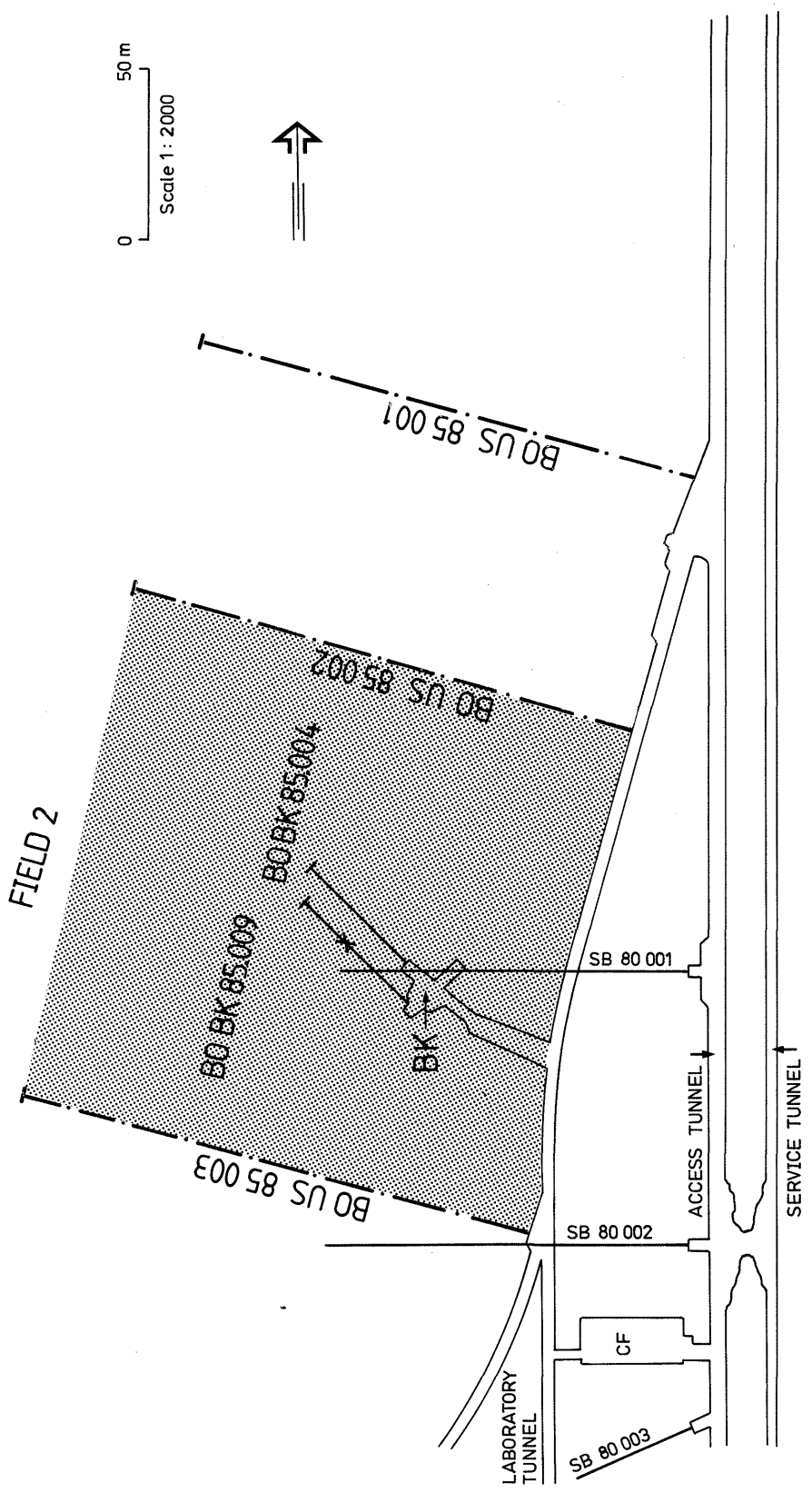

Fig. 1.2 Map of the US-site where the Radar Crosshole Tomography measurements were performed. The injection point for saline tracer during phase 2 is indicated.

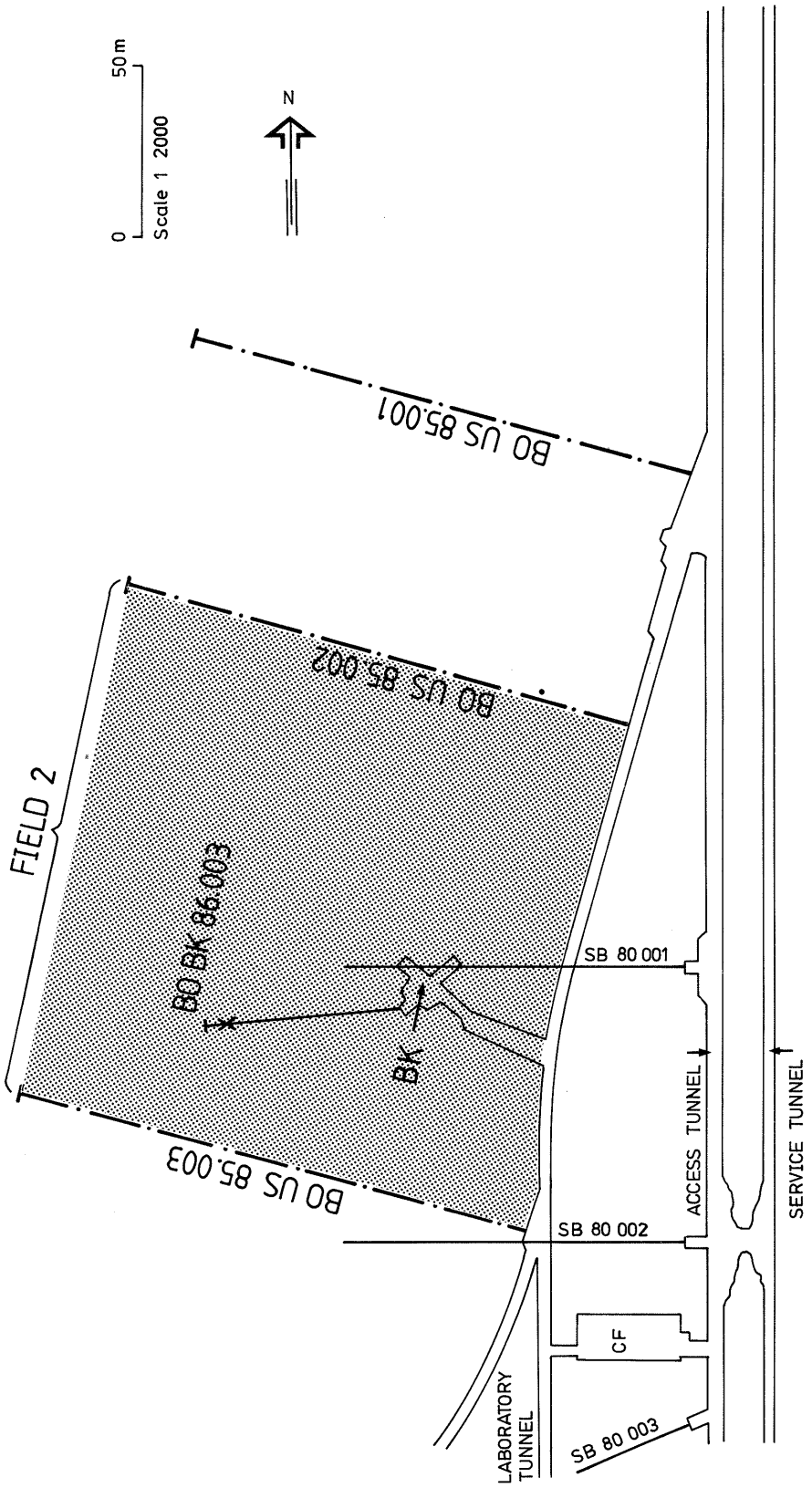

Fig. 1.3 Map of the US-site where the Radar Crosshole Tomography measurements were performed. The injection point for saline tracer during phase 3 is indicated.

2 EXPERIMENTAL SETUP

2.1 Equipment used

A short pulse borehole radar system (RAMAC) has been used for these measurements. The system was originally developed by the Swedish Geological Co. (SGAB) as a part of the International Stripa Project. A continued development to make the system adapted for field work on a production basis has later been funded by SKB.

The radar system (RAMAC) consists of four different parts;

- a microcomputer with two 5 inch floppy disc units for control of measurements, data storage, data presentation and signal analysis.
- a control unit for timing control, storage and stacking of single radar measurements.
- a borehole transmitter for generation of short radar pulses.
- a borehole receiver for detection and digitization of radar pulses.

The RAMAC system works in principle in the following manner: A short current pulse is fed to the transmitter antenna, which generates a radar pulse that propagates through the rock. The pulse is made as short as possible to obtain high resolution. The pulse is received by the same type of antenna, amplified, and registered as a function of time. The receiver may be located in the same borehole as the transmitter or in any other borehole. From the full wave record of the signal the distance (travel time) to a reflector, the strength of the reflection, and the attenuation and delay of the direct wave between transmitter and receiver may be deduced.

The recording of the signal is similar to that of a sampling oscilloscope, i.e. for each pulse from the transmitter only one sample of the received electric signal is taken at a specific time. When the next pulse is generated a new sample is taken which is displaced slightly in time. Thus, after a number of samples a replica of the entire signal is recorded. The sampling frequency and the length and position of

the sampled time interval can be set by the operator.

Optical fibers are used for transmission of the trigger signals from the computer to the borehole probes and for transmission of data from the receiver to the control unit. The optical fibers have no electrical conductivity and will not support waves propagating along the borehole. Another advantage of optical fibers is that they can not pick up electrical noise and as the signal is digitized down-hole there will be no deterioration of the signal along the cable. The quality of the results will thus be independent of cable length.

There is no direct connection between the transmitter and the receiver. Both probes are instead connected directly to the control unit and the transmitter and the receiver can be put into the same as well as into separate holes. In other words, the radar may be used both for single hole and crosshole measurements. The system also provides absolute timing of the transmitted pulses and a calibrated gain in the receiver which makes it possible to measure travel time and amplitude of the radar pulses in a crosshole measurement and hence provide data for a tomographic analysis. The absolute time depends on the length of the optical fibers and is hence a quantity which has to be obtained through calibration for a given set of optical fibers. The block diagram of the control unit, transmitter, and receiver is shown in Fig. 2.1 and the technical specifications of the system are given in Table 2.1.

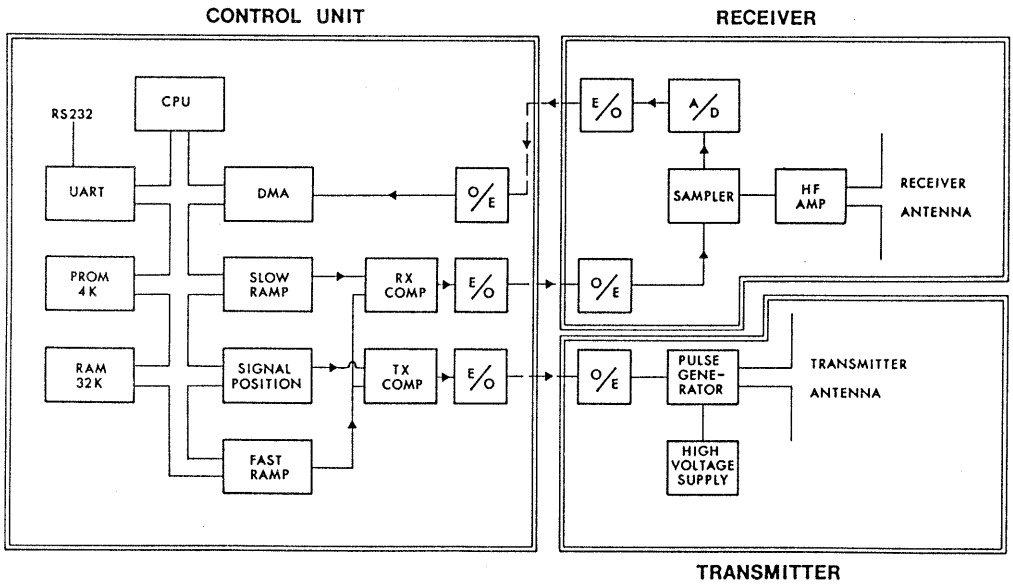

Fig. 2.1 Block diagram of the borehole radar system.

Table 2.1 Technical specifications of the borehole radar system.

General	
Frequency range	20-80 MHz
Total dynamic range	150 dB
Sampling time accuracy	1 ns
Maximum optical fiber length	1000 m
Maximum operating pressure	100 bar
Outer diameter of transmitter/receiver	48 mm
Minimum borehole diameter	56 mm
Transmitter	
Peak power	500 W
Operating time	10 h
Length	4.8 m
Weight	16 kg
Receiver	
Bandwidth	10-200 MHz
A/D converter	16 bit
Sensitivity	1 µV
Data transmission rate	1.2 MB
Operating time	10 h
Length	5.4 m
Weight	18 kg
Control unit	
Microprocessor	RCA 1806
Clock frequency	5 MHz
Pulse repetition frequency	43.1 kHz
Sampling frequency	30-1000 MHz
No of samples	256-4096
No of stacks	1-32767
Time window	0-11 µs

2.2 Measurement program

The experimental programme comprised three phases. the first phase included radar measurements of all three fields at the US-site. The second and third phases comprised repeated radar measurements of Field 2 during injection of saline tracer.

The crosshole radar measurements during phase 1 were carried out to cover three fields of investigation. Fields 1 and 2 were measured with a dense ray

coverage while Field 3 was covered with about one fourth the ray density used for the other fields. The Laboratory tunnel (L-tunnel) and the boreholes from which the measurements were made are shown in Fig. 1.1. The actual location of all points which were used either as source or receiver points are shown in Fig. 2.2.

The source and receiver positions used for the respective fields are listed in Tables 2.2-2.4. Field 1 corresponds to the plane between the boreholes BO US 85.001 and BO US 85.002 while Field 2 is between holes BO US 85.002 and BO US 85.003. The separation of measurement points for Fields 1 and 2 were 2.5 m in the boreholes and 5 m in the L-tunnel. A point separation of 5 m in the holes and 10 m in the tunnel was used for Field 3.

Table 2.2 Radar Crosshole Tomography source and receiver points for Field 1.

Transmitter	Receiver	Transmitter spacing	Receiver spacing
BO US 85.002	BO US 85.001		
0-142.5 m	0-142.5 m	2.5 m	2.5 m
L-tunnel*	BO US 85.001		
85.014	0-142.5 m		2.5 m
85.016	0-142.5 m		2.5 m
85.020	0-142.5 m		2.5 m
85.023-85.039	0-142.5 m	5 m	2.5 m
85.002	0-142.5 m		2.5 m
L-tunnel	BO US 85.002		
85.001	0-142.5 m		2.5 m
85.014	0-142.5 m		2.5 m
85.016	0-142.5 m		2.5 m
85.020	0-142.5 m		2.5 m
85.023-85.039	0-142.5 m	5 m	2.5 m

Total number of rays 4872.

* A number of short boreholes with a depth of about 0.5 m were drilled along the tunnel during the seismic crosshole tomography program. These boreholes were originally used to ensure good coupling of the seismic receivers. For the radar program these short boreholes were not used directly. Instead the centre of the transmitter was placed at the location of these boreholes. The positions are indicated in Fig. 2.2.

Table 2.3 Radar Crosshole Tomography source and receiver points for Field 2.

Transmitter	Receiver	Transmitter spacing	Receiver spacing
BO US 85.003	BO US 85.002*		
0-142.5 m	0-142.5 m	2.5 m	2.5 m
L-tunnel	BO US 85.002		
85.042-85.076	0-142.5 m	5 m	2.5 m
85.083-85.095	0-142.5 m	5 m	2.5 m
85.003	0-142.5 m		2.5 m
L-tunnel	BO US 85.003		
85.002	0-142.5 m		2.5 m
85.042-85.076	0-142.5 m	5 m	2.5 m
85.083-85.095	0-142.5 m	5 m	2.5 m

Total number of rays 6380.

*The borehole to borehole measurements of phases 2 and 3 were performed with the transmitter in BO US 85.002 and the receiver in BO US 85.003.

The crosshole measurements have been performed in sets which are termed 'scans'. During each scan one of the probes (transmitter or receiver) is kept at a fixed position while the other probe is moved in the other borehole. The moving probe has normally been the transmitter in the borehole to borehole measurements and the receiver, which was moved in the boreholes, during the tunnel to borehole measurements. The following exceptions to this rule apply: during the phase 2 measurements the moving probe in the hole to hole measurements was the receiver (in BO US 85.003), and the L-tunnel to borehole BO US 85.003 measurements during phase 3 were performed with the moving probe (transmitter) in the tunnel.

The phase 3 measurements of Field 2 did only total 6328 rays as two scans with the receiver in BO US 85.003 closest to the borehole mouth and the transmitter in the L-tunnel were not measured.

Table 2.4 Radar Crosshole Tomography source and receiver points for Field 3.

Transmitter	Receiver	Transmitter spacing	Receiver spacing
BO US 85.003 0-140 m	BO US 85.001 0-140 m	5 m	5 m
L-tunnel	BO US 85.001		
85.014	0-142.5 m		2.5 m
85.016	0-142.5 m		2.5 m
85.020	0-142.5 m		2.5 m
85.023-85.039	0-142.5 m	5 m	2.5 m
85.002	0-142.5 m		2.5 m
85.044-85.076	0-140 m	10 m	5 m
85.083-85.095	0-140 m	10 m	5 m
L-tunnel	BO US 85.003		
85.001	0-140 m		5 m
85.016	0-140 m		5 m
85.020	0-140 m		5 m
85.023-85.035	0-140 m	10 m	5 m
85.039	0-142.5 m		2.5 m
85.002	0-142.5 m		2.5 m
85.042-85.076	0-142.5 m	5 m	2.5 m
85.083-85.095	0-142.5 m	5 m	2.5 m

Total number of rays 3741.

The system parameters used for these measurements are listed in Table 2.5. The change in sampling frequency between the different phases is due to changes in the time base of the radar system which is further discussed in section 2.5.

Table 2.5 Borehole radar system parameters used for the RCT measurements.

Centre frequency	22 MHz
Number of samples	512
Number of stacks	256
Sampling frequency (phase 1)	349 MHz
Sampling frequency (phase 2)	333.5 MHz
Sampling frequency (phase 3)	367.6 MHz

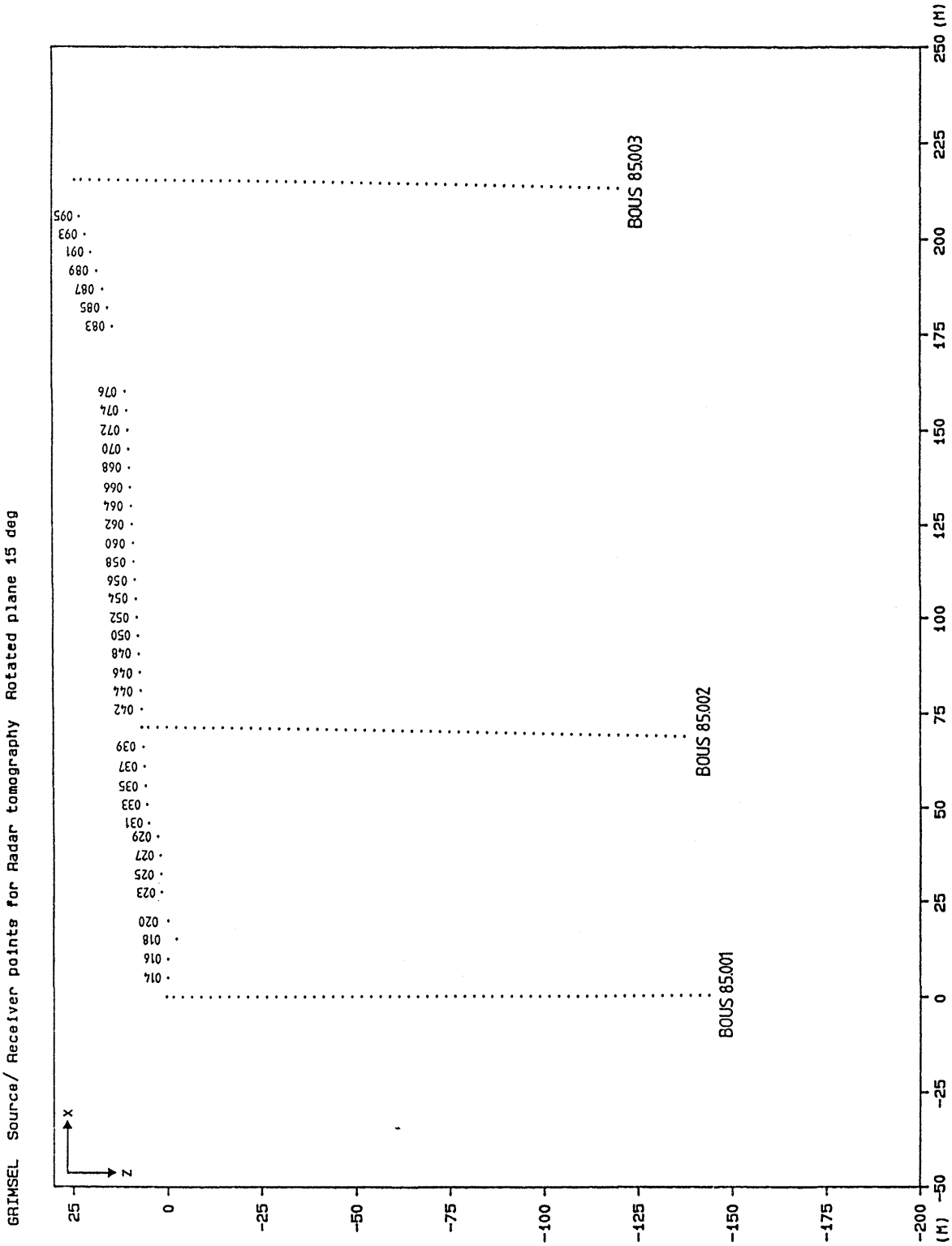

Fig. 2.2 Location of source and receiver points projected to the plane spanned by the boreholes (dip 15 degrees).

2.3 Injection of saline tracer

2.3.1 Phase 2

During phase 2 a saline tracer (NaCl) was injected in a section of the borehole BO BK 85.009 isolated by packers. The active section was located at a borehole depth of about 29 m (Fig. 1.2). At this depth the borehole intersects a minor fracture zone.

The injection was started on April 1, 1987 at 15:00 Hrs. The pump rate in the beginning was about 15 l/min and the concentration of NaCl about 0.1 %. The pump rate was successively lowered to 2.5 l/min and reached that level on April 3. The pump rate was thereafter kept at 2.3 ±0.2 l/min until April 15 when the radar measurements were completed (Fig. 2.3). The salt concentration was increased to 0.88 % by April 2 and was then kept within ±0.02 % of that value during the radar measurement period (Fig. 2.4).

The radar measurements were initially started on April 2. However, the concentration and spatial distribution of the saline tracer was not considered to have reached steady state conditions during the first two days as the salt concentration of the water flowing out of borehole BO BK 85.004 was still increasing. In order to obtain a data set with as small errors as possible these measurements were repeated. The collection of the data which were later used for the tomographic inversion was started on April 6 and continued until April 15. Hence, the flow rate and salt concentration were essentially constant during the entire data collection period (Figs. 2.3 and 2.4).

The salt concentration of the outflowing water from the nearby borehole BO BK 85.004 (Fig. 1.2) increased nearly linearly from 0.35 % on April 4 to 0.43 % on April 15. The outflow rate was roughly constant during the testing period, 4-4.5 l/min (Fig. 2.5). During the measurement period no changes in the salinity were observed in the water flowing out of the boreholes BO US 85.002 and BO US 85.003 in which the radar measurements were made.

A more detailed account of the experimental procedures used for the salt water injection experiments at the Grimsel Test Site is given by Liedtke and Pahl, 1987.

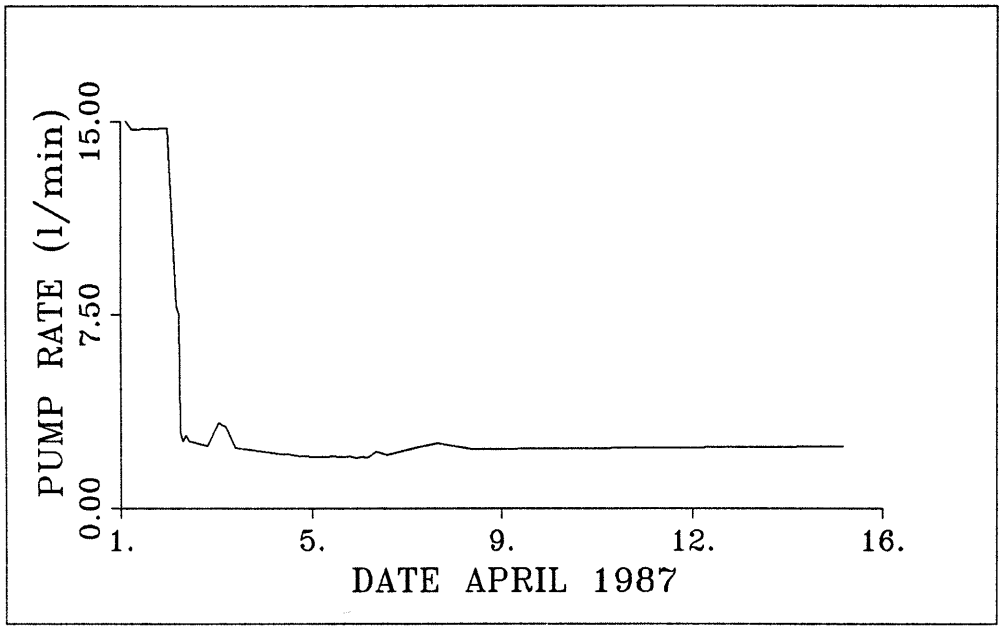

Fig. 2.3 Pump rate for saline tracer injected in borehole BO BK 85.009 as a function of time during the phase 2 experiments.

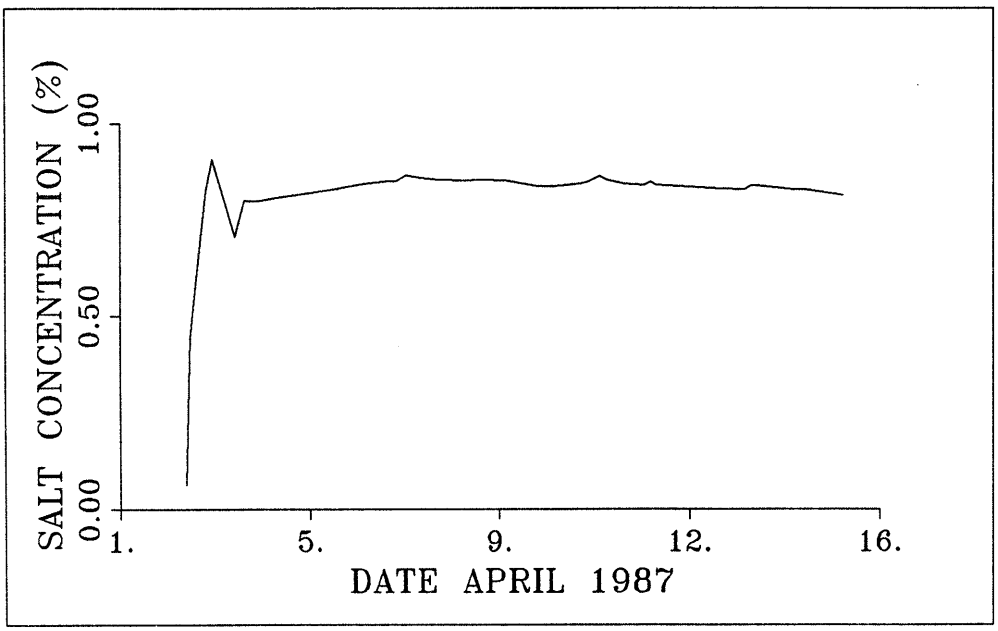

Fig. 2.4 Salt concentration of fluid injected in borehole BO BK 85.009 as a function of time during the phase 2 experiments.

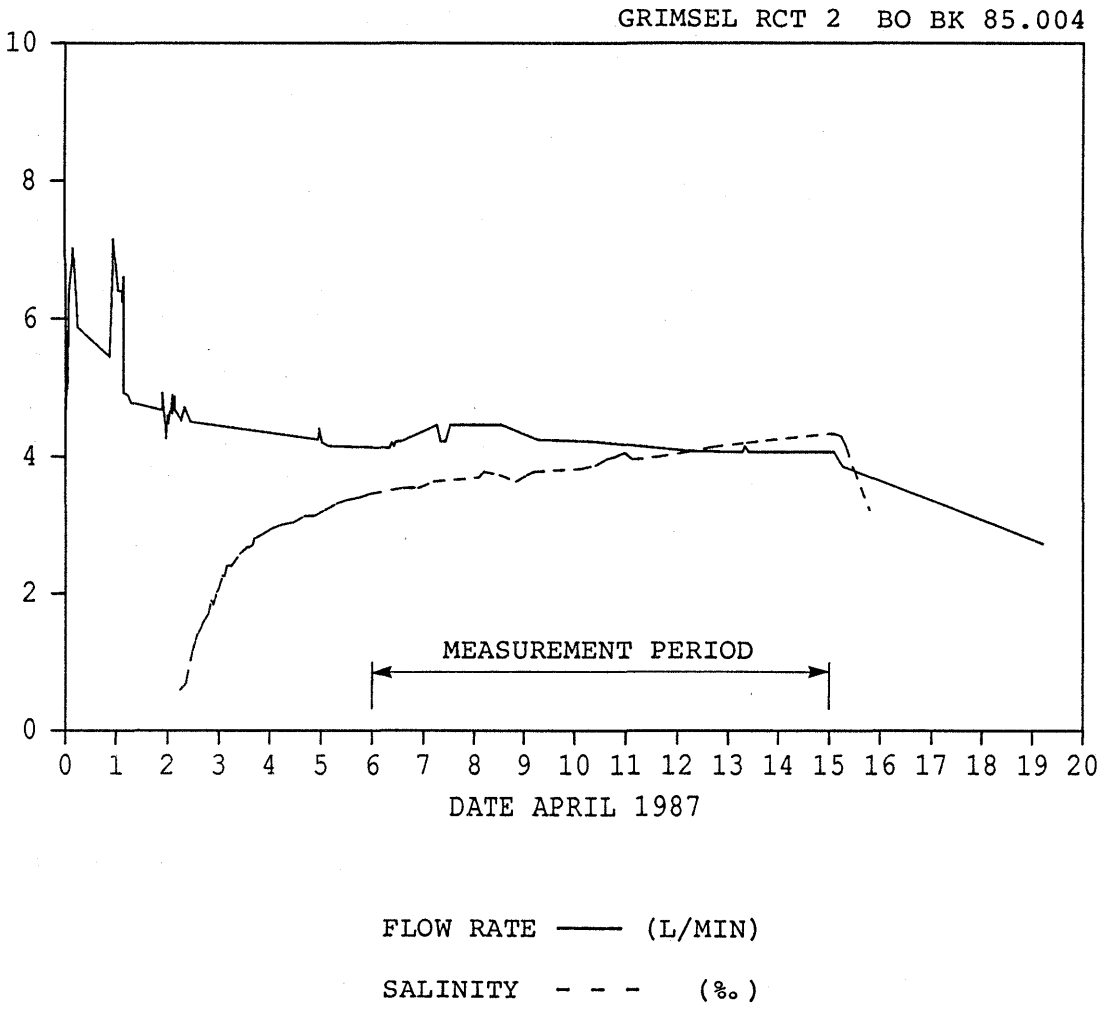

Fig. 2.5 Flow rate and salinity of water flowing out of the borehole BO BK 85.004 during the phase 2 experiment.

2.3.2 Phase 3

During phase 3 the saline tracer (NaCl) was injected in a section of the borehole BK 86.003 isolated by packers. The active section was located at a depth of about 62 metres (Fig. 1.3).

The injection was started on Friday, December 4, 1987 at 15:00 hrs. The pump rate was initially set to 2.5 l/min and the concentration of NaCl to 0.8% . Due to a technical failure during the weekend the pump rate increased to 6 l/min. The pumping continued from Sunday (December 6) night until Monday morning with a flow rate of approximately 1 l/min. On Monday morning the pump rate was increased to 2.1 l/min. Pumping continued with that rate until Thursday when it was reduced to 1 l/min. The pressure required to keep a constant flow rate increased successively during the experiment. At the beginning of the experiment a pressure of 8-10 bars was sufficient to achieve a pump rate of 2.1 l/min but on Thursday December 10 the required pressure had increased to 18 bars. This pressure increase was the main reason to reduce the pump rate on December 10. After Thursday an injection rate of 1 l/min was achieved by applying a pressure of approximately 15 bars. The pumping continued until 05:00 hrs on Saturday morning when the radar measurements were completed.

2.4 Measurement procedure

The performance of the radar crosshole measurements comprised the following steps:

Power (220 V, 50 Hz) is supplied to the computer and the control unit. The units are connected through a serial communication link. The three optical fibers which connect the control unit to the borehole probes are attached and the battery packs are mounted on the transmitter and receiver, respectively. Power is switched on to all units and the control program is started on the computer unit.

After initialization of a data disc and selection of the variable parameters the borehole probes are put into the hole. In these horizontal holes the probes were pushed into the boreholes by glass fiber rods with a length of 2.5 meters (Fig. 2.6). If the holes are slightly dipping it is possible for two persons to push the probes to a borehole depth of 250 to 300 m. In this case the length of the investigated holes was 150 m and there were no problems to reach the bottom of the holes. In vertical or steeply dipping

holes the probes are lowered down the borehole with a specially designed optical fiber cable mounted on a motor driven winch. When both probes have been put at the appropriate positions the measurement is started by the operator. When the measurement of a single trace is completed the computer displays the recorded signal as a function of time. The signal is also displayed with the amplitude coded in different colors. When several measurements are made the colour coded traces are displayed beside each other on the screen and thus a radar map is generated. When a signal trace has been recorded on the floppy discs the computer unit gives an audio signal to indicate that it is time for the operator to move the probes to the next measuring position.

The measurements were performed in sets which have been termed scans. For each scan one probe is kept fixed in one hole or the tunnel while the other probe is moved stepwise in another hole in such a way that it will pass over its entire length. After the completion of a scan the 'fixed' probe is moved to a new position and the measurement in the other hole is repeated. This procedure is repeated until each field is fully measured (cf. Tables 2.2-2.4).

The measurements in the boreholes were made with a point separation of 2.5 m for Fields 1 and 2, while the separation was 5 m for Field 3. The separation between source points in the tunnel was 5 m for Fields 1 and 2 and 10 m for Field 3.

In principle the transmitter and receiver are interchangeable and it is thus irrelevant which probe is fixed or which is moving during each borehole scan. In the borehole to borehole measurements the receiver was fixed while the transmitter was moved along the borehole. This choice was made as it is slightly easier to move the transmitter as it is connected with only one optical fiber (exceptions to this rule are given in Section 2.2).

In the tunnel to borehole measurements the transmitter was used as the fixed probe and placed in the tunnel. The reason for this is that a lot of electrical noise is generated in the tunnel by electrical power lines, instrumentation and so forth. This noise exists mostly in the vicinity of the tunnel and is rapidly attenuated in the rock surrounding the tunnel. The receiver is sensitive to this noise which is not the case for the transmitter. Hence, in order to obtain low noise data the receiver has to be kept in the rock, i.e. in the boreholes. During the tunnel measurements the transmitter was placed on a wooden plank approximately 0.5 m above the floor of the tunnel (Fig. 2.7). The transmitter

was positioned so that the centre of the transmitter antenna was just at the mouth of one of the short boreholes drilled from the tunnel (BO US 85.014 to 095).

The drilled parts of the tunnel have very smooth walls and the coupling of the radar antenna to the rock is expected to be essentially the same for all measurement points. The L-tunnel, with a few exceptions, has no metallic installations which could disturb the radiation from the antenna on the side of the tunnel where the measurements were made. There were also measurement points where the tunnel wall is rough due to blasting. In these cases the coupling will become less efficient and likely to vary between measurement points.

The source positions at the beginning of the L-tunnel behind the equipment storage facility represent a special case (BO US 85.023 to 029). This part of the tunnel includes some installations of metallic material on the side of the tunnel from which the measurements were made. At these points the transmitter was placed against the rough tunnel wall in the small space available between the wall and the wire fence of the storage facility. The small distance between the wall and the fence posed some practical problems to position the transmitter at the measuring point. The fence affects the radiation pattern of the antenna in an unknown way and the radiation pattern for these positions is expected to be different from the other source positions in the tunnel.

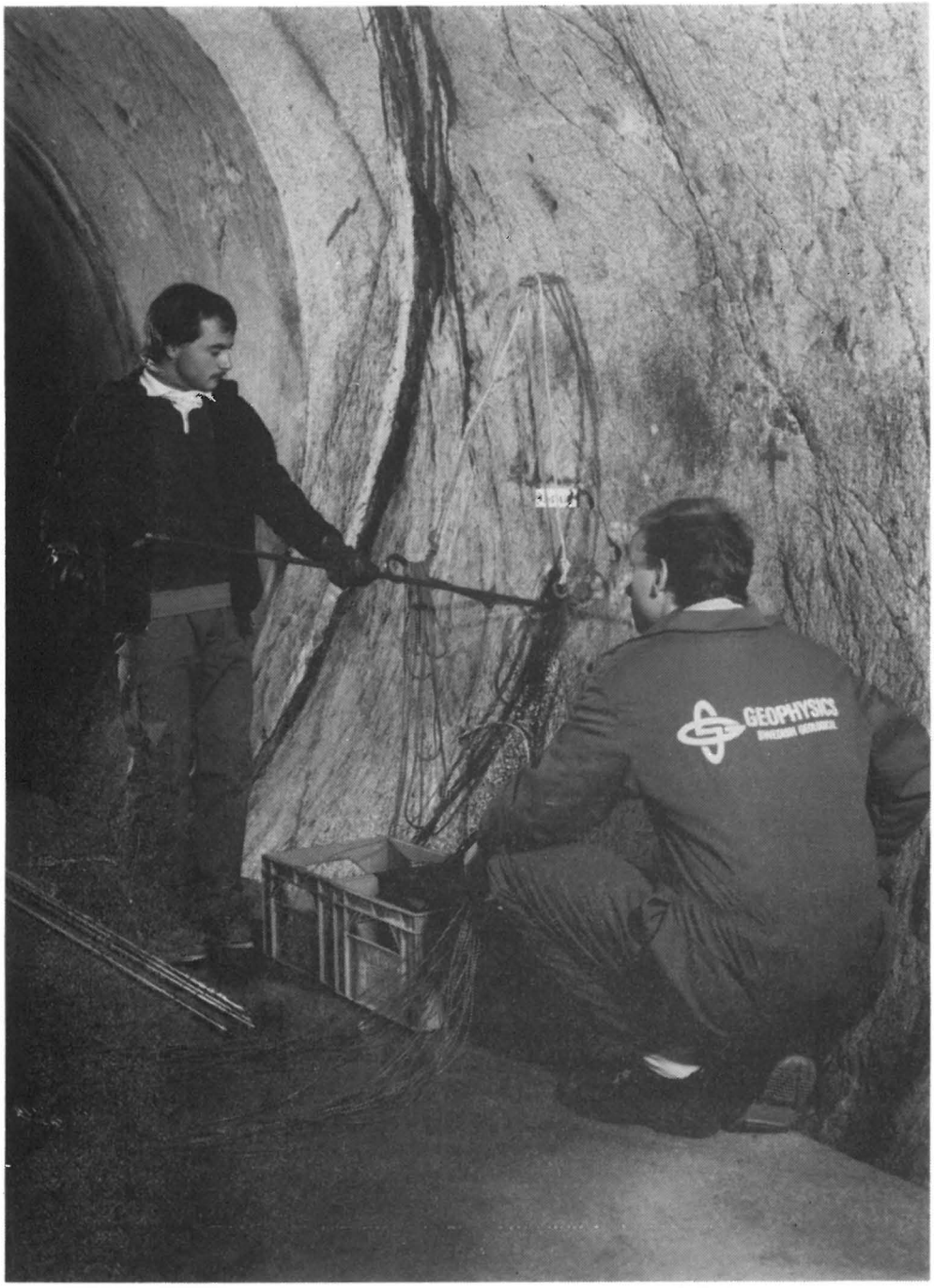

Fig. 2.6 Borehole radar system in operation at the Grimsel Rock Laboratory.

Fig. 2.7 Arrangement for positioning the transmitter in the tunnel during the tunnel to borehole measurements.

2.5 Calibrations

Calibration measurements were performed in order to control any drift in the system with respect to measurements of time or amplitude of the received signals. The requirements of the radar system with respect to long term time and amplitude stability are very high for an experiment of this type where the difference between measurements made more than a year apart are studied. Control of system drifts during each phase and between phases are crucial for positive results of tomography surveys in general and difference tomography surveys in particular.

During phase 1 a calibration measurement programme was setup which comprised time base calibrations and measurements between a set of reference points.

The objective of the time base calibrations were to determine the time base of the RAMAC system in absolute terms. The time base calibration is carried out by increasing the length of the optical fibre to the transmitter by inserting an extra fibre. The increase in fibre length will cause a time delay which is proportional to the length of the fibre. As the velocity of light in the fibre (201 m/μs) is known the theoretical delay can be calculated and compared to the delay measured by the radar system. The accuracy of the time base calibrations is dependent on the length of the inserted fibre and the reduction in light intensity caused by introduction of an extra optical joint. The attained accuracy in the obtained time base of the system is estimated to 1-2 %. Time base calibrations were performed twice a week during the three measurement phases.

The calibration procedure adopted during phase 1 included measurements at two pairs of referential points (i.e. two rays) included in the part of the field measured the day the calibrations were made. Hence, the calibration rays were changed during the course of the measurement. This made it difficult to compare data from different fields of parts of fields (borehole to borehole rays or borehole to tunnel rays) as there were no common calibrations which could be used to quantify drifts in time base or gain. Calibrations were performed each day in the morning before the commencement of the measurements and at the end of the working day.

During the phase 1 measurements a drift in the time base was observed and it was thought that the calibration data could be used to compensate for the drift. However, as the reference rays were changed during the course of the measurements it was

impossible to compare calibrations relating to different parts of the measurements and to determine the drift corrections needed with sufficient accuracy. This leads to relatively large artifacts in the phase 1 slowness tomograms for Fields 2 and 3. The drift during the measurements of Field 1 were negligeable and consequently the Field 1 slowness tomogram did not contain significant artifacts.

The drift in the time base of the system was caused by a few temperature sensitive components in the system. The critical parts of the system were redesigned and no significant time base drifts could be observed during the phase 2 and 3 measurements. The drift of these components did not affect the amplitude measurements and therefore it did not create artifacts in the difference tomograms.

The calibration procedure used during phase 1 had not been satisfactory and a new procedure was devised for phases 2 and 3. The basic principle of the revised calibration procedure was that the same referential rays should be used during the entire measurement period. The spatial distribution of the referential rays were also chosen in such a way that the calibration measurement contained rays of significantly different lengths. The calibrations during phases 2 and 3 were carried out as complete borehole scans where the transmitter was located in the L-tunnel and the receiver moved in one of the boreholes. The same transmitter locations (in the L-tunnel at boreholes BO US 85.070 and BO US 85.085) were used during both phases while the receiver was moved in borehole BO US 85.003 during phase 2 and in BO US 85.002 during phase 3. This calibration procedure proved to be satisfactory as it was possible to compare results during the entire measurement period and to determine the necessary corrections.

Calibration measurements were carried out twice a day and on some instances three times per day. An example of the results from the calibrations are displayed in Fig. 2.8 which shows the variation in residual travel time for a specific calibration ray during phase 2. The residual travel times have a variation which is within ±3 ns. This corresponds to ±1 time sample interval and we may in this case conclude that the time drift of the system is less than one sample and that the main source of error in the travel time reading is the quantization error.

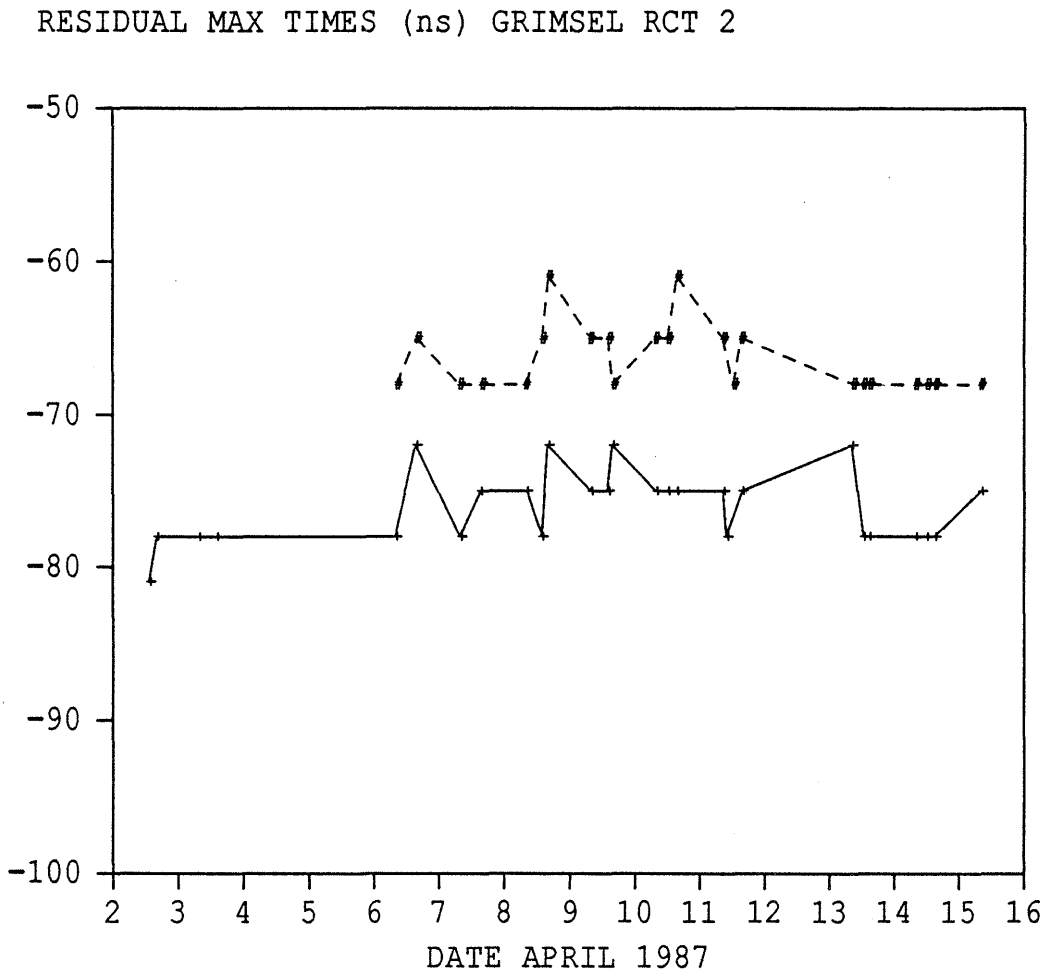

Fig. 2.8 Residual travel times obtained from calibration measurements during phase 2. Transmitter located in L-tunnel at BO US 85.070 (+) and BO US 85.085 (#). Receiver located at a borehole depth of 121.46 m in BO US 85.003.

The amplitude calibrations generally showed variations around the average value of about ±1 dB. This variation appeared to have a stochastic nature and no corrections were made to the data based on the amplitude calibration data.

2.6 Conclusions and recommendations

The RAMAC system used for the measurements performed well during the execution of the relatively comprehensive RCT-programme. During phase 1 serious problems were caused by temperature sensitive components which caused a drift in the time base of the system. The system was modified and no problems of that type occurred during phases 2 and 3. The comprehensive measurement programmes of each phase could be completed within the allocated time frames.

The calibration procedure applied during phases 2 and 3 provided sufficient control on any system drifts. During experiments of this type where saline tracer is injected into the rock it is strongly recommended that the calibration measurements are taken in a part of the experimental site where no saline tracer is expected to appear. Difference tomography requires very good control on system drifts. It is essential to be able to separate effects caused by the injected salt and the measurement system itself.

The measurement procedure described in section 2.4 has proved to be efficient and well suited for experiments of this type. A reduction of the total measurement time is however of interest. Difference tomography can be considered as taking a snapshot of the changed conditions when the second tomography is made. The exposure time is the time it takes to perform the tomographic survey of the investigated section or "field". To obtain good results the conditions in the investigated rock volume should not change during the time it takes to measure the tomographic section. Changes in conditions during the measurement time can be expected to cause a "blurred" image. The time extension for measurement of Field 2 during phase 2 was 10 days and during phase 3 it was reduced to 5 days. A reduction of total measurement time is recommended and can be achieved either by reducing the time to take a reading with the radar system or by reducing the investigated area and hence the number of rays to be measured.

Ensuring steady state conditions during the performance of the radar measurements also requires a good control of the hydrogeologic situation.

Hydraulic parameters should preferably be known in boreholes at the site before the commencement of the second radar survey included in a difference tomography experiment. Conductivity and injection rates of the saline tracer should be monitored closely during the experiment. If the time required for the radar measurements is extensive then the radar measurements should not begin until monitoring of saline concentrations in suitable boreholes show that steady state conditions apply. Good control of the hydrogeological conditions at the site is likely to facilitate better planning of an experiment of this type and the understanding of the results.

3 PRINCIPLES OF TOMOGRAPHIC INVERSION

3.1 Definition of the problem

The general idea behind tomographic reconstruction is that information about the properties of the interior of a region can be obtained through measurements at the boundary. In general the transmitter and receiver probes are located at the boundary of the area and each ray connecting transmitter and receiver can in principle be considered to represent the average of a measured property of the rock along the ray path. In order to obtain an estimate of this property at a given point it is necessary that several rays are passing close to the same point and that the rays have different directions and hence different information content. The requirement that several rays should intersect the same point puts some severe constraints on the borehole geometry. The main one being that the source and receiver positions and hence the boreholes have to be confined to the same plane.

In mathematical terms the tomographic problem can be formulated in the following way

$$d_i = \int_{T_i(m)} m(x) \cdot ds \qquad (3.1)$$

where d_i is the measured data for ray number i. The objective of the tomographic inversion is to estimate the spatial distribution of some property, $m(x)$, characteristic of the medium (x denotes the spatial coordinates). The data is thought of as being a sum (line integral) of this property along the ray path, $T_i(m)$, from the transmitter to the receiver. The actual ray path is dependant on the properties of the medium, $m(x)$, and is normally the curve which gives the least possible travel time. The complex dependance of the ray paths, T_i, on the properties of the medium, $m(x)$, makes the problem nonlinear. The problem can be linearized by replacing the curves T_i with straight line segments, L_i, connecting sources and receivers.

In a borehole radar crosshole measurement data on the travel time and the amplitude of the direct wave between transmitter and receiver, i.e. the first arrival, can be extracted. It is assumed that the travel time can be constructed as the line integral of the slowness, $s(x)$, along each ray, i.e.

$$d_i = \int_{L_i} (1/v(x)) \cdot ds = \int_{L_i} s(x) \cdot ds \qquad (3.2)$$

The ray paths have been assumed to be straight lines in order to make the equations linear and in this way simplify the inversion problem.

The amplitudes can not be obtained from a line integral directly. The logarithm has to be taken of the data in order to linearize the problem and to allow tomographic inversion. The amplitude of the electric field sent out by the transmitter decays with distance according to

$$E = c_t \, a(\theta) \, \exp(-\alpha r)/r \qquad (3.3)$$

where $a(\theta)$ is the antenna radiation pattern and c_t some constant which gives a measure of the radiated power. The received signal amplitude is also dependant on the directionality of the receiver antenna gain. The received amplitude is thus obtained by multiplying (3.3) with the directional antenna gain pattern of the receiver antenna. This directional gain is identical to that of the transmitter if the same type of antennas are used. Hence the received amplitude is

$$E_m = c \, \frac{\exp(-\alpha r)}{r} \, a(\theta_1) a(\theta_2) \qquad (3.4)$$

Taking the logarithm and rearranging terms we obtain

$$\alpha r = \int_{L_i} \alpha(x) \cdot ds = \ln \frac{c \, a(\theta_1) a(\theta_2)}{r \, E_m} \qquad (3.5)$$

Here it has been assumed that the product αr can be constructed as a line integral of the attenuation along each ray. Thus, an inversion of the logarithm of the received amplitudes should give an estimate of the distribution of attenuation in the investigated plane. In equation (3.5) 'c' represents a normalization constant describing the combined effects of transmitted power and receiver gain and 'E_m' is the amplitude of the received electric field.

The next problem is to devise a procedure for inverting the data to obtain the distribution of slowness or attenuation in the plane between the boreholes. First a discretization is made of the problem. The plane between the boreholes is divided into a number of cells and the line integral is calculated as a sum where the contribution from each cell is considered in proportion to the length of the

ray within each cell, cf. Fig. 3.1. A discretization of (3.1) assuming straight ray paths transforms the equation into the following form

$$d_i = \sum_{j=1}^{M} G_{ij}\, b_j \qquad (3.6)$$

where G_{ij} represents the length of ray 'i' in cell 'j' and b_j the attenuation or slowness of cell 'j'.

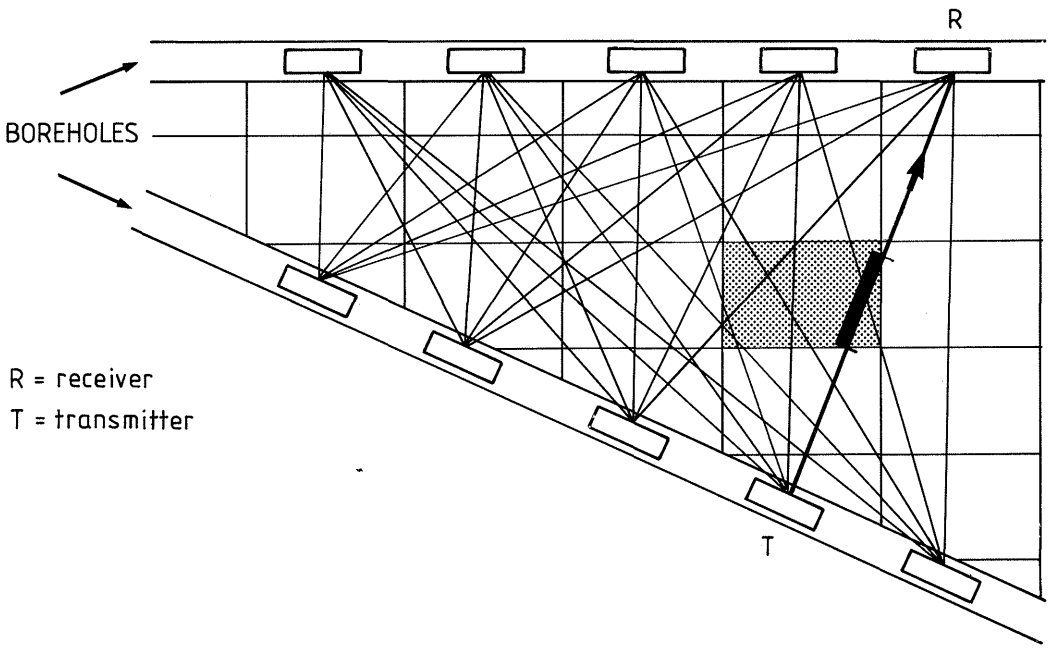

Fig. 3.1 Generalized crosshole tomography geometry with a decomposition into cells and an example of a ray pattern.

The problem has now been transformed into a system of linear equations, where the number of equations correspond to the number of rays, N, and the number of unknowns, b_i, to the number of cells, M. Hence, we may write

$$\mathbf{d} = \underline{\mathbf{G}} \cdot \mathbf{b} \qquad (3.7)$$

This equation system can be both overdetermined and underdetermined at the same time and errors in the data may cause some equations to be in conflict. The most common solution concept for this type of equation is through minimization of the functional $|\mathbf{d}-\underline{\mathbf{G}}\cdot\mathbf{b}|^2$.

Experience shows that the equation system is often unstable and it is necessary to introduce some form of damping. An effective and natural way of introducing damping is to assume that the slowness (or attenuation) of adjacent cells are equal. Introducing equations constraining the solution in this way gives that a minimization should be made of the functional

$$|\mathbf{d} - \underline{\mathbf{G}}\cdot\mathbf{b}|^2 + \lambda^2 \, |\underline{\mathbf{C}}.\mathbf{b}|^2 \qquad (3.8)$$

where the parameter λ is a measure of the strength of the damping and $\underline{\mathbf{C}}$ is a matrix containing the equations for equal slowness (or attenuation) in adjacent cells. λ determines the weight of the constraining equations and the practical consequence is that the differences in slowness between adjacent cells are limited to a certain extent. This type of damping gives a smoothed tomographic image without creating serious artifacts.

The solution to (3.8) has the following form

$$\mathbf{b} = (\underline{\mathbf{G}}^T \cdot \underline{\mathbf{G}} + \lambda^2 \cdot \underline{\mathbf{C}}^T \cdot \underline{\mathbf{C}})^{-1} \cdot \underline{\mathbf{G}}^T \cdot \mathbf{d} \qquad (3.9)$$

Here $\underline{\mathbf{G}}$ and $\underline{\mathbf{C}}$ are known and depend on the ray pattern and the division of the investigated area into cells. In other words they contain the geometrical information about the measurement setup. The term in the parenthesis is a square matrix which may be inverted through standard procedures and when this has been done a least squares estimate of $\mathbf{b}$ is obtained through matrix multiplication. However, the direct inversion of the matrix has its practical limitations as the matrix is large. The number of elements of $\underline{\mathbf{G}}^T \cdot \underline{\mathbf{G}}$ is M^2, i.e. the number of cells squared, and this is for most problems a very large number (in this case up to 10 000 000) which prohibits direct inversion of the matrix due to the enormous computing times involved. Note that the

computing time required for inversion of a matrix is proportional to M^3.

Normally the number of unknowns in the equation system is too large for direct inversion and iterative procedures will have to be used to obtain the solution. The conjugate gradient (CG) method which was developed as a part of the Stripa Project, Phase 2, is considered to be an efficient inversion procedure. The convergence is fast and hence few iterations are needed to arrive at the final solution. The CG-method has been shown to give smaller computing times and better reconstructions of model examples than the other iterative methods (Ivansson, 1984). Hence, the CG-method has been used for all tomographic inversions presented in this report.

A comprehensive description of the theory behind tomographic inversion and details about the CG-method can be found in Ivansson (1984).

3.2 Residual attenuation and velocity

The radar velocity (or slowness) has small variations around a certain average value. We have found it useful to put the crosshole data in such a form that these variations are studied rather than the absolute values of these properties. The concept has also been adopted for the amplitude data. In this context we define the terms 'residual travel time' and 'residual amplitude'. These residual data correspond to the measured data after subtraction of the expected data value which would have been obtained in a homogeneous medium with properties close to those of the investigated rock.

The residual travel time, t_r, is defined as the measured travel time, t_m, minus the estimated travel time for a homogeneous medium with a constant velocity, v_0. The residual travel time then becomes

$$t_r = t_m - r/v_0 \qquad (3.10)$$

where r is the distance between transmitter and receiver.

The residual amplitude is defined as the quotient (expressed in dB) of the received amplitude, E_m, and the estimated amplitude in a homogeneous medium with constant attenuation α_0. The residual amplitude, d_r, thus becomes

$$d_r = -20 \log_{10} \frac{E_0}{E_m} \frac{\exp(-\alpha_0 r)\ a(\theta_1)\ a(\theta_2)}{r} \qquad (3.11)$$

where E_0 represents a reference level corresponding to the ratio of transmitted power to receiver sensitivity. Through the use of the base 10 logarithm and the multiplication by 20, the residual amplitudes become represented in dB.

With this conversion into residual data it is possible to look at small variations from large average values. The residual data are also suitable for detecting systematic errors in the data and can be used for calibration of some system parameters.

3.3 The effect of saline tracer on radar wave propagation

The attenuation of radar waves is proportional to the electrical conductivity of the rock. To a first approximation the dependance of the electrical conductivity of the rock on the conductivity of the pore fluid can be estimated according to Archies law:

$$\sigma_r = a\ \sigma_w \Phi^m \qquad (3.12)$$

where

σ_r = bulk conductivity of the rock
σ_w = pore fluid conductivity
Φ = porosity
m = cementation factor (approximately 1.5)
a = dimensionless parameter (approximately 1)

In low porosity rocks like granite surface conduction along grain boundaries plays a significant role and a surface conduction term should be added to the right hand side of Archies equation above (Brace, Orange, and Madden, 1965, Magnusson, Carlsten, and Olsson, 1987). At higher frequencies the dielectric losses in water start to become significant (Sen, Scala, and Cohen, 1981) and a loss term has to be added to Archies law. Including these additions to Archies law we obtain an effective conductivity, σ^*, of the form

$$\sigma^* = \sigma_s + (\sigma_w + \omega\varepsilon_0\varepsilon_w'')\,\Phi^m \qquad (3.13)$$

where

σ_s = surface conductivity
ε_w'' = dielectric loss of water.

It has not been within the scope of this work to estimate the magnitude of these parameters. However,

equation (3.12) can serve as an illustration that the bulk conductivity is not expected to increase proportionally to the increase in pore fluid conductivity caused by the saline tracer. The conductivity of the saline fluid injected during these experiments has been about 1.5 S/m which is more than 100 times higher than the conductivity of the natural groundwater. Considering the modified Archies equation and that the pore fluid will not be completely replaced by the saline tracer, increases in bulk conductivity by a factor significantly less than 100 should be expected.

4 PROCESSING OF RADAR DATA FOR TOMOGRAPHIC ANALYSIS

4.1 Travel time and amplitude picking

A typical example of a radar signal recorded from a crosshole measurement is shown in Fig. 4.1. From this signal trace we want to obtain the time of first arrival and the magnitude of the signal.

A tomographic survey normally includes a large number of rays (in this case about 30 000 rays). It is therefore of utmost importance to arrive at some automatic procedure which can pick the data from the recorded traces, especially as a manual treatment of each ray would be extremely time consuming and hence costly. For the radar data we have adopted a simple approach which has in a number of cases proven to be reasonably efficient. An algorithm has been devised which picks out the maximum and the minimum for each trace and the time instances at which these events occur. The travel time is then defined as the time to the maximum or minimum of the pulse and the amplitude is defined as the difference between the maximum and the minimum, i.e. peak-to-peak amplitude.

This scheme is useful for radar signals where the first pulse in most cases also is the largest one. The procedure is normally not useful for seismic crosshole investigations as the maximum signal in that case is normally not obtained within the first pulse cycle. The first arrival has one significant maximum and two minima of almost equal magnitude. As there is some dispersion of the pulse the relative magnitude of the two minima will vary somewhat and the minimum time will be picked from either of these two minima. The minimum travel times are thus sensitive to small changes in the pulse form which is not the case for the maximum times. The minimum travel times will normally be picked inconsistently between different rays while the maximum times are picked consistently and have consequently been used for the analysis. The peak-to-peak amplitudes have been shown to provide a satisfactory data set even if they also are affected by the dispersion of the pulse.

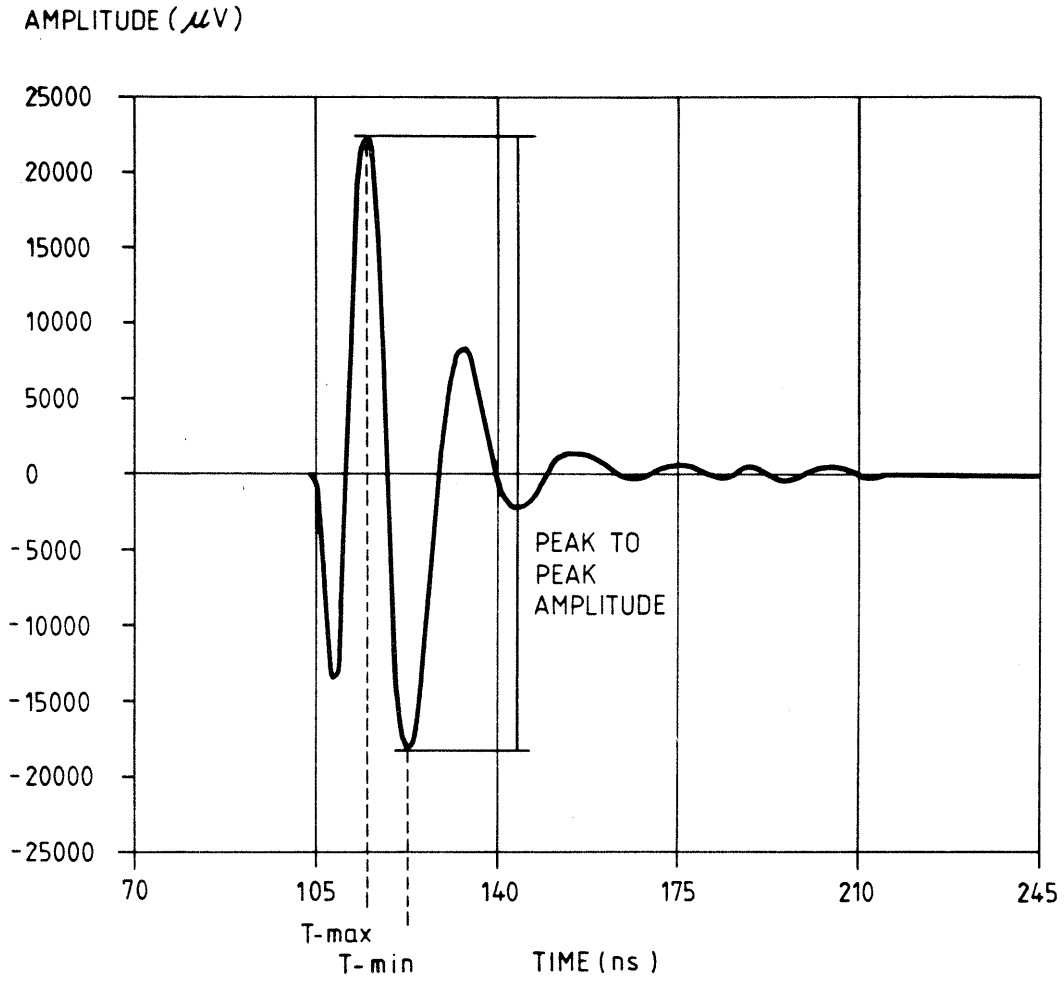

Fig. 4.1 Radar signal obtained from a crosshole measurement. The data identified by the automatic routine for extraction of travel times and amplitudes are indicated.

4.2 Attachment of coordinates to data

The basic step in preparing data for tomographic inversion is the attachment of coordinates to the picked travel times and amplitudes. The accuracy required in source and receiver coordinates is of the same order as the propagation distance during a sampling interval. In these measurements the sampling interval corresponds to approximately 0.3 m. Borehole and tunnel coordinates have been supplied by NAGRA.

After the travel time and amplitude data have been combined with the coordinates of the source and receiver points the residual data are calculated according to (3.10) and (3.11).

The tomographic inversion software requires the source and receiver points to be in the X-Z plane and in order to accomplish this the coordinate system is rotated. In this case the coordinate system is rotated around the point where the borehole BO US 85.001 begins. The rotation is made in such a way that the X-axis is horizontal and has a declination of 200° relative to the coordinate system of the Grimsel Rock Laboratory. The Z-axis has a plunge of 15° and a declination of 290°. Hence, the Z-axis essentially coincides with borehole BO US 85.001.

4.3 Data quality checks and corrections

The tomographic data is subject to a number of errors such as; errors in time and amplitude picking, quantization errors, constant offset errors in time and gain, and coordinate errors. It is essential to get a grasp of both the stochastic and systematic errors which may exist in the data set. The errors must be understood, quantified and corrected before a tomographic inversion is attempted. A good way to reveal errors is to plot the residual data as a function of the length of the rays. From these plots an offset and a slowness or attenuation correction is determined. A grey scale plot (or ray check plot) is then made of the average slowness or attenuation for all rays. In this plot individual rays containing errors (e.g. due to errors in time and amplitude picking) can be identified. Rays containing errors are then removed from the data set before the tomographic inversion. Below follows a discussion on the most common types of errors included in the data and how they can be corrected for.

The main sources of stochastic errors are noise on the recorded traces and digitization errors.

Digitization errors are due to the finite sampling frequency and the limited (16-bit) resolution of the A/D-converter in the receiver. Digitization errors are noteable in the travel time data and limits the resolution of the slowness tomograms. Digitization errors and noise affect amplitude data only ror traces with very low amplitudes (i.e. the longest rays).

The main errors in the residual travel time are due to imprecise knowledge of the zero time, i.e. the start time of the pulse, and the assumed velocity of the medium. Let us denote the picked travel time by, t_m, where we assumed the pulse to have been sent at a time, t_0. Now, assume there is an error in the start time, Δt_0, and in the velocity used for calculation of the residual travel time. The assumed velocity, v_0, is related to the real velocity, v, in the following way

$$v = v_0 \ (1+\delta v) \tag{4.1}$$

If these assumptions are inserted in (3.10) we obtain

$$\begin{aligned} t'_r &= t_m - t_0 - \Delta t_0 - r/(v_0(1+\delta v)) \\ &\approx t_m - t_0 - r/v_0 - \Delta t_0 + r\delta v/v_0 \\ &= t_r - \Delta t_0 + r\delta v/v_0 \end{aligned} \tag{4.2}$$

In this equation we can see t_r as the real residual travel time while t'_r is the residual time including the errors caused by the last two terms. In the case of a homogeneous medium the real data, t_r, would be zero and $t'_r = -\Delta t_0 + r\delta v/v_0$ would be a straight line in a t_r versus r diagram. The offset, $-\Delta t_0$, and the error in the estimated velocity (slope) can directly be read from such a plot.

If we divide equation (4.2) by the length of the ray we get the residual slowness for the ray, s'_r;

$$s'_r = s_r - \Delta t_0/r + \delta v/v_0 \tag{4.3}$$

Again we let the unprimed quantity define the error free value. Here it is important to note that an error in the assumed velocity will pose no problems as this will only lead to a constant offset in the residual slowness values and the error in the slowness estimate will be the same for all rays. Errors in the pulse transmission time will cause errors in the slowness estimate which are dependant on the length of the rays and hence different for different rays. Offset errors of this type normally generate artifacts in the resulting tomograms. A typical artifact caused by offset errors is a

diagonal cross in the tomogram. This is consistent with the different size of error for the longest (i.e. diagonal) rays compared to the shorter ones.

The amplitude data can be analyzed in a similar fashion. Here we assume an average attenuation, α_0, with an error, $\Delta\alpha_0$, such that

$$\alpha=\alpha_0+\Delta\alpha_0 \qquad (4.4)$$

We also assume that we have a percentage error, δE_0, in the reference level, E'_0, such that

$$E_0=E'_0 * \delta E_0 \qquad (4.5)$$

In an analogue fashion to the error analysis of the residual travel times we obtain

$$d'_r=d_r-20 \log_{10} \delta E_0+20\Delta\alpha_0 r/\ln(10) \qquad (4.6)$$

for the residual amplitudes. Again the offset error in the received amplitude levels is the error which will most severely affect the tomographic inversion as it gives rise to a systematic error which is different for rays of differing lengths.

The corrections to apply can generally be deduced from plots of the residual data as a function of the distance between the source and receiver points. The residual data will in most cases form a cluster centered along a line. The slope of this line will then give the error in the estimated velocity or attenuation and the intersection with the Y-axis (i.e. the value for zero distance) will give the offset error in time or power.

An example of a plot of the residual travel times versus distance is given in Fig. 4.2. The residual travel times were calculated using an assumed velocity of 117 m/μs. This velocity is evidently smaller than the actual average velocity as long rays have shorter residual travel times than short rays. The travel times form a cluster along a line with a negative slope of $\delta v/v_0$=.00049 μs/m which gives an actual average velocity of 124 m/μs. From this plot the offset error is estimated to -15 ns.

There will also be a number of cases where the algorithm for getting the travel time and amplitude data has failed. Such erroneous data have to be identified and removed from the data set. It is normally not cost efficient, but sometimes necessary, to go back to the original recorded traces and to perform a manual retrieval of the travel times and amplitudes. Instead such data is removed from the data set used for tomographic inversion. The ray

density in the radar crosshole measurements at Grimsel is in general high and the result of the tomographic inversion is not critically dependant on if a few rays are skipped. It should be noted that it is essential to exclude rays containing significant errors as only a few such rays are sufficient to introduce artifacts in the tomograms.

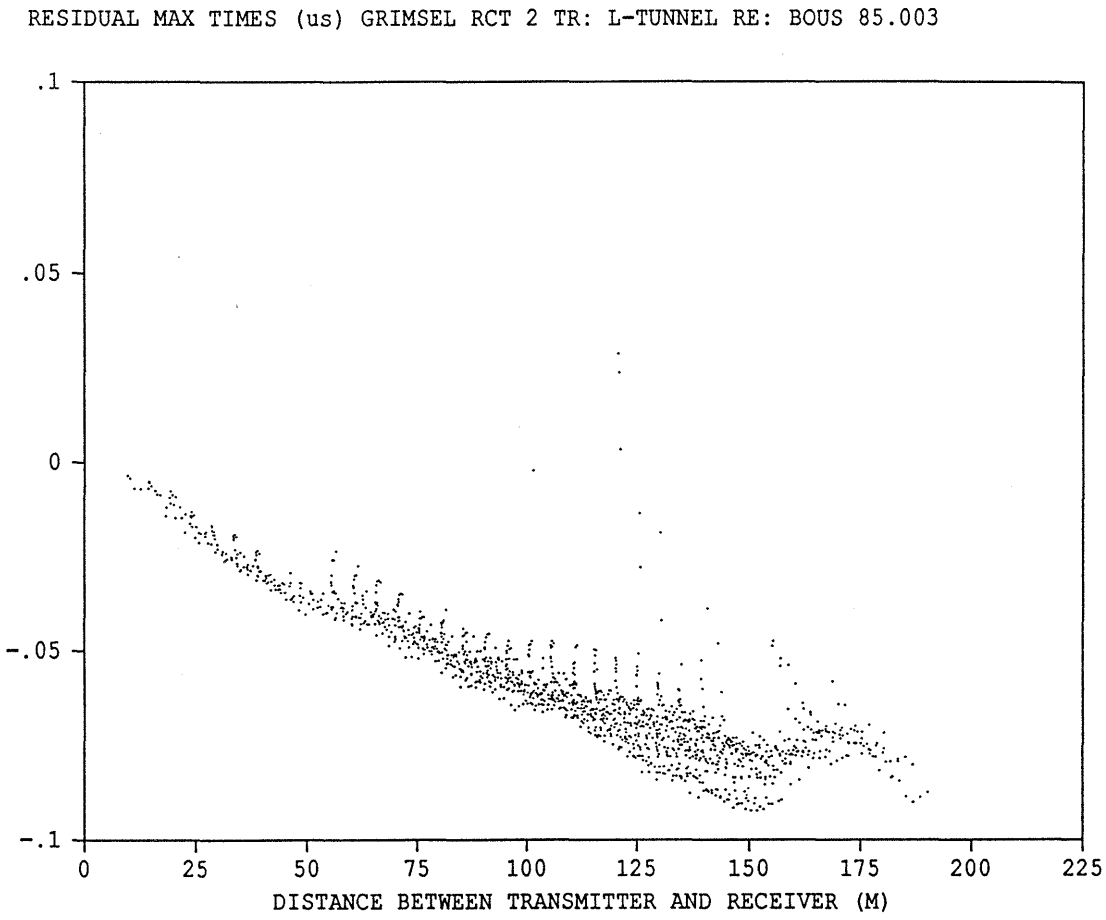

Fig. 4.2 Residual travel times as a function of ray length. Data shown are rays belonging to Field 2 from L-tunnel to borehole BO US 85.003 collected during phase 2.

In this case the data obtained from the hole to hole measurements have been of high quality and there has been no errors in the picking of these data. However, the tunnel to hole rays have in some cases been disturbed by electric noise and refracted waves along the tunnel which has caused errors in the travel times and amplitudes. An example of a tunnel to borehole scan is shown in Fig. 4.3. Here we can see that the algorithm used works well for practically all traces. However, there is one trace of the ones displayed where the time picked will be in error due to interference of the first arrival with a refracted and a reflected wavelet (arrow).

Identification of erroneous rays are made by means of ray check plots which display the average slowness or attenuation for each individual ray. Fig. 4.4 shows the ray check plot for the L-tunnel to borehole BO US 85.003 data. The position of the probes along the L-tunnel and borehole, respectively, is shown along the coordinate axis. Each pixel corresponds to a specific ray and individual rays are easily identified in this type of plot, which was not the case for the residual plot shown in Fig. 4.2. Erroneous rays normally have significantly larger or smaller average slowness compared to neighboring rays and stand out as either white or black pixels in the ray check plot.

Artifacts in the tomograms may also be caused by anisotropic properties of the rock. One consequence of anisotropy is that the property (velocity or attenuation) of each cell is not uniquely defined as the value depends on the direction of the rays passing through the cell. It is therefore necessary to correct the data to remove the anisotropy effect in order to get input data to the tomographic inversion algorithm which are consistent with the theoretical assumptions.

The effect of anisotropy on the data is that the slowness or attenuation will vary according to a cosine curve depending on the direction of the rays. If such a correction is added to the residual data the equations for corrections of the data become:

residual travel times

$$t'_r = t_r - \Delta t_0 + r\delta v/v_0 - e \cos 2(\phi - \phi_0)\ r/v_0 \qquad (4.7)$$

residual amplitudes

$$d'_r = d_r - 20 \log_{10} \delta E_0 + 20\Delta\alpha_0 r/\ln(10) - e \cos 2(\phi - \phi_0)\ r\alpha_0 \qquad (4.8)$$

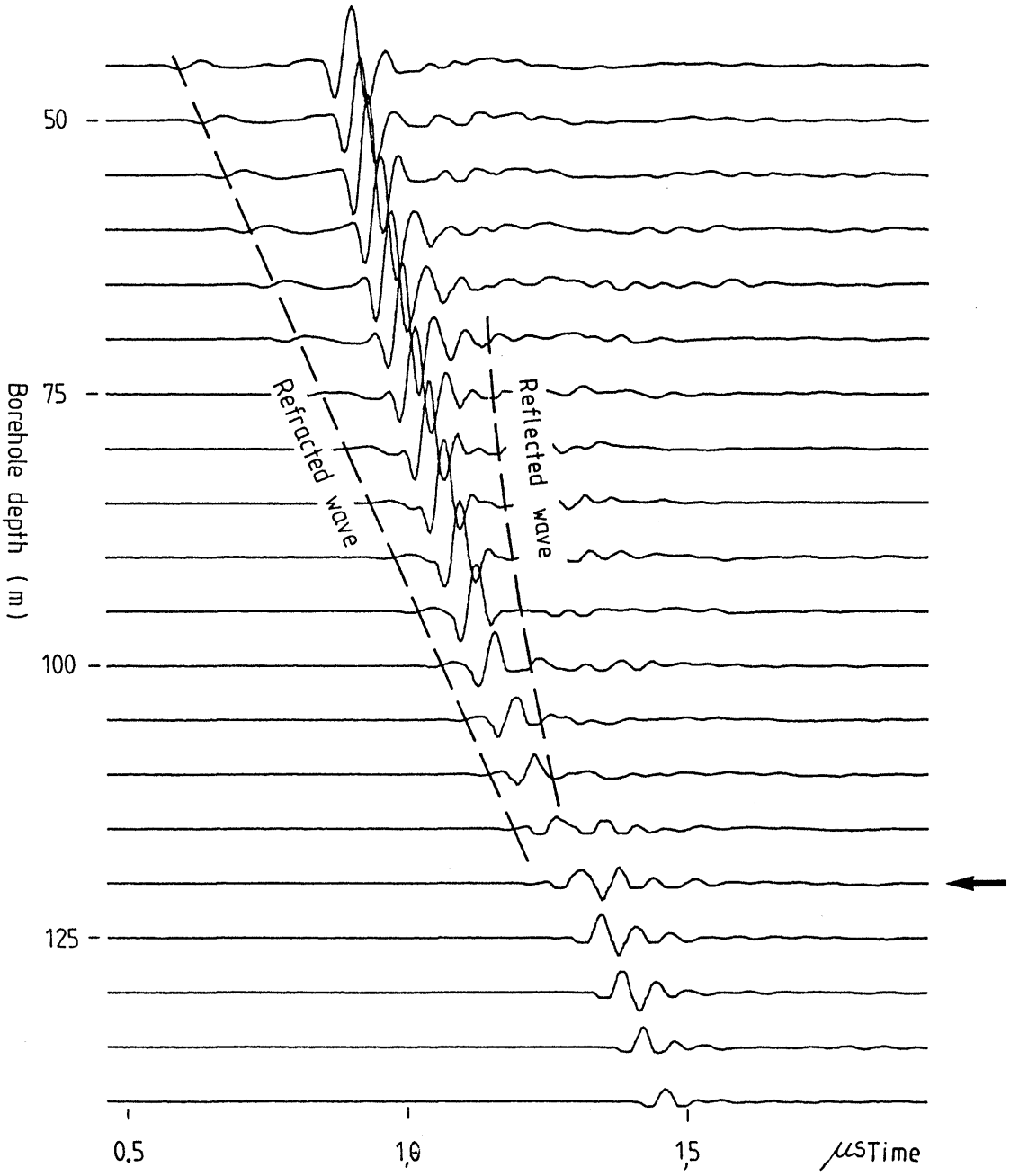

Fig. 4.3 Radar signals obtained from the crosshole scan between the L-tunnel (BO US 85.050) and BO US 85.003. Data collected during phase 1.

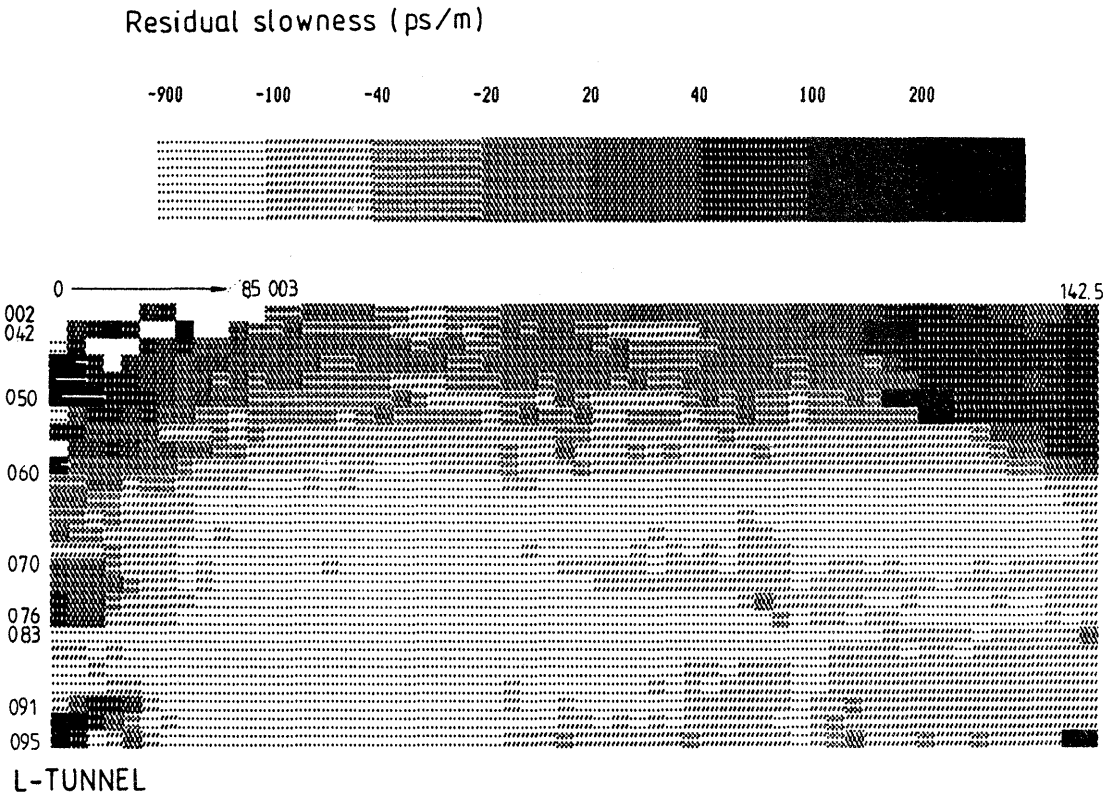

Fig. 4.4 Map of residual slowness for each ray from Field 2 belonging to the L-tunnel to BO US 85.003 data. Data are from phase 2. A slowness correction of 0.00049 µs/m has been applied.

where e is the magnitude of the anisotropy, ϕ the direction of the ray and ϕ_0 the reference direction for maximum slowness or attenuation.

The anisotropy correction is determined from plots of average slowness or attenuation as a function of ray direction. Anisotropic effects were discovered both in the amplitude and the travel time data. Fig. 4.5 shows the residual attenuation as a function of ray direction for the borehole to borehole data from Field 1. The reference direction was in this case determined to 45° (relative to the Z-axis of the coordinate system used for tomographic inversion, Fig. 2.2) and the magnitude of the anisotropy to 7%. The slowness anisotropy magnitude was determined to 0.3 % and the reference direction was the same as for the attenuation data. The borehole to borehole data from Field 1 provided the best data for determination of anisotropy as this data set contained the largest variation in the direction of the rays.

The ray direction plots for the L-tunnel to borehole data of the average attenuation showed that the antenna radiation lobes are significantly affected by the tunnel. A discrepancy in the actual radiation pattern compared to the theoretical pattern used in the calculation of the residual amplitudes will cause systematic errors in the data which will generate artifacts in the attenuation tomograms. The deviations from the theoretical formula should in principle be corrected for but this requires knowledge of the antenna radiation pattern in the presence of a tunnel. It has not been within the scope of the current program to quantify the radiation pattern of antennas located in a tunnel and a simplified approach has been adopted for these corrections. It was noted that the magnitude of the L-tunnel to borehole rays generally were smaller than the borehole to borehole rays. To compensate for this difference a larger offset correction (4-7 dB) was applied to the L-tunnel to borehole data than to the borehole to borehole data.

The L-tunnel to borehole rays which showed a large discrepancy with the applied offset correction were removed from the data set and not used for amplitude tomography. The following criteria for removal of tunnel to hole rays were adopted: Tunnel to hole rays where the angle between the ray and the tunnel was less than 25° and rays almost parallel to the boreholes (angle less than 10°) were removed from the data set. In addition rays with a length less than 20 m were excluded because of near field effects.

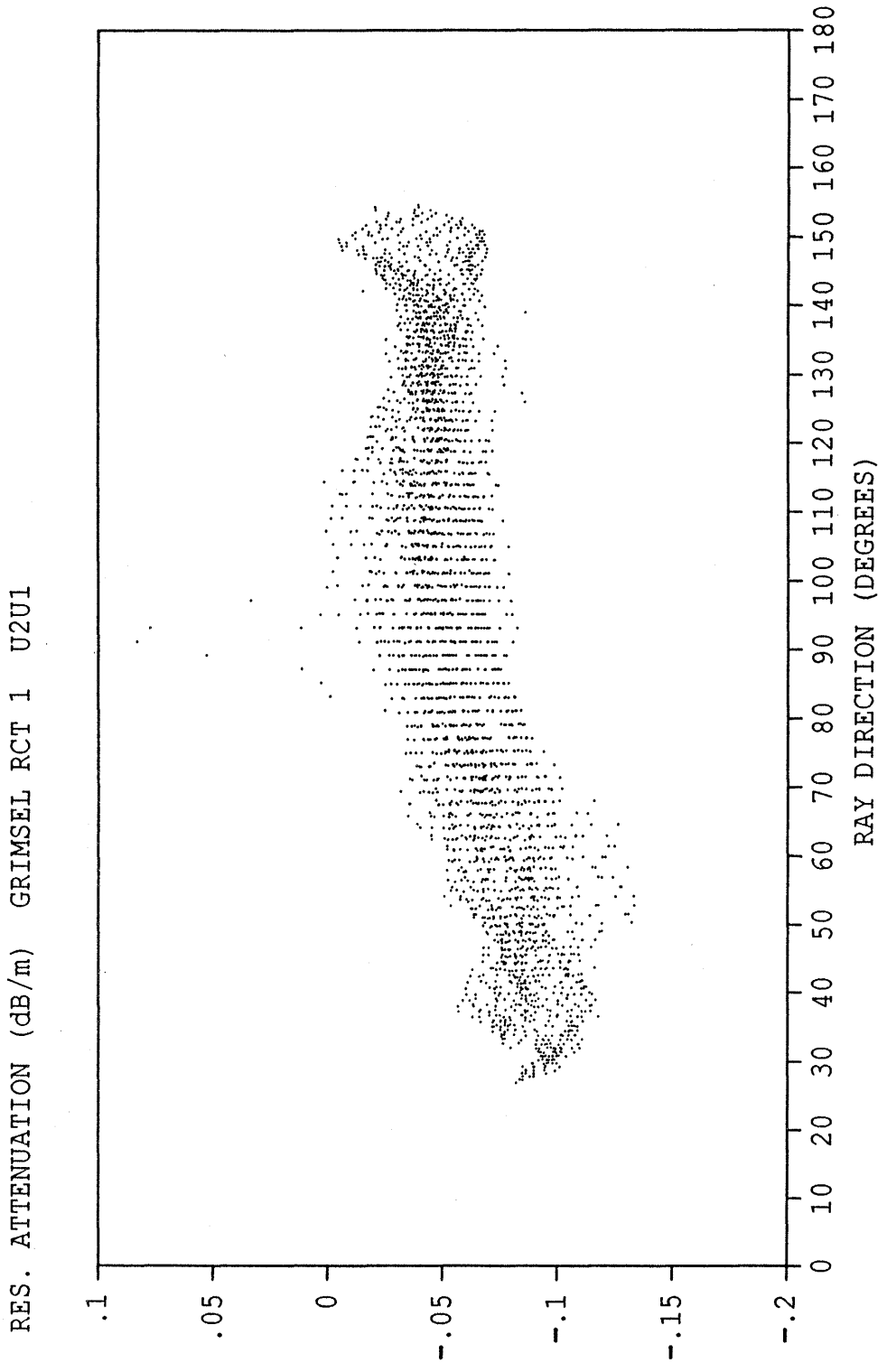

Fig. 4.5 Residual attenuation versus ray direction. Data displayed are borehole to borehole data from Field 1 (Phase 1). An offset correction of 5 dB has been applied to the data.

For information on the corrections used for each Field and phase the reader is referred to the internal reports describing the results of the individual phases (Niva and Olsson, 1987, 1988a, 1988b).

4.4 Tomographic inversion procedure

Tomographic inversions were performed of the residual travel times and the residual amplitudes after corrections and removal of erroneous rays as described in the previous section. The inversion was made with the Conjugated Gradient (CG) method described by Ivansson (1984).

The inversion was made with rectangular basis functions, i.e. the velocity of each cell is assumed to be constant within that cell. This means that no interpolation is made of the values between adjacent cells. In the tomographic inversion of a data set the following parameters may be varied:

- the cell size
- the number of iterations
- the damping constant (λ).

For this project cell sizes of approximately 2.5 m and 5 m have been used. All results presented in this report are calculated with the smaller cell size. The damping constant is a measure of the length over which the slowness or attenuation is averaged.

The tomographic inversion has been carried out in two steps. The first step consisted of inversion of the data sets where rays assumed to contain errors had been removed manually. The rays to be removed were identified on the ray check plots and in the case of the amplitudes also according to the criteria described in the previous section.

The general strategy of the two step inversion procedure is first to make a tomographic inversion with a large cell size and a large damping constant in order to identify any remaining rays containing errors. The large cell size and damping constant will give a smoothed solution and rays inconsistent with this solution will be identified and removed. The criteria for removal of rays has been that the error should be greater than 2.5 times the RMS-error of all rays compared to the solution obtained by the tomographic inversion. In the next step smaller cell size and damping constant are used to obtain a high resolution image. The first step has in all cases been made with a cell size of approximately 5 m and

the second step with a cell size of approximately 2.5 m.

The number of iterations and the value of the damping constant has changed during the course of the project based on the experience gained. In the analysis of the phase 1 data 50-100 iterations were used but a study of Ivansson, Hammarström, and Pihl (1987) showed that when a large number of iterations were used systematic errors tended to be concentrated to regions of low ray density. When a small number of iterations were used errors tended to be more evenly distributed. However, fewer iterations results in smaller anomalies and hence tomograms with less contrast.

Experience from the project has also shown that it is essential that the damping constant in the first inversion is large in order to assure that only the rays which have poor quality are removed. If the damping constant is too small it may well happen that a ray containing a large error will distort the solution with the consequence that rays adjacent to the one containing the error are removed incorrectly.

In the inversion of the phase 3 data a damping constant of 50 m and 11 iterations were used in the first step. The second step was made with 21 iterations and the damping constant was 3 m for the travel time inversions and 2 m for the amplitudes. A small damping constant improves the resolution but the errors in the slowness and attenuation estimates will increase. The smallest acceptable value for the damping constant depends on the noise in the input data. There is relatively more noise in the travel time data than in the amplitudes and the damping constant for the travel times has thus been given a larger value.

A complete tomographic inversion according to the procedure described above takes about 2 hours of CPU-time on a Prime 2250 minicomputer.

4.5 Difference tomograms

Difference tomography is based on the principle that there are two nearly identical sets of measurements available and by studying the difference between these two sets we can obtain information on changes in the investigated regions between the two measurements. In this case we have studied changes in Field 2 caused by injection of saline water at two different locations on two different occasions (phase 2 and 3). The measurement made during phase 1 serves

as a reference measurement to which the other measurements are compared. The introduction of a saline tracer into the rock causes an increase in the attenuation of radar waves and efforts have mainly been concentrated on difference tomography of amplitude data. As major changes in dielectric constant, and therefore radar wave velocity, are not expected only minor efforts have also been made in using the travel time data for difference tomography.

There are two possibilities for making radar difference tomography. One possibility is to construct the difference of the residual amplitudes corrected for any changes in offset levels. The difference data

$$\mathbf{d}_{diff}=\mathbf{d}_2-\mathbf{d}_1 \qquad (4.9)$$

are then used as input to the tomographic inversion algorithm (cf. equation 3.9) which yields an estimate of the changes in attenuation, $\mathbf{b}_{diff}$, between the two measurements. The other possibility is to construct the tomograms from each measurement in order to obtain two attenuation distributions, $\mathbf{b}_1$ and $\mathbf{b}_2$, and then take the difference of these two results to get the distribution of attenuation change

$$\mathbf{b}_{diff}=\mathbf{b}_2-\mathbf{b}_1. \qquad (4.10)$$

The two procedures should in principle give the same result as equation (3.9) is linear. The problem is that the data sets contain errors and these errors are not necessarily the same for the two data sets. Errors will generate artifacts in the tomograms and these are likely to be different for the two data sets.

The residual amplitudes from the tunnel to hole rays generally contain errors caused by the modification of the radiation pattern by the tunnel. It can be assumed that this modification of the radiation pattern has been the same during all phases. This implies that a change in amplitude for a ray is caused by the change in attenuation along its path and hence that the errors in the radiation pattern cancel in the difference data.

In the attenuation tomograms the data errors caused by modification of the radiation pattern have been transformed into artifacts. The details as to how errors propagate through the tomographic inversion procedure are not clear and an analysis is not easy to perform.

In order to resolve which procedure produces the best difference tomograms both procedures were used. Better and more stable results were obtained by taking the difference of the amplitudes for each ray according to equation (4.9) followed by a tomographic inversion of the difference data. This procedure was used for all results shown in this report. In this case rays which had been identified as containing errors in either of the two phases were removed before calculation of the difference tomograms.

There were changes in transmitter output power between the different phases which appear as offset errors in the data. The difference in offset between the different phases was estimated from crossplots of the residual amplitudes obtained for each ray in the two phases (Fig. 4.6). Most of the data points fall along a straight line in the figure. This line represents a best fit of the phase 1 and phase 2 results for rays not affected by the saline tracer. The lines indicate an offset of 7.2 dB between the phase 1 and phase 2 data. The average difference between the data sets is actually 2.2 dB as an offset correction of 5 dB had been applied to the phase 1 data before plotting. Thus there has been a reduction in the output power of the transmitter by 2.2 dB since the phase 1 measurements were performed.

The data points above the line indicate points where the amplitude is smaller in the phase 2 data set and points below the line correspond to rays where the amplitude has increased. The spread of the points around the lines give an indication of the errors (noise) in the raw data. The errors can be estimated to approximately ±1 dB. It can be noted that most of the points which do not fall along the line are located above it, i.e. the amplitude is smaller for the phase 2 data. This indicates that the saline tracer has caused a measurable reduction in amplitude which is larger than the noise in the data.

After the difference for each ray of the residual amplitudes from each phase has been calculated ray check plots are produced in the same manner as for the ordinary tomographic analysis. As an example the ray check plot corresponding to the data shown in Fig. 4.6 is shown in Fig. 4.7. An area with higher attenuation is clearly distinguished close to borehole BO US 85.003 at the depths of 100 to 130 metres.

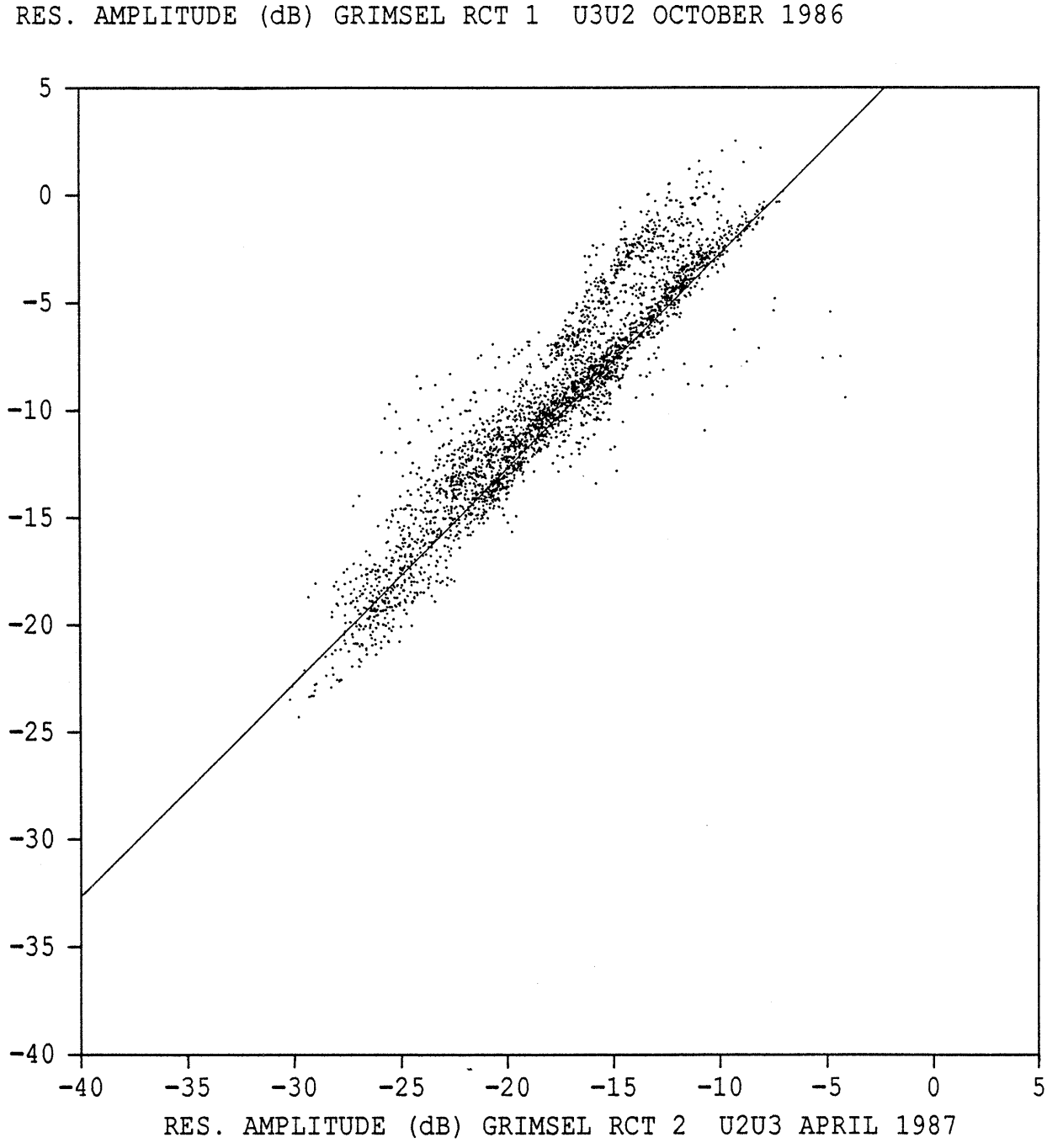

Fig. 4.6 Crossplot of residual amplitude of hole to hole rays for Field 2 obtained from phase 1 and phase 2 measurements.

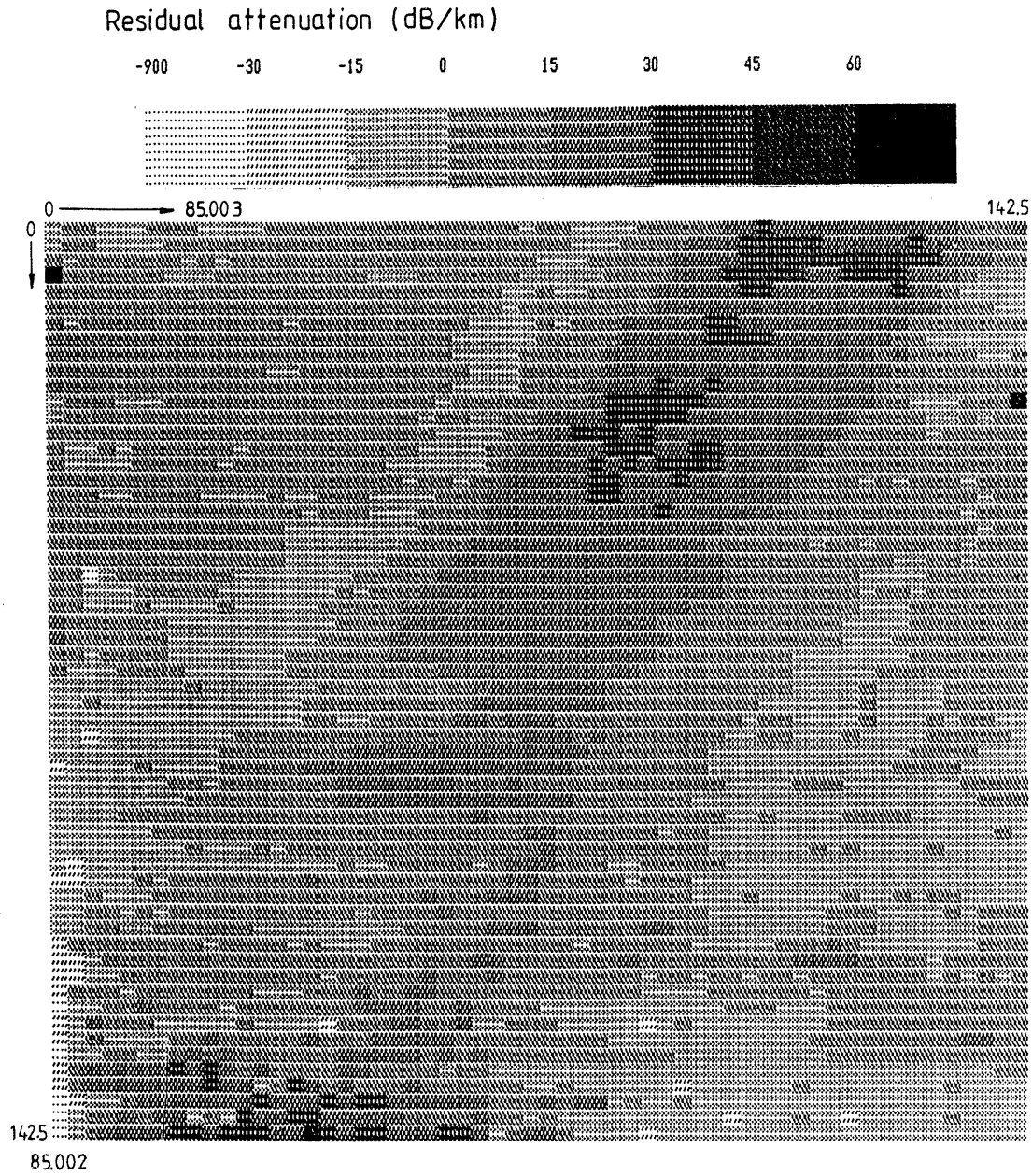

Fig. 4.7 Map of attenuation increase for each ray between phase 1 and phase 2 measurements of Field 2. Borehole to borehole data after offset correction of 2.2 dB.

4.6 Conclusions and recommendations

The procedures adopted for travel time and amplitude picking have been shown to be reasonably efficient. The algorithm used has worked properly except for a small proportion of the rays. The corresponding rays have been identified and removed from the data set. The exclusion of these rays have not had a significant effect on the resulting tomograms essentially due to the large ray density used in this tomographic survey. The procedure used has performed satisfactorily but other procedures for extracting travel time and amplitude can of course be discussed.

The procedure used for checking the data set and correcting for errors is considered to be reasonably efficient. The most significant errors found in the amplitude data were caused by the effect of the tunnel on the radiation pattern of the antenna. No efficient way was found for correcting for this error instead a significant portion of the tunnel to hole rays had to be excluded from the data set. However, the errors caused by the unknown radiation pattern cancel when the difference data is calculated between two phases and the effect on the difference tomograms has thus been negligeable. Further research on the radiation patterns from antennas located in tunnels is needed in order to obtain improved results from amplitude tomography including measurements from the tunnel locations.

The only significant errors in the travel time data occurred during phase 1 when there were relatively large drifts in the time base of the radar system. These errors could not be corrected sufficiently due to inadequate calibration procedures (cf. Chapter 2). The dominating errors in the travel time data from the latter two phases were quantization errors caused by the relatively large sampling interval ($\approx$3 ns). These errors could be reduced by increasing the sampling frequency.

The parameters used in the tomographic inversion have changed during the project based on the experience gained. The parameters used in phase 3 appear to give good results and are recommended for future use. The Conjugated Gradient method is an effective inversion method which converges quickly. A large number of iterations appear to concentrate errors and artifacts to regions of low ray density. A modification of the damping procedure could possibly reduce artifacts and give a more homogeneous distribution of inconsistencies. Further research in this area is warranted.

With respect to the difference tomography the method based on the difference of the residual amplitudes for each ray followed by a tomographic inversion of the difference data proved to give the best results.

5 TOMOGRAPHIC RESULTS FROM THE REFERENCE MEASUREMENT

5.1 Slowness

The slowness tomograms obtained from Fields 1 and 2 are shown in Figs. 5.1 and 5.2. The first figure contains only the tomographic information while the geologic information available along tunnels and boreholes have been included in the second figure. The tomogram of Field 1 is based on data collected during phase 1 while Field 2 is based on the data collected during phase 2. The errors in the travel time data during phase 1 for Fields 2 and 3 were large and this generated significant artifacts in the corresponding tomograms (cf. Fig. 5.3 and Niva and Olsson, 1987). The tomographic inversion has been made separately for each Field and the resulting plots have been merged in the same figure.

In the computation of the Field 1 slowness tomogram 9 % of the rays were excluded out of a total of 4872. For Field 2 only 3.3 % were excluded out of a total of 6380. The relative number of tunnel to hole rays excluded was significantly larger than the relative amount of hole to hole rays. This was due to more noise in the tunnel to hole data and interference of the direct wave with refracted tunnel waves.

The RMS-error obtained for the Field 1 and 2 tomograms was 1.3 ns and 2.2 ns, respectively. This error is smaller than the sampling interval which is approximately 3 ns.

A number of linear features can be identified in the tomograms and the resolution is comparatively high close to the L-tunnel where the ray density is high and rays of practically all directions pass through the pixels. Towards the end of the boreholes the resolution gets poorer. In this part, approximately midway between the boreholes, two dark areas can be observed indicating increases in slowness. Here the rays are all nearly parallel and there is no information in the data on the position of a feature between the boreholes. Therefore all structures will be relatively smoothed in this part of the tomogram. In this case we can note that an area of increased slowness is obtained surrounded by two regions with relatively low slowness values. This is an artifact caused by the tomographic inversion technique and the way damping is introduced into the CG-method (Ivansson, Hammarström, and Pihl, 1987).

The slowness tomogram for Field 3 is shown in Fig. 5.3. In the computation of the Field 3 slowness tomogram 7 % of the rays were excluded out of a total of 2116. The RMS-error obtained for Field 3 was 2.8 ns. We can note that this tomogram shows very little resemblance to the tomograms shown in Fig. 5.1. Practically all structures seen in the Field 3 tomogram can be considered as artifacts and they are caused by the drift in the time base of the system. This tomogram can not be used for any predictions of the geological conditions at the site.

As mentioned above the inadequate calibration routine during phase 1 did not allow a suitable correction of the travel time data for Field 3. A hardware modification between phase 1 and 2 and the use of a better designed calibration procedure during phase 2 and 3 (Field 2) demonstrated that these problems are solved and the described error will not occur in future investigations.

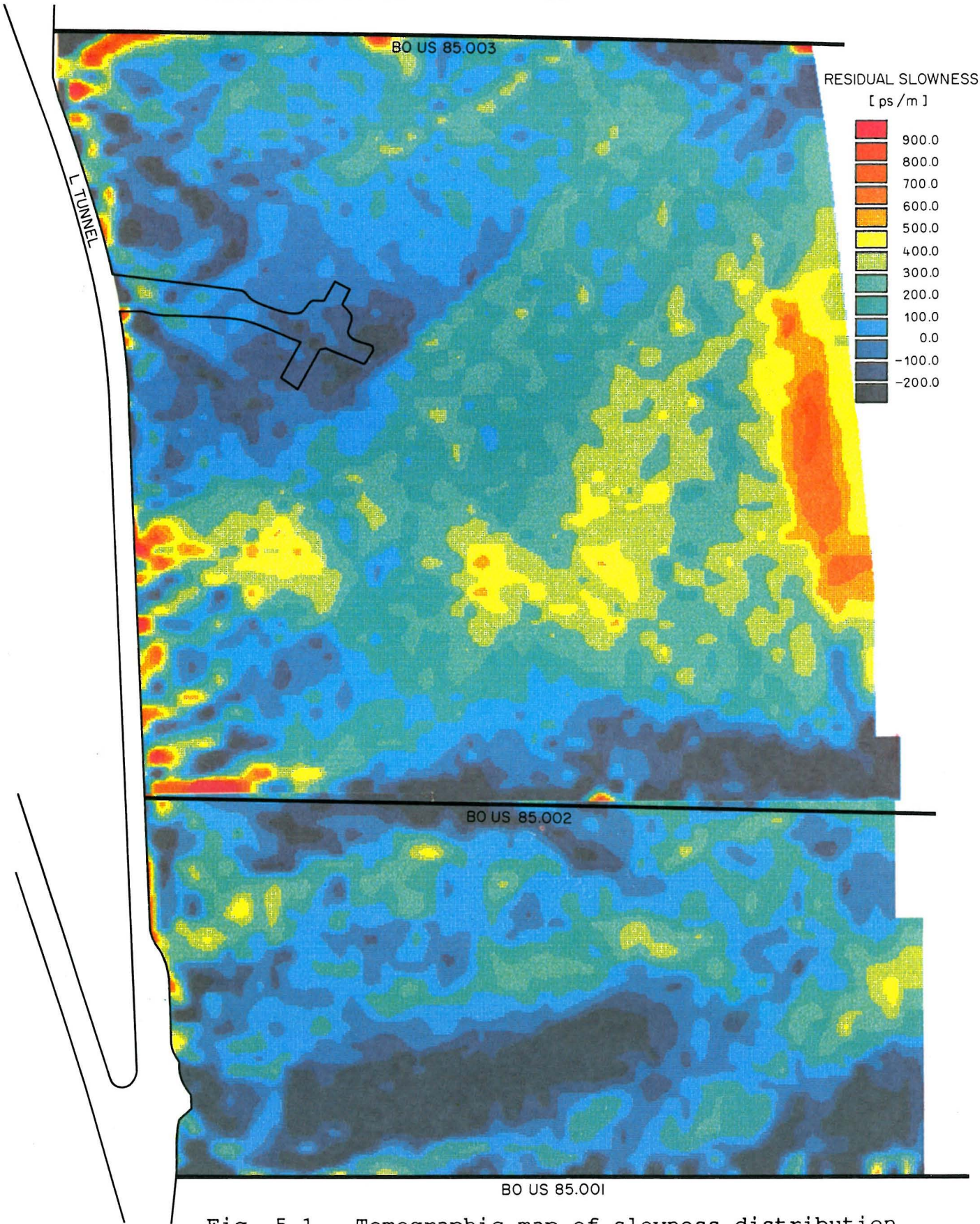

Fig. 5.1 Tomographic map of slowness distribution for Fields 1 and 2. A slowness value of zero corresponds to a velocity of 124 m/µs. Scale 1:1000.

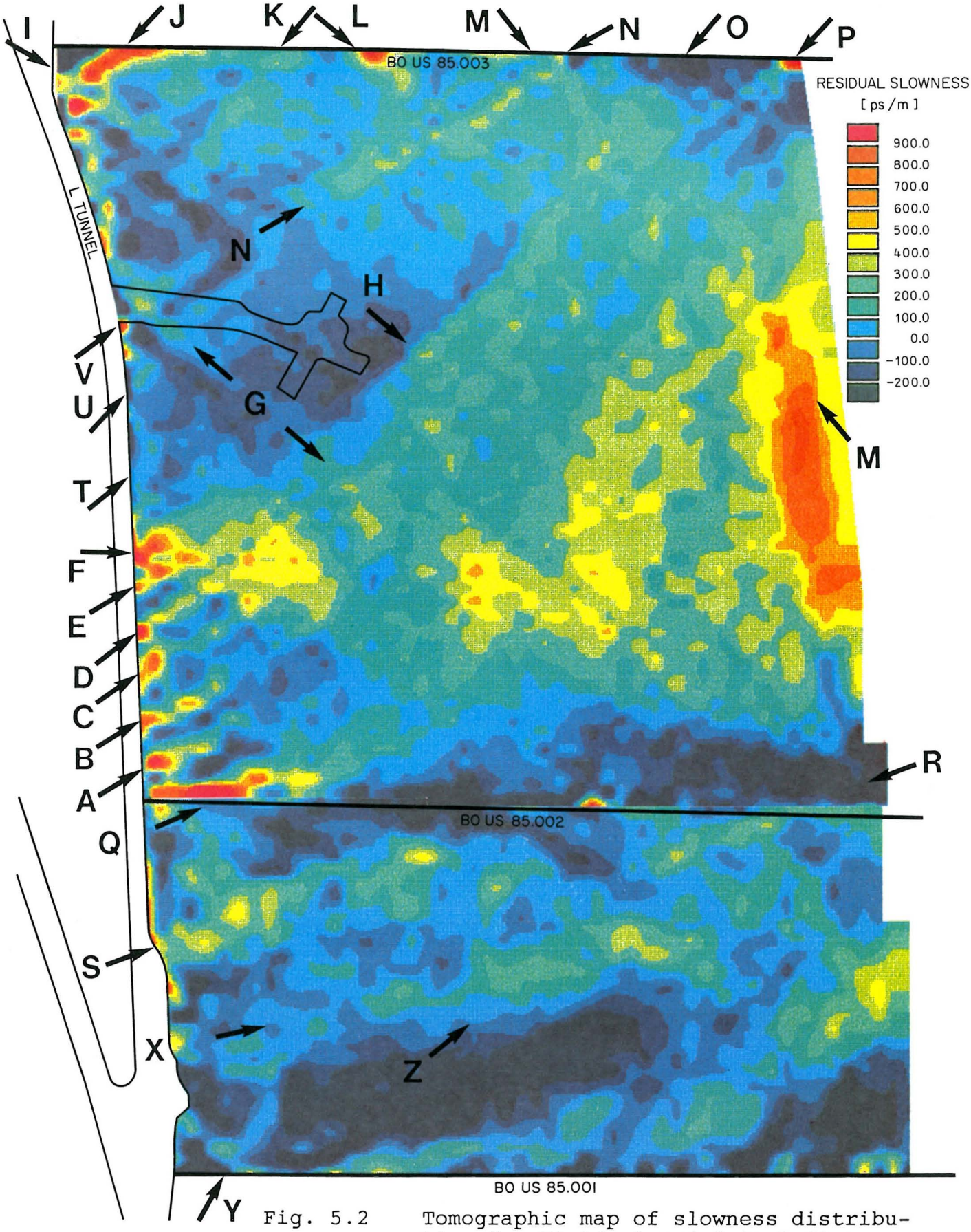

Fig. 5.2 Tomographic map of slowness distribution for Fields 1 and 2 including labels which identify the observed structures. A residual slowness value of zero corresponds to an actual velocity of 124 m/µs. Scale 1:1000.

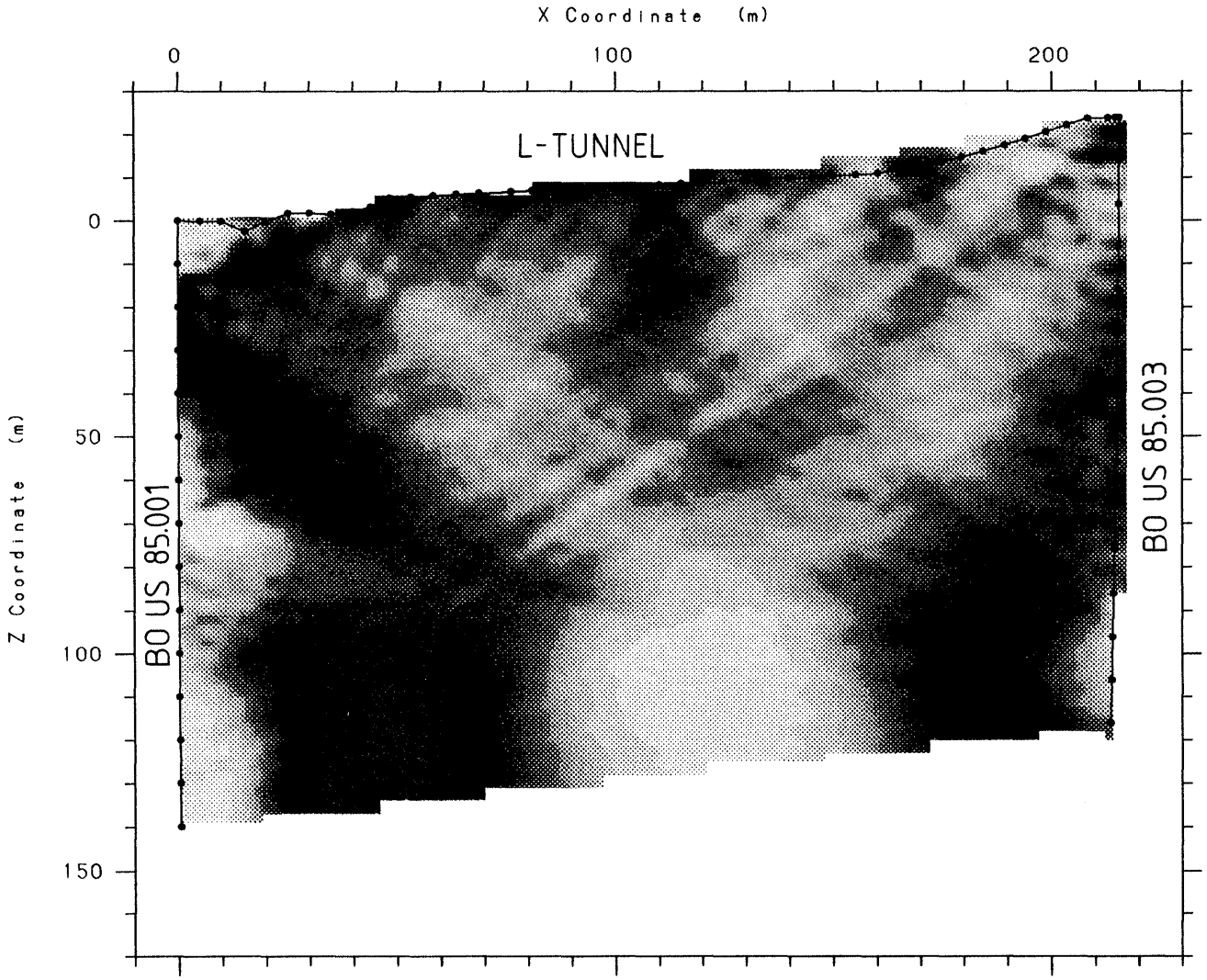

Fig. 5.3 Tomographic map of slowness distribution for Field 3. A slowness value of zero corresponds to a velocity of 124 m/μs. Scale 1:1600.

5.2 Attenuation

The attenuation tomograms obtained for Fields 1 and 2 are shown in Figs. 5.4 and 5.5. These figures display the tomograms obtained from the inversion of the data collected during phase 1, the reference measurement. As was the case for the slowness tomograms the tomographic inversion has also in this case been made separately for each Field and the resulting plots merged in the same figure.

The fraction of excluded rays in the computation of these tomograms was 16% for Field 1 and 20% for Field 2. The majority of the rays were excluded based on the criteria described in Section 4.3 which stipulated that certain tunnel to borehole rays should be excluded based on their direction relative to boreholes and tunnels. A comparison was made between excluding a large number of rays based on these criteria and exclusion of a significantly smaller number of rays. It was found that the attenuation tomogram obtained by excluding a large number of rays were more similar to the slowness tomograms and contained less artifacts than the one obtained with a smaller number of rays excluded. The procedure adopted for removing rays was therefore considered efficient in reducing the artifacts caused by inadequate knowledge of the antenna radiation pattern for antennas located in tunnels (Niva and Olsson, 1988a).

Fig. 5.6 shows the residual attenuation tomogram obtained for Field 3. It should be noted that this Field was measured with a point separation of 5 m in the boreholes and 10 m in the L-tunnel which is twice as large as the point separation used for Fields 1 and 2. Hence, we can expect poorer resolution but there is a general similarity between the features observed in the Field 3 tomogram and the Field 1 and 2 tomograms.

A general observation can be made concerning the three tomograms. Close to the L-tunnel a number of relatively narrow and well defined features can generally be identified. At a larger distance from the tunnel features become smeared and diffuse. The distance from the L-tunnel at which this appears is different between the three fields. This difference is attributed to the differences in angular coverage of rays for the three Fields. In Field 1 structures are well defined to a distance of approximately 120 m from the L-tunnel which should be compared to the measured section of the boreholes which is about 145 m. The corresponding distances for Field 2 and 3 are 100 m and 50 m, respectively.

For these Fields data has been collected along three sides of a rectangle and if the length to width ratio is 2 to 1, as for Field 1, good resolution is obtained for nearly the entire area of the field. For a 1 to 1 ratio as in Field 2 we obtain good data from about two thirds of the investigated area. If the length to width ratio becomes 1 to 1.5 as for Field 3 good data is only obtained for about a third of the area and this is generally not sufficient.

The RMS-error obtained for the Field 1 and 2 tomograms was 0.34 dB and 0.75 dB, respectively. The corresponding error for Field 3 was 0.95 dB. The proportion of excluded rays for Field 3 was 5% out of a total of 2117 rays.

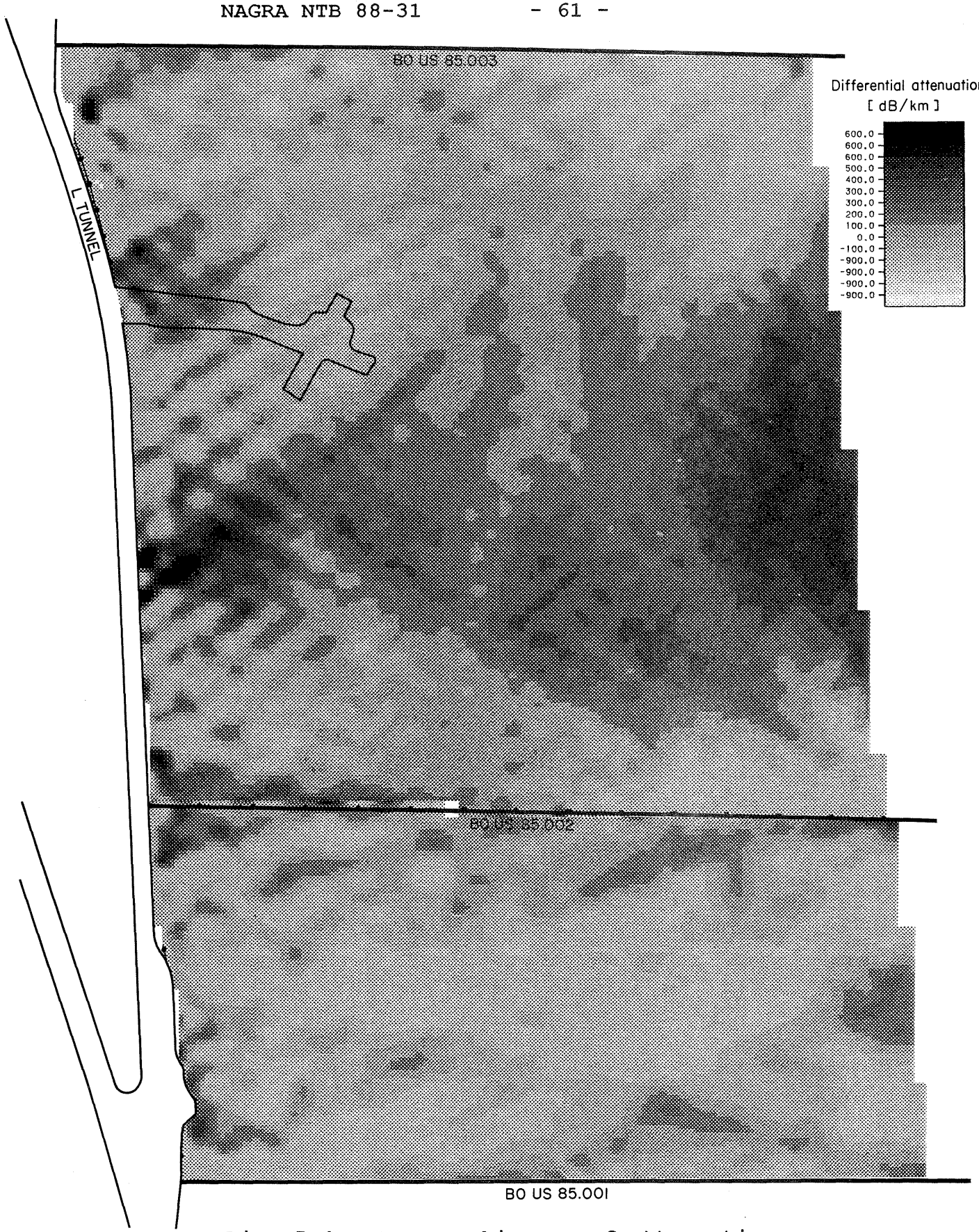

Fig. 5.4 Tomographic map of attenuation distribution for Fields 1 and 2. A residual attenuation of zero corresponds to an actual attenuation of 25 dB/100 m. Scale 1:1000.

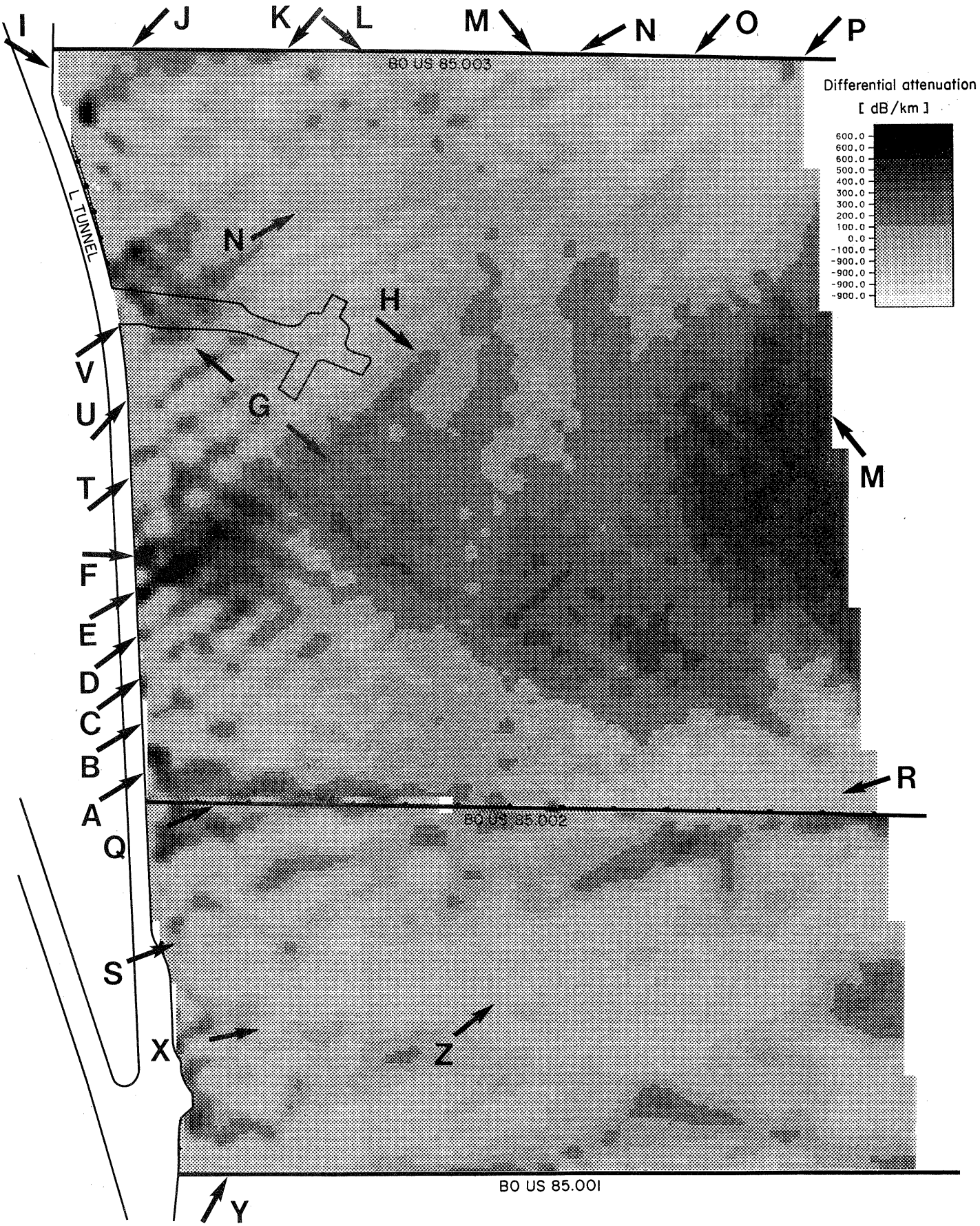

Fig. 5.5 Tomographic map of attenuation distribution for Fields 1 and 2 including labels which identify the observed structures. A residual attenuation of zero corresponds to an actual attenuation of 25 dB/100m. Scale 1:1000.

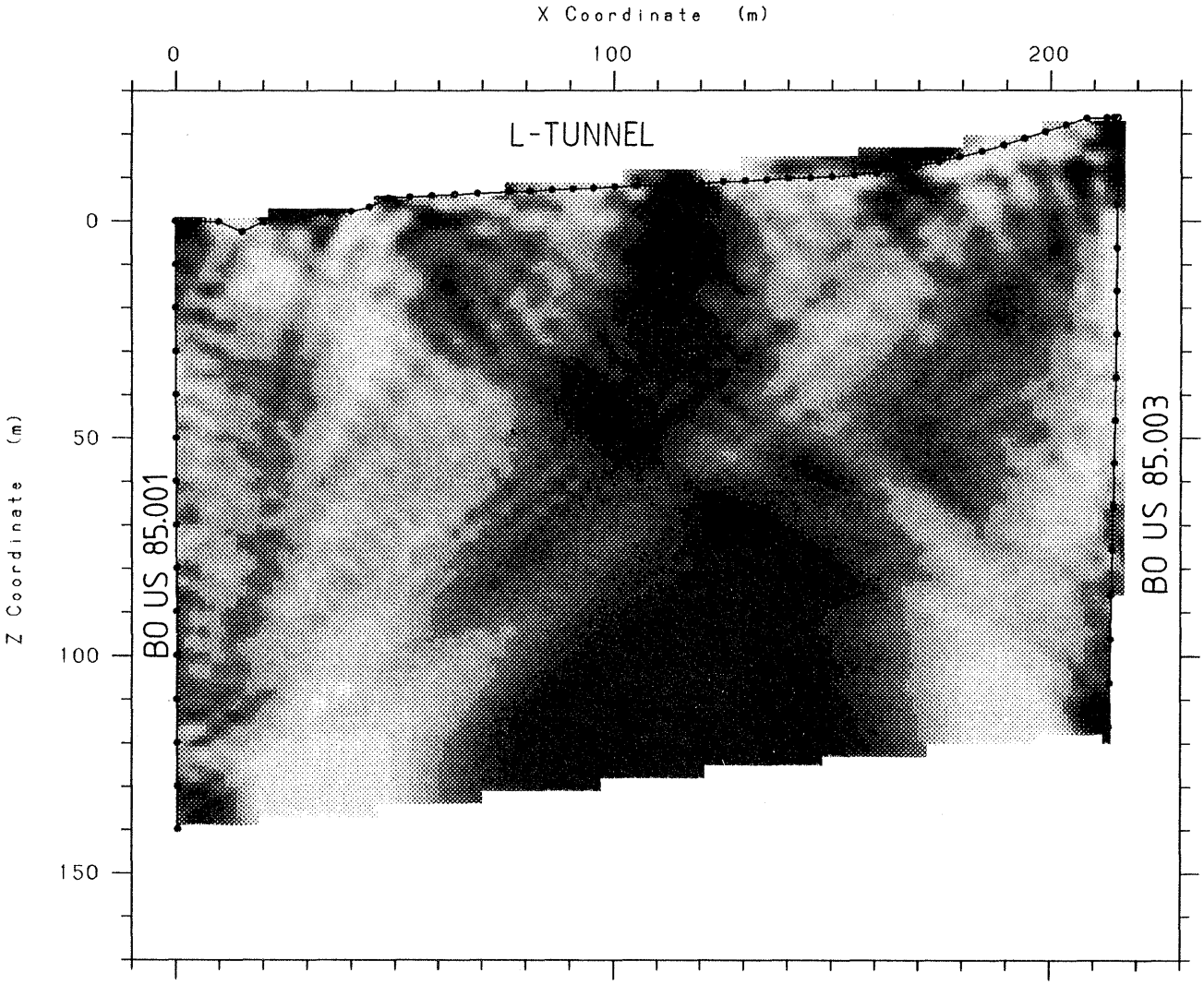

Fig. 5.6 Tomographic map of attenuation distribution for Field 3. A residual attenuation of zero corresponds to an actual attenuation of 25 dB/100 m. Scale 1:1600.

5.3 Geophysical interpretation

The interpretation of structural features at the test site is based on the slowness and attenuation tomograms for Fields 1 and 2 as they provide the best resolution. Figs. 5.2 and 5.5 display the tomograms together with geological information obtained from boreholes and tunnels. These figures also contain identification letters of the features identified in the tomograms.

The reference values for the residual slowness and attenuation shown in the figures is 124 m/μs and 25 dB/100 m, respectively. The range of variation in the slowness data is roughly 700 ps/m which should be compared to the reference value of 8050 ps/m (or 124 m/μs). The magnitude of the slowness anomalies is thus about 9 %. The range of variation for the attenuation values is about 60 dB/100 m which is 250% of the reference value. The contrast in attenuation is thus considerably larger than the contrast in slowness (velocity). It is also instructive to look at the magnitude of the anisotropy in the slowness and attenuation data and compare it to the range of variation. The anisotropy was 0.3% and 7% for the slowness and amplitude data, respectively, which is about 3 % of the corresponding range of variation.

The dominating feature in the tomograms is the lamprophyre (F) which intersects the L-tunnel at the borehole BO US 85.060. The lamprophyre gives rise to a zone of significantly increased slowness and attenuation of irregular shape extending almost parallel to the boreholes. The appearance of the lamprophyre in the slowness and attenuation tomograms is similar.

Starting from the north-eastern corner of the investigated area there is an irregular anomaly (X) extending in a direction almost parallel to the boreholes. The attenuation anomaly is displaced towards the south relative to a similar anomaly observed close to the tunnel in the slowness tomogram.

The dominating features in Field 1 are (R) and (S) which extend nearly parallel to the boreholes. Feature (S) starts at a position in the L-tunnel where a lamprophyre intersects the tunnel and it has the same general direction as feature (R). It is possible that they actually represent the same feature but that there has been faulting along a line with north-westerly orientation. The slowness and attenuation anomalies associated with these features show a relative displacement with respect to each

other. This displacement of the anomalies is evident already in the raw data and is not an artifact caused by the tomographic inversion procedure or data errors. The physical cause for a displacement of slowness and attenuation anomalies is not clear but it has also been observed at other sites (Olsson, Eriksson, Falk, and Sandberg, 1988). The attenuation anomaly of (S) intersects borehole BO US 85.002 at a depth of about 110 m which coincides with a resistivity anomaly identified in the borehole. Two features (Y and Z) striking roughly N50°E can also be identified. (Y) intersects BO US 85.001 at about 15 m and seems to continue to BO US 85.002 which it intersects at about 65 m (this is most clear in the attenuation tomogram).

A zone of increased slowness (Q) extending in a westerly direction is observed close to the beginning of borehole BO US 85.002. At the location where the anomaly intersects the borehole there is a zone of increased fracturing which is associated with a resistivity anomaly. In the attenuation tomogram the feature Q appears as a wide area of increased attenuation from the beginning of borehole BO US 85.002 to a borehole length of about 60 m. This appearance of Q might be considered as an artifact which is caused by the removal of a large number of rays in the attenuation tomogram.

Between borehole BO US 85.002 and the location where the lamprophyre (F) intersects the tunnel there are five parallel zones (A, B, C, D, and E) which extend towards WSW. Increased fracturing and lamprophyric dikes are observed where these anomalies intersect the L-tunnel. These structures appear to cross the lamprophyre (F) and continue through it. However, on the southern side of the lamprophyre only two nearly parallel structures can be identified (O and P). The orientation of the zones is slightly different on the northern and southern sides of the lamprophyre. The geometry of the structures appears to be quite complex where the zones (A, B, C, D, E, O, and P) intersect the lamprophyre. Included in this complex is the feature G which extends from the start of the BK-drift to borehole BO US 85.002, which it intersects at a borehole depth of approximately 90 m. The slowness anomaly associated with G is small north of the BK-drift and close to BO US 85.002. At the positions where G intersects the BK-drift and the borehole BO US 85.002 increased fracturing is observed but the orientation of the fractures is not the same as the orientation of zone G (cf. Fig. 5.2). There is a weak indication in the tomogram of a structure (H) which is located to the south of G and parallel to it.

A few features not clearly observed in the slowness tomogram are seen in the attenuation tomogram. The most clear features are T, U, and V which strike WSW. Zone V which is located at the beginning of the BK-drift is the strongest anomaly. It is possible that V is connected to N seen in the travel time tomogram. The anomalies T and U could be artifacts caused by the removal of a large number of rays to the end of BO US 85.003.

Close to the beginning of borehole BO US 85.003 there is an indication of a structure (I) striking NW. The structure can be followed approximately 50 m from the L-tunnel. Structure I is intersected by a feature (J) extending from a borehole depth of approximately 12 m in BO US 85.003 to the L-tunnel with a strike in the direction WSW. Two other features (K and N) almost parallel to J can also be observed. The two northwesterly striking features L and M are probably associated with lamprophyres intersecting borehole BO US 85.003.

Another interesting feature in the tomogram is the slowness anomaly associated with the L-tunnel. The anomaly closely follows the wall of the tunnel and the width of the slowness anomaly is approximately one pixel, i.e. about 2.5 m. This anomaly can possibly be caused by increased water content in the immediate vicinity of the tunnel due to stress release and microfracturing caused by the excavation of the tunnel.

5.4 Conclusions and recommendations

The slowness and attenuation tomograms produced within the project have a good correlation with geological features observed in boreholes and tunnels. High resolution is obtained near the L-tunnel. The distance from the tunnel where high resolution prevails is determined by the length to width ratio of the investigated field. It is recommended that the length to width ratio is not less than 1 as this will give acceptable data for at least two thirds of the investigated area and that measurements points are located on at least three sides of the area as has been done in this case.

The slowness tomograms from phase 1 contained significant artifacts for Fields 2 and 3 due to the drift in the time base of the radar equipment. Before the commencement of phase 2 the equipment was modified and no significant time base drifts could be observed during phases 2 and 3. The time base drift does not affect the amplitude measurements so the

quality of the amplitude data was roughly the same for all phases.

A consequence of the improved quality of the travel time data was that the travel time tomogram showed a significant improvement in resolution and reduction of artifacts. This is a demonstration of the high data quality required for a successful outcome of a tomographic survey. The results also show that the modified radar system meets those requirements.

The main feature identified in the tomograms is the lamprophyre which extends in a direction almost parallel to the boreholes. Two additional sets of features can also be identified which extend in almost orthogonal directions (NW and WSW). These features can be identified with good resolution in the slowness tomogram. There is a good correlation between the existence of geophysical anomalies known from borehole logging, fracturing and tomographic features at the locations where these features intersects the boreholes or the drifts.

Only the major features can be identified in the attenuation tomograms and the resolution is relatively poor due to the artifacts caused by the systematic errors in the tunnel to hole data. It has also been shown that the artifacts can be reduced to some extent by excluding the rays where the errors in the radiation pattern are largest.

6 RADAR RESPONSES DUE TO SALINE TRACER MIGRATION

6.1 Results from Phase 2 tracer injection

During phase 2 saline tracer was injected in a section at an approximate depth of 29 m in borehole BO BK 85.009 (Fig. 1.2). The injection of the tracer was started 5 days before the commencement of the radar tomography survey. The saline injection continued during the entire radar survey which lasted for 10 days.

The difference tomograms were obtained through inversion of the difference amplitude for each ray as described in Section 4.5. For the phase 2 data tomographic inversion of the difference data was performed with three different sets of excluded rays.

The first tomogram was made after removal of the rays assumed to contain large errors due to the effect of the L-tunnel on the antenna radiation pattern (the criteria for removal are described in Section 4.3). The total number of excluded rays were 1464 (23% out of a total of 6380) for the tomogram shown in Fig. 6.1. The RMS-error for this tomogram is 0.5 dB.

The second tomogram was made with only those rays removed found to contain errors. The total number of excluded rays were 433 (7% out of a total of 6380) for the tomogram shown in Fig. 6.2. The RMS-error for this tomogram is 0.6 dB.

The same features are seen at the same locations in both tomograms but small differences in anomaly magnitude can be observed in some places. The similarity of these two results shows that including the rays which are known to contain errors in the radiation pattern due to the effect of the L-tunnel does not produce significant artifacts in the difference tomogram. In other words the expected cancellation of errors of this type actually takes place. If these results are compared to the result obtained by taking the difference of two tomograms it is clear that the best result is obtained by first taking the difference of the data for each ray and then making a tomographic inversion of that data (Niva and Olsson, 1988a)

A general characteristic of the tomograms shown in Figs. 6.1 and 6.2 are the linear anomalies which

seem to go to the corners of the field, in particular to the end of BO US 85.002. In order to study if these structures were artifacts the rays going to the end of BO US 85.002 were removed and a third tomogram was produced. The resulting tomogram (Fig. 6.3) shows that practically all the anomalies remain the same. The location of anomaly (3) has shifted somewhat towards the new corner and (2) is identified only with difficulty in Fig. 6.3. This is partly due to the loss of resolution in this part of the field due to the removal of the rays. These results show that the tomographic anomalies are not affected significantly by removal of rays going to one corner and hence that the structures seen in the tomograms are real and not artifacts.

The dominating feature in the difference tomogram is the anomaly in the centre of the Field. The location of the maximum anomaly coincides with the injection point for the saline tracer. The neighborhood of the injection point is also the point where the largest concentration of the tracer is expected and hence also the largest radar anomaly. It is also interesting to note that the largest anomaly in all tomograms from Field 2 the lamprophyre (F in Fig. 5.2 and 5.5) does not show up at all in the difference tomogram. These observations taken together indicate that the anomalies observed in the difference tomogram are basically an effect of the saline tracer and are not caused by experimental measurement errors or conceptual errors in the data processing.

However, there are a number of anomalies at the boundaries of the investigated area. These anomalies are most likely artifacts caused by the tomographic inversion procedure. A number of small anomalies can also be seen scattered all over the tomogram. Such anomalies should be considered as noise and are probably caused by the random noise in the original data which amounted to ±1 dB.

The magnitude of the maximum anomaly in the region around the injection point is approximately 12 dB/100 m which should be compared to the average attenuation of the rock at the Grimsel Test Site which has been estimated to 25 dB/100 m. Thus, the saline tracer has caused an increase in the attenuation of about 50% in the region where the concentration has been highest.

The saline tracer does not spread radially out from the injection point instead it extends linearly towards WSW (1). The spreading of the saline tracer (1) appears to follow the feature (P) identified in the slowness tomogram (cf. Fig. 5.2). The anomaly does not reach the borehole BO US 85.003, instead

starting at a distance of about 20 m from BO US 85.003 the tracer appears to spread in a direction almost orthogonal to the feature P (or 1). This feature (2) does not directly correspond to any feature identified in the slowness tomogram but it is parallel to the features L and M. The distribution of the saline tracer in this region is very irregular with a series of patches of increased attenuation (or saline concentration). This type of tracer distribution can be expected if the fracture zone followed by the tracer is channeled. It should be remembered that the tomogram shows the tracer distribution in a plane and that migration out of the plane is likely, especially as most of the fracture zones are known to be steeply dipping. If the tracer is transported out of the plane and if the fracture zones are channeled then a tomographic study of the plane will show only where the channels intersect the plane, which could give rise to a number of pointlike anomalies as observed in Figs. 6.1 and 6.2.

There is also a weak anomaly extending in the north-westerly direction from the injection point towards the north-western corner of the Field (3). This anomaly appears to be an extension of the feature I identified in the slowness tomogram. The magnitude of the anomaly is relatively small close to the injection point but it increases as it approaches the end of borehole BO US 85.002. This could indicate that the main transport path within this feature is out of the investigated plane.

Two relatively large anomalies can also be observed close to the BK-drift (H and 4). The location of these anomalies coincides with regions of fracturing observed in the BK-drift and the L-tunnel and the orientation coincides with G, H, and I identified in the slowness tomogram. It is interesting to observe that the location of 4 is a few meters to the north of G while the slowness and saline tracer anomaly coincide for H. A strong anomaly of small extent (5) is also seen close to where borehole BO US 85.002 intersects the L-tunnel. All of these anomalies are not connected to the injection point which implies that transport of tracer in the third dimension out of the plane of investigation must have occurred for the tracer to reach these positions.

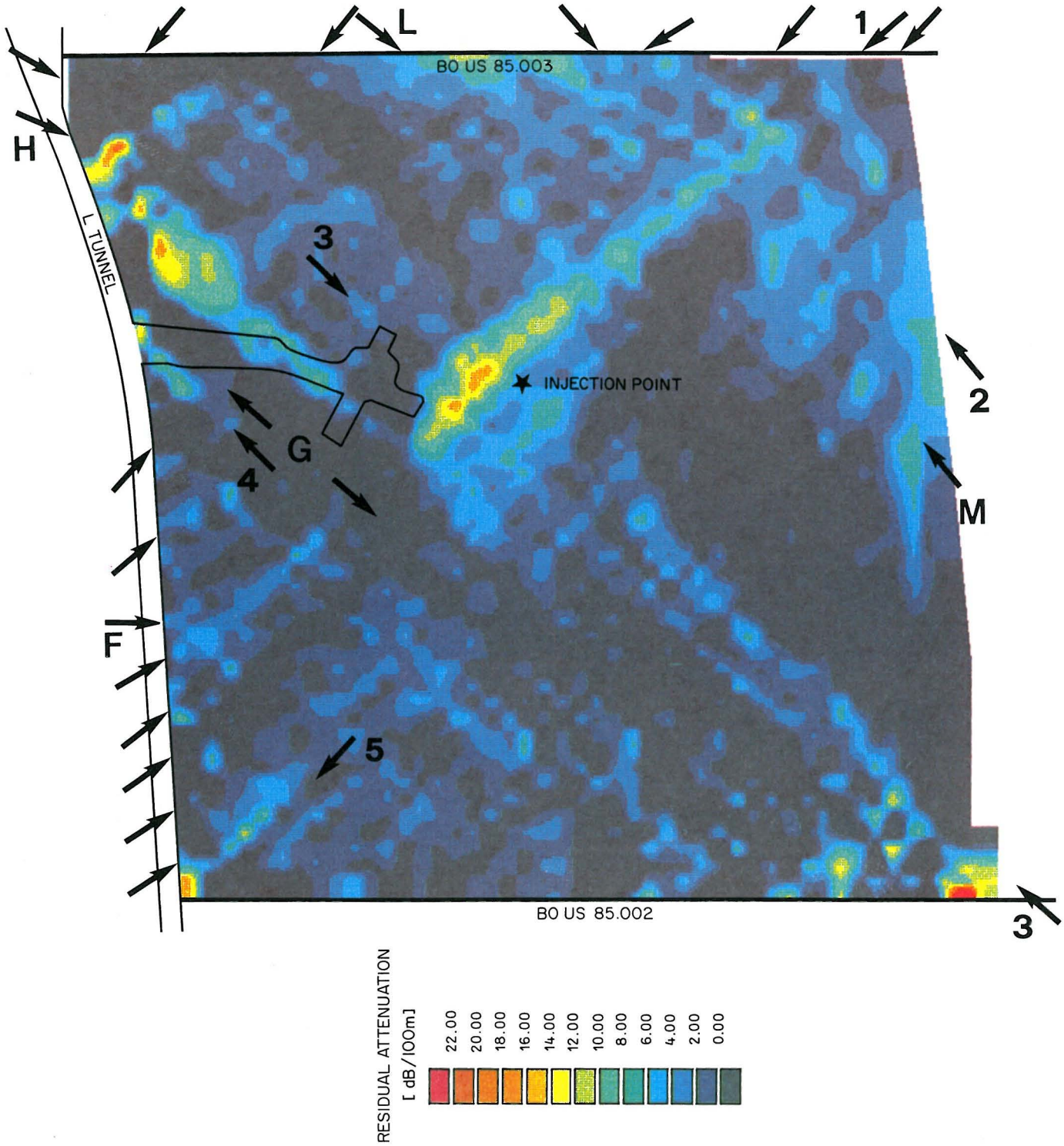

Fig. 6.1 Tomographic map showing the increase in radar attenuation of Field 2 from phase 1 to phase 2 obtained after removal of 1464 rays. The map shows the parts of the plane where the saline tracer has migrated. Unlabeled arrows indicate the position of fracture zones identified in the reference tomograms. Scale 1:1000.

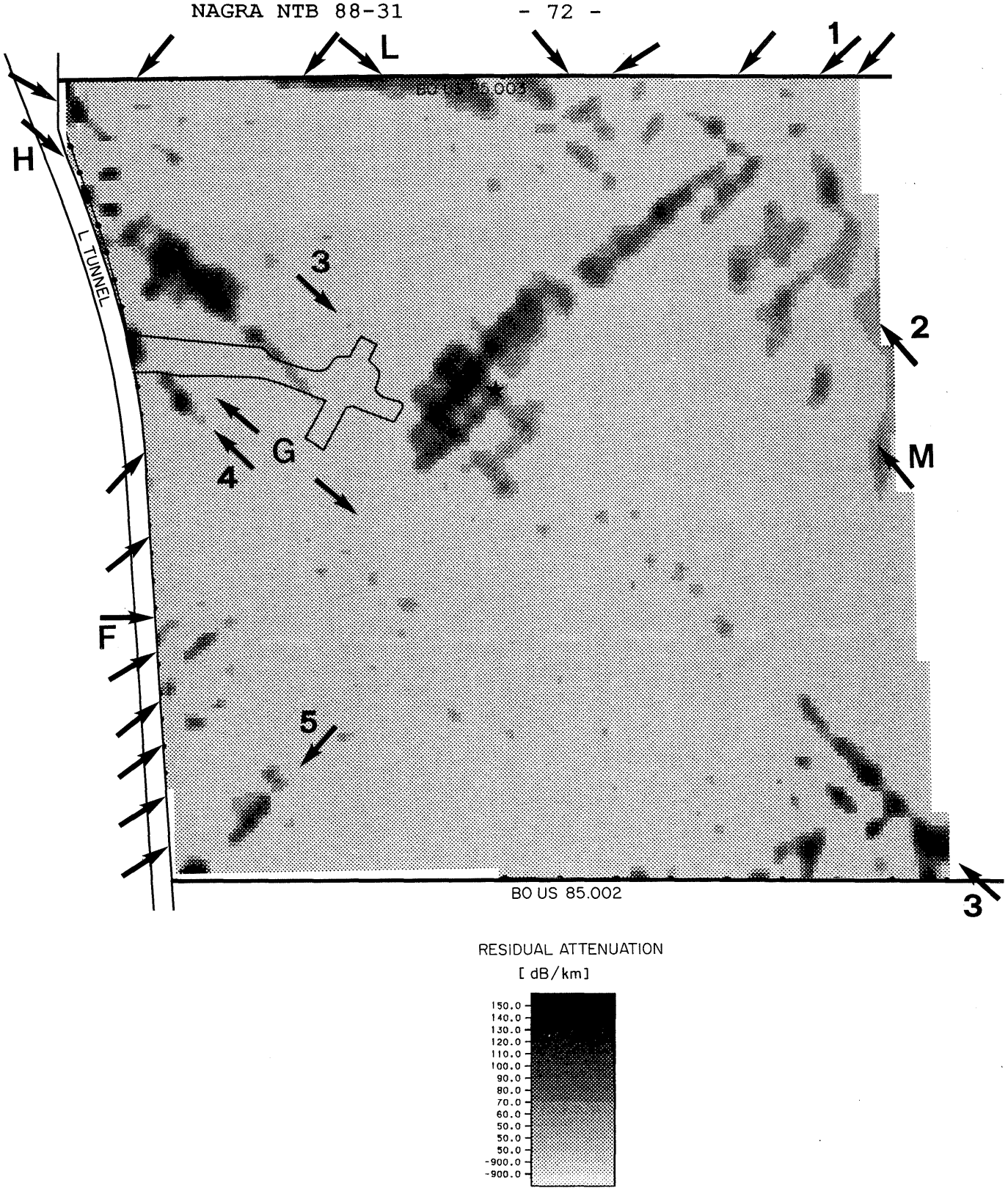

Fig. 6.2 Tomographic map showing the increase in radar attenuation of Field 2 from phase 1 to phase 2 obtained after removal of 433 rays. The map shows the parts of the plane where the saline tracer has migrated. Scale 1:1000.

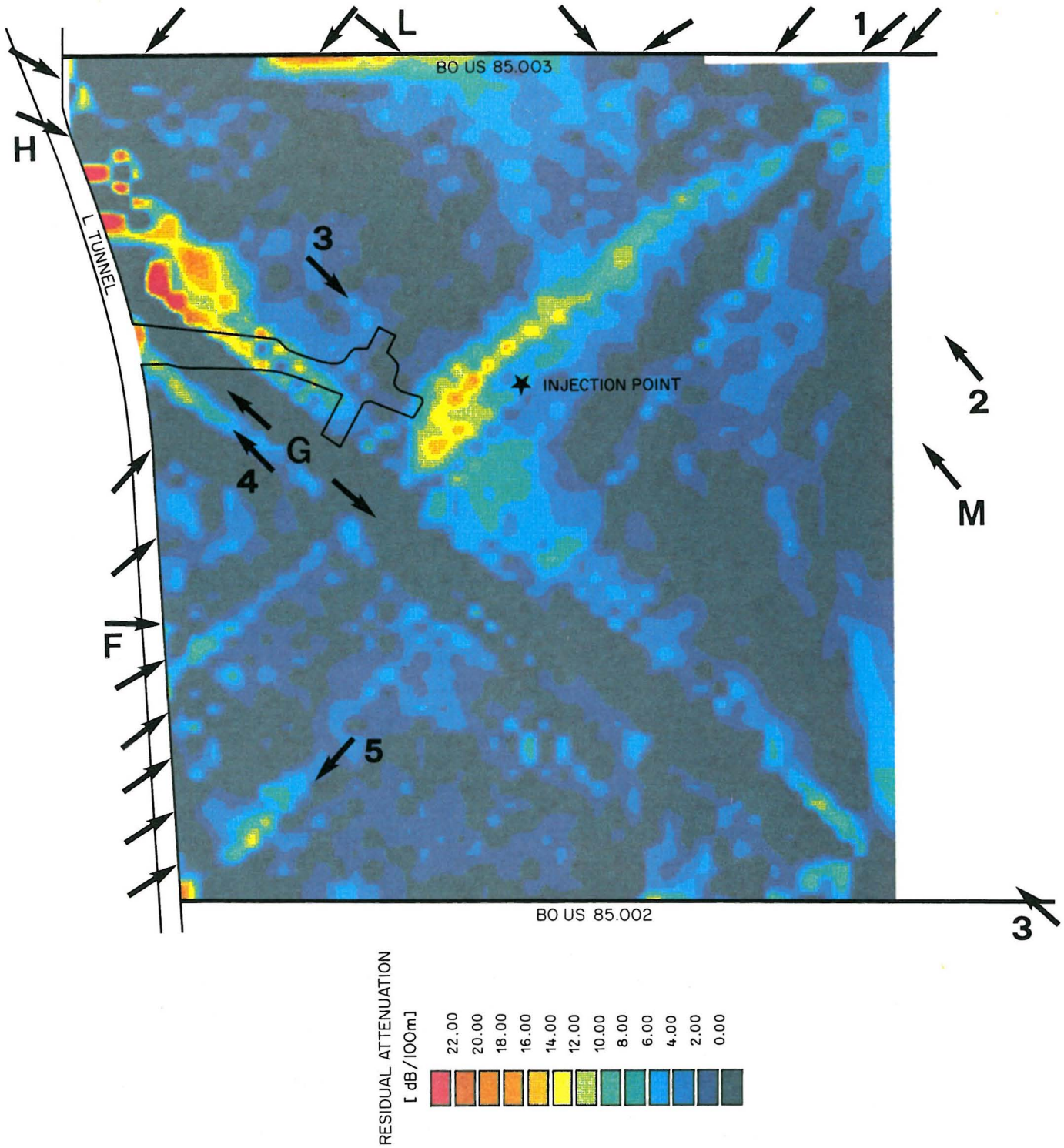

Fig. 6.3 Tomographic map showing the increase in radar attenuation of Field 2 from phase 1 to phase 2 obtained after removal of the rays going to the end of BO US 85.002. A total of 856 rays were removed. Scale 1:1000.

6.2 Results from Phase 3 tracer injection

During phase 3 saline tracer was injected in a section at an approximate depth of 62 m in borehole BO BK 86.003 (Fig. 1.3). The injection of the tracer was started 3 days before the commencement of the radar tomography survey. The saline injection continued during the entire radar survey which lasted for 5 days.

The measurement configuration between the tunnel and borehole BO US 85.003 was changed during this phase compared to previous phases in order not to disturb the conditions in the borehole. In accordance with the results of the seismic tomography program and previous hydraulic tests an inflow of saline tracer to the borehole was expected as a result of the injection. The receiver antenna was therefore kept fixed in the borehole while the transmitter antenna was moved in the tunnel between the measurement points.

An attempt was made to make difference tomography on the travel time data from phases 2 and 3. The resulting tomogram (Fig. 6.4) is dominated by a large slowness anomaly in the bottom part of the area between the boreholes which must be considered an artifact. The tomogram is also very "noisy" with a lot of small pointlike anomalies confined to a single pixel. The anomalies observed in the slowness difference tomogram are considered to be artifacts and hence not representative of any effect of the saline tracer. From this result we may conclude that the effect (if any) of a saline tracer on radar velocities is smaller than the errors in the measurement.

Two tomograms have been made of the difference between phase 3 and phase 1 amplitudes. One where the rays identified by the manual and automatic removal process from both phase 1 and 3 were removed. For the other tomogram the rays going to the bottom part of borehole BO US 85.002 were removed in addition to the removed rays from phase 3 in order to study the effect on one dominating structure in the tomogram.

The first difference tomogram between phase 3 and 1 was made containing a total of 4959 rays. The total number of removed rays was 1421 (22.2 % out of a total of 6380). The RMS-value was 0.9 dB after the first inversion and 0.7 dB after the final inversion.

The tomogram (Fig. 6.5) is dominated by a structure (H) which was identified in the difference tomogram from phase 2 to phase 1 (Figs. 6.2 and 6.3). This

feature extends partly beyond the BK-drift and appears to be connected to a number of structures starting close to the point of the phase 3 injections. These anomalies seem to end up at structure (H). Structure (4) identified earlier also appears to have obtained increased attenuation between phase 3 and 1. Water inflow to the L-tunnel has been observed at the intersection points of (H) and (5) with the tunnel. Close to the injection point a strong attenuation increase (6) appears which extends to a fractured part of borehole BO US 85.003 and represents the known hydraulic connection between the boreholes BO BK 86.003 and BO US 85.003.

Tomographic inversion was also made with those rays removed which goes to the bottom part of borehole BO US 85.002 and the ones with errors identified during phase 3. This was done in order to determine whether anomaly (3) was an artifact caused by rays from the tunnel to the end of borehole BO US 85.002. The remaining number of rays was 5032, subsequently 1348 out of 6380 had been removed. The resulting tomogram is shown in Fig. 6.6. The tomogram shows the same overall pattern as the previous one except close to the bottom part of borehole BO US 85.002 where data has been removed. Some minor differences in the bottom part of the tomogram are visible presumably created by the inversion process as the ray density in that part has been changed. The anomalies caused by the saline tracer show the same pattern in the injection area.

The difference tomograms based on phase 3 results show only minor residual effects from the phase 2 injections. The large attenuation increase observed in the phase 1 to phase 2 tomograms is now hardly visible. In the area between the tunnel close to borehole BO US 85.003 and the BK-drift the attenuation increase that was identified during phase 2 still appears but with higher intensity compared to the phase 1 results.

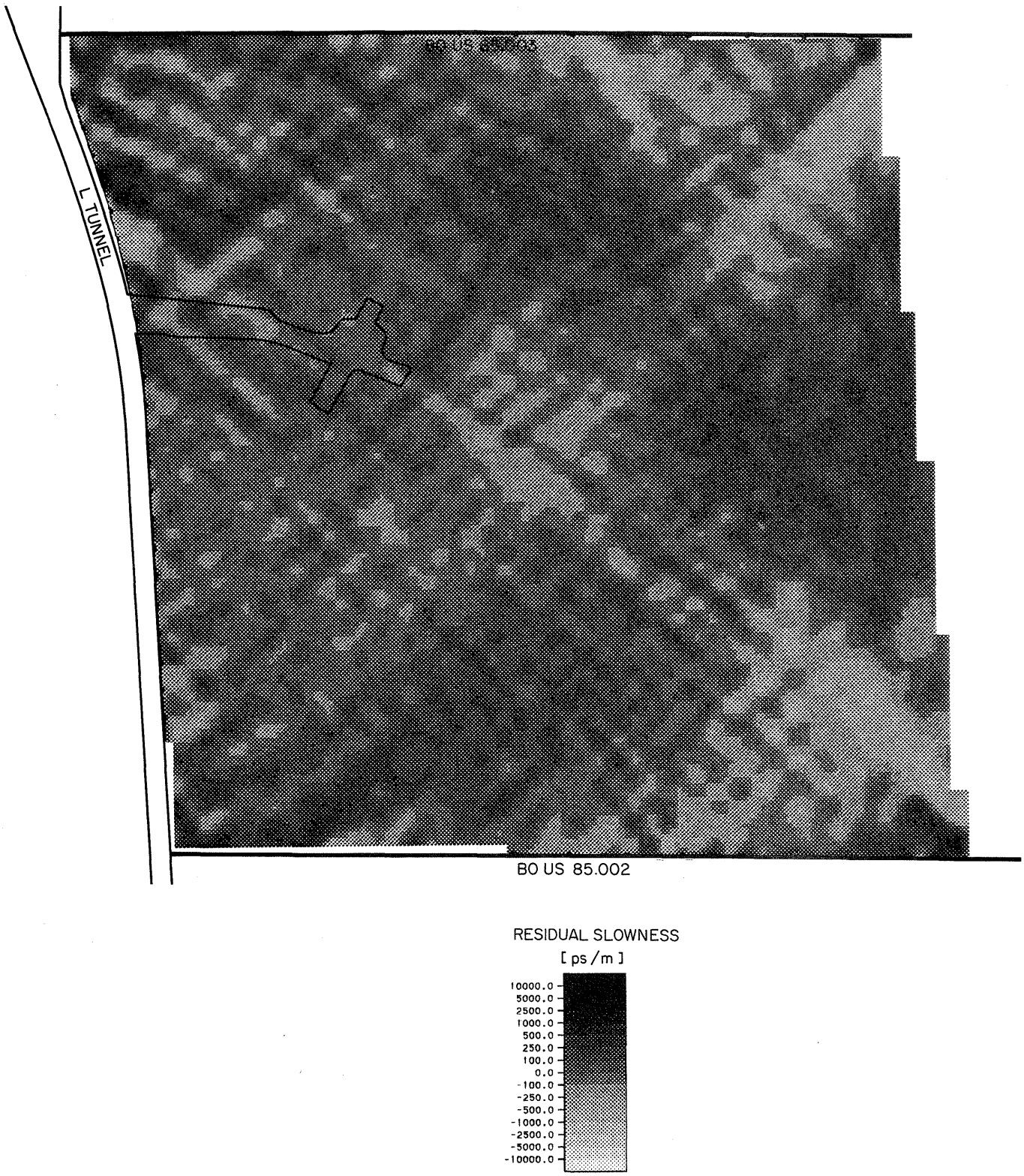

Fig. 6.4 Tomographic map showing the increase in radar slowness of Field 2 from phase 2 to phase 3. Scale 1:1000.

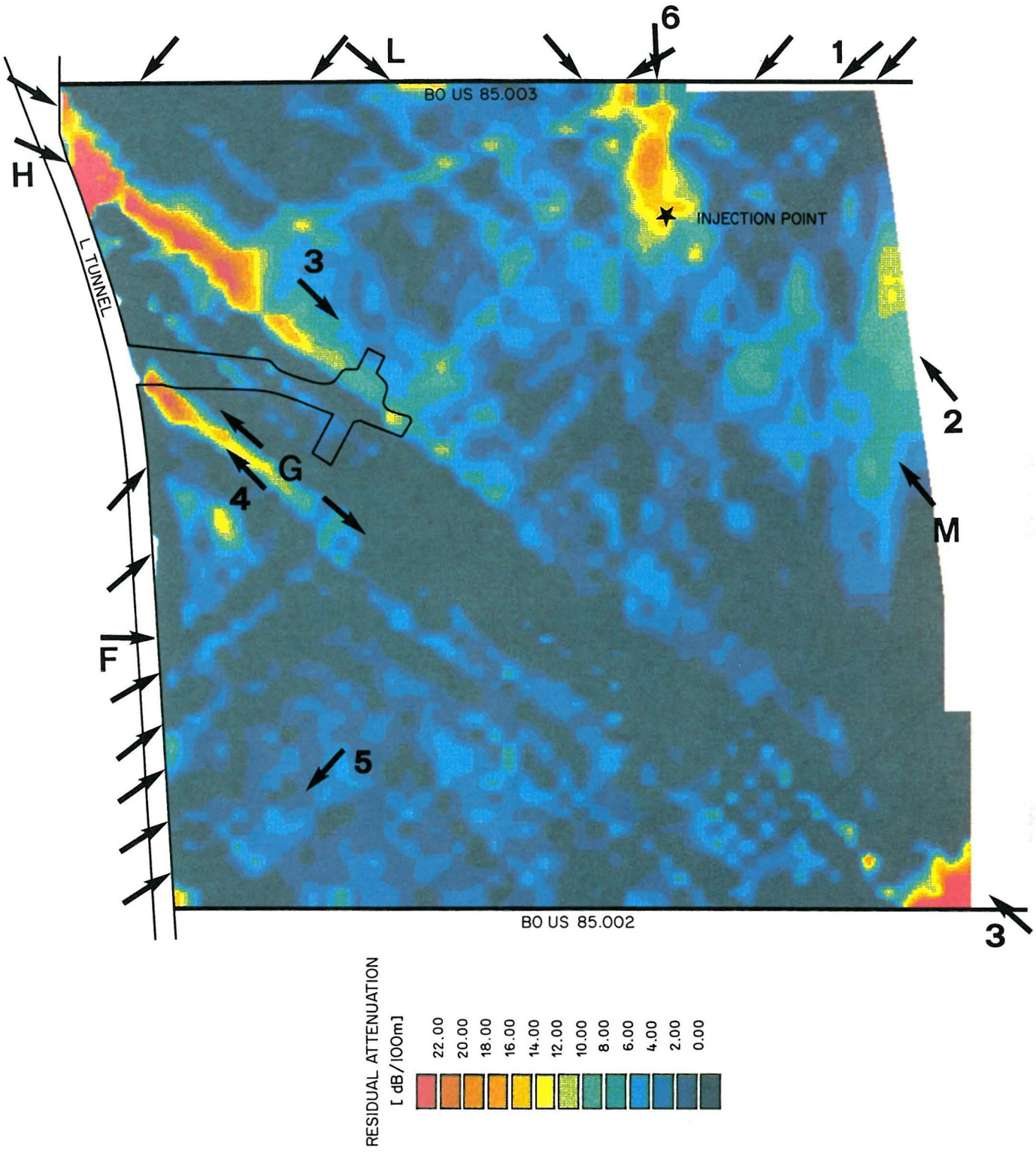

Fig. 6.5 Tomographic map showing the increase in radar attenuation of Field 2 from phase 1 to phase 3 obtained after removal of 1421 rays. The map shows the parts of the plane where the saline tracer has migrated. Scale 1:1000.

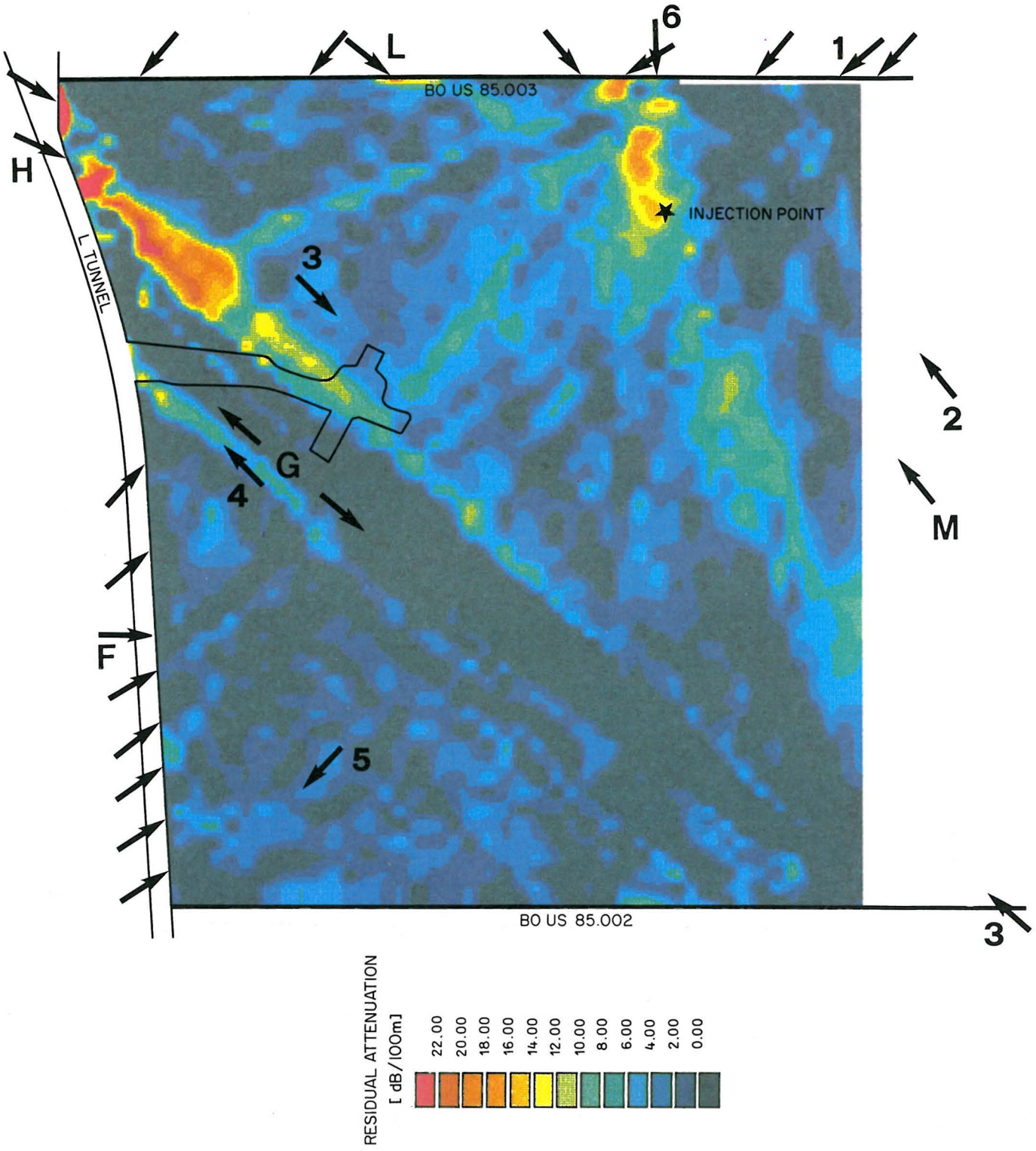

Fig. 6.6 Tomographic map showing increase in radar attenuation of Field 2 from phase 1 to phase 3 obtained after removal of the rays going to the bottom of borehole BO US 85.002. Scale 1:1000.

6.3 Conclusions and recommendations

The main task during the second and third phases of the RCT-programme was to investigate whether radar tomography could be used to study the spreading of a saline tracer through the rock mass and if radar tomography successfully can map the spreading of the tracer.

Saline tracer was injected from boreholes BO BK 85.009 during phase 2 and BO BK 86.003 during phase 3, both drilled from the BK-drift. The salinity of the tracer was selected to 0.9% for phase 2 and 0.8% for phase 3. This high salinity was chosen to ensure that there was a reasonable chance of measuring the increased attenuation with the radar system. Another important aspect of this type of experiment is that the results from two measurements are compared and that radar data are collected over a relatively long period of time (10 days for phase 2 and 5 days for phase 3). As all data from each measuring period is used in the tomographic inversion it is a prerequisite that the properties of the rock mass are not changed during the measurement period. If there is a change in radar attenuation with time this will cause an inconsistent data set which will generate artifacts in the difference tomogram. The reduction of the measurement time for phase 3 was made as an attempt to reduce any such changes.

The basic experimental requirements for mapping the transport of a saline tracer in rock with a difference measurement like the one performed here is that the measuring equipment is extremely stable during the entire experiment and that the distribution and concentration of the saline tracer in the investigated rock volume does not change significantly during the experimental period. These conditions are actually quite difficult to satisfy and control. The data from the calibrations performed during phases 2 and 3 and comparison with the amplitude data from phase 1 indicate that the radar equipment meets the experimental requirements. Some of the radar data actually indicates that the concentration of the saline tracer has not been the same throughout the experimental volume and time duration. Hence, the condition that steady state conditions should apply during the experiment has not been totally fulfilled. The amount of variation is difficult to quantify and the effect on the difference tomogram is uncertain. However, results of the daily calibrations indicate that especially the anomalies at the end of borehole BO US 85.002 could represent artifacts due to changes in salt concentration in the area during the radar

measurement period. A further analysis of the radar data to see if the transport of the tracer as a function of time can be observed and quantified is certainly of interest.

The difference tomogram was calculated in two ways; by taking the difference of the amplitude tomograms produced from phases 1 and 2; and from the difference of the residual amplitude data for each ray obtained in phases 1 and 2. It was shown that better and more stable results were obtained by taking the difference of the amplitudes for each ray. In this case the errors introduced on the ray pattern by locating the transmitter antenna in the L-tunnel will cancel. This procedure is considered superior to taking the difference of two tomograms each containing large artifacts.

The difference tomograms define the distribution of increased attenuation (i.e. the location of the saline tracer) with high resolution and the tomograms do not appear to contain any significant artifacts. The results should however be viewed with some caution as it is known that steady state conditions have not totally been met. Most likely the distribution of the tracer is indicated in general terms but the details of the distribution can be in error. The absence of the largest anomaly, the lamprophyre (F), in the difference tomograms indicates that the difference procedure works and that no errors proportional to the magnitude of the anomalies in the attenuation tomograms exist. The magnitude of the anomalies in the difference tomograms is about 10-20% of the attenuation anomaly caused by the lamprophyre (F) in normal tomograms.

The difference tomogram from phase 2 shows the largest increase in attenuation at the point of injection of the saline tracer and the tracer follows one of the structures identified in the slowness tomogram until this structure intersects another feature which also shows a significant increase in attenuation. A relatively large anomaly close to borehole BO US 85.003 indicates that the saline tracer flows towards this hole.

The phase 3 results also show a large increase in attenuation close to the injection point which extends to borehole BO US 85.003. Inflow of saline water in the borehole was also observed at the location indicated by the difference tomography.

An interesting feature is marked by the anomalies close to the L-tunnel which appear in the difference tomograms from both phases. These anomalies are associated with the features (G) and (H) identified

in the slowness and attenuation tomograms. There is no direct connection between the injection points and these anomalies. This implies that the tracer possibly has been transported along a path out of the investigated plane. This is not unreasonable considering that the fracture zones at the site have a steep dip. If the tracer follows the fracture zones it is likely to move out of the investigated plane. It should also be noted that the L-tunnel constitutes a hydraulic drain and the flow paths are likely to end near the tunnel.

Increased attenuation was also observed in the difference tomograms at the end of borehole BO US 85.002. The phase 2 difference tomogram had an indication of a structure extending from the injection point to the end of this borehole where saline tracer had migrated. A weaker indication was also observed in the phase 3 data. Initially this anomaly was suspected to be an artifact and tests were made where rays from the end of borehole BO US 85.002 were removed from the data set (Figs. 6.3 and 6.6). The anomaly (3) still remained even if its location changed somewhat due to the removed rays. It must be concluded that these anomalies are real. A detailed study of the data indicate that the tracer has arrived close to the end of borehole BO US 85.002 towards the end of the measurement periods of both phase 2 and phase 3. Hence, we may conclude that there is a transport of tracer from both injection points towards the end of borehole BO US 85.002 on a path which is probably out of the investigation plane.

7 DISCUSSION AND CONCLUSIONS

The Radar Crosshole Tomography (RCT) programme has had two goals. The first was to investigate the potential of the method for mapping the geologic structures at the US-site in the Grimsel Rock Laboratory and the second was to use difference tomography to map the transport paths of saline tracer. Both tasks have been successfully completed.

Generally good correlation has been obtained between the slowness and attenuation tomograms and the geological features observed in boreholes and tunnels. The tomograms have high resolution in an area extending from the L-tunnel. The extent of this area depends on the length of the boreholes in relation to the distance between the boreholes. The results obtained shows that the distance between the boreholes should not exceed their length if high resolution is required for a sufficient portion of the investigated area. If the length of holes is equal to the distance between holes as in the case of Field 2 good resolution is obtained for about two thirds of the investigated area.

Tomograms are more sensitive to systematic errors than stochastic errors. Stochastic errors generally produce a noisy image which reduces the attainable resolution while systematic errors produce artifacts, i.e. false structures, in the tomograms. During phase 1 a drift in the time base of the radar system occurred caused by some temperature sensitive components. This resulted in systematic offset and velocity errors which were different for several parts of the data sets. The slowness tomograms, except from Field 1, from phase 1 therefore generally contained significant artifacts which results in poor correlation with geological features observed in boreholes and tunnels. The equipment was modified before the start of the phase 2 measurements and no significant time base drifts occurred during the last two phases. The quality of the slowness tomograms made after the modification of the equipment was greatly enhanced.

The amplitude data from the L-tunnel to borehole rays contained systematic errors due to the inadequate knowledge of the radiation pattern of an antenna located in a tunnel. The radiation pattern for antennas located in a borehole is well known and no systematic errors were found in the borehole to borehole data. The errors in the amplitude data

generated significant artifacts in the tomograms especially at large distances from the L-tunnel and close to the borehole. A significant reduction in the artifacts was obtained by excluding the rays containing the largest errors based on their direction relative to the tunnel and the boreholes.

The average velocity of radar waves at the site was estimated to 124 m/μs and the average attenuation was about 25 dB/100 m. The measured contrasts in slowness and attenuation amounted to about 9% and 250%, respectively. The attenuation contrasts are thus considerably larger than the velocity (or slowness) contrasts. Anisotropic effects were observed both in slowness and amplitudes the magnitudes of the anisotropy were 0.3% and 7%, respectively.

The main feature identified in the tomograms is a lamprophyre which extends in a direction almost parallel to the boreholes. Two additional sets of features, probably fracture zones, can also be identified which extend in almost orthogonal directions (NW and WSW). These features can be identified with good resolution only in the slowness tomogram.

The main task during the second and third phases of the RCT-programme was to investigate the transport of a saline tracer by means of difference tomography. Saline tracer was injected in borehole BO BK 85.009 during phase 2 and from borehole BO BK 86.003 during phase 3. The salinity of the tracer was just below 1%. This high salinity was chosen to ensure a reasonable chance of detecting an attenuation increase caused by the saline tracer.

The injection of the saline tracer was started a couple of days before the radar tomography measurements began. The injection continued during the radar measurements which took 10 days for phase 2 and 5 days for phase 3. Steady state conditions during the radar measurements are mandatory for a successful outcome of a difference tomography experiment. For these experiments it does not appear as if the hydrological situation has been completely under control. The difference tomograms give very good results but there are aspects of the data which indicate that there has been minor changes in the distribution of the tracer during the measurements. It is recommended that saline injection is started a considerably longer time before the radar measurements than was the case for the RCT-programme. Salt concentrations should be monitored in available boreholes and the radar measurements should not be started until steady state conditions prevail.

Difference tomograms were obtained by taking the difference between the amplitude data from two different phases for each ray followed by a tomographic inversion of this data. The technique for producing the difference tomograms performed very well. An indirect demonstration of this is the complete disappearance of the largest anomaly in the attenuation tomograms, the lamprophyre dike. This implies that errors in the residual amplitudes due to modification of the radiation pattern caused by the tunnel cancel as expected.

Strong attenuation was observed at both injection points and the tracer followed fracture zones extending from each injection point. Transport of tracer from the injection points to the L-tunnel along paths which must have been out of the investigated plane were also observed. The tracer generally followed features which were observed in the slowness tomograms. But the features where the tracer transport has taken place were not the strongest and most significant anomalies in the slowness tomograms. Significant water flow can evidently take place along smaller fracture zones which are visible in tomograms but may not be considered significant. This is an item which has to be carefully considered in future interpretation of tomograms in geological and hydrological terms.

The results from the RCT-programme show that the radar method can be used successfully to map the transport of saline tracer through a fractured rock mass. Experiments of the type performed within the RCT-programme open new possibilities for obtaining a description of the uneven distribution of groundwater flow through fractured crystalline rock. The radar is a remote sensing technique and an application of the radar difference technique to monitor groundwater transport can give reliable two or three dimensional images of flow paths. This should be compared to the uncertain extrapolations that have to be made between sparsely distributed measurement points in conventional migration experiments. The techniques developed within the RCT-programme have an enormous potential for exploring some of the complexities of groundwater transport through crystalline rock such as channeling.

8 ACKNOWLEDGEMENT

The assistance given by the personnel both from NAGRA and BGR at the Grimsel Test Site has been of great value for the successful performance of the measurements. The discussions, assistance, and encouragement given by Dr. G. Sattel, and Dr. L. Liedtke is greatly appreciated. G. Stoll, C. Gustavsson, and L. Lundmark made the field measurements. A. Wettervik, M. Smellie and B. Kunz made the drafting work.

9 REFERENCES

Brace, W. F., Orange, A. S., Madden, T. R. (1965): The effect of pressure on the electrical resistivity of water saturated crystalline rocks. Journal of Geophysical Research, 70 (22), 5669-5678.

Falk, L., Magnusson, K.-Å., Olsson, O., Amman, M., Keusen, H. R., Sattel, G., (1987): Analysis of radar measurements performed at the Grimsel Rock Laboratory in October 1985. NAGRA NTB 87-13, NAGRA, Baden, Switzerland.

Ivansson, S. (1984): Crosshole Investigations - Tomography and its application to crosshole seismic measurements. Stripa Project IR 84-08, SKB, Stockholm, Sweden.

Ivansson, S., Hammarström, M., Pihl, J. (1987): Tomographic calculations for synthetic data. Internal report, NAGRA, Baden, Switzerland.

Liedtke, L. and Pahl, A. (1987): Transport of dissolved substances in fissured granite. In Proc. from DOE/AECL '87 Conference on Geostatistical Sensitivity and Uncertainty Methods for Groundwater Flow and Radionuclide Transport Modelling, September 1987, San Francisco.

Magnusson, K.-Å., Carlsten, S., Olsson, O. (1987): Crosshole investigations - Physical properties of core samples from borehole F1 and F2. Stripa Project TR 87-10, SKB, Stockholm, Sweden.

Niva, B., Olsson, O. (1987): Radar crosshole tomography at the Grimsel Test Site - Results from phase 1. Internal report, NAGRA, Baden, Switzerland.

Niva, B., Olsson, O. (1988a): Radar crosshole tomography at the Grimsel Test Site - Results from phase 2. Internal report, NAGRA, Baden, Switzerland.

Niva, B., Olsson, O. (1988b): Radar crosshole tomography at the Grimsel Test Site - Results from phase 3. Internal report, NAGRA, Baden, Switzerland.

Olsson, O., Lundmark, L. (1985): Documentation of radar measurements performed at the Grimsel Rock Laboratory, Switzerland, in October 1985. Swedish Geological Co. Report IRAP 85245. Swedish Geological Co., Uppsala, Sweden.

Olsson, O., Falk., L., Forslund., O., Lundmark, L., Sandberg, E. (1987): Crosshole investigations - Results from borehole radar investigations. Stripa Project TR 87-11, SKB, Stockholm, Sweden.

Olsson, O., Black, J., Cosma, C., Pihl, J. (1987): Crosshole investigations - Final report. Stripa Project TR 87-16, SKB, Stockholm, Sweden.

Olsson, O., Eriksson, J., Falk, F., Sandberg, E. (1988): Site characterization and validation - Borehole radar investigations, Stage I. Stripa Project IR 88-03, SKB, Stockholm, Sweden.

Sen, P. N., Scala, C., Cohen, M. H. (1981): A self-similar model for sedimentary rocks with application to the dielectric constant of fused glass beads. Geophysics, 46, 781-795.